Bottom Up Study of $K_L \to \pi^0 \nu \bar{\nu}$ experiment

Kenichi Manabe
High Energy Physics Group
Department of Physics at Osaka University

March 25, 2000

Abstract

The $K_L \to \pi^0 \nu \bar{\nu}$ decay is a good probe to measure η which is an imaginary component in the CKM matrix which describes CP violation. By using Monte Carlo simulation, we studied the necessary condition to measure η to 10% of itself with a lead/scintillator sandwich calorimeter, while suppressing the number of major background from $K_L \to \pi^0 \pi^0$ below signal events. With a semi-ideal detector, we found required K_L momentum range for the following four cases; a)if we only measure gammas energy and position, K_L momentum $\geq$ 10GeV/c, b)if we know the decay vertex in addition to gammas energy and position, K_L momentum $\geq$ 5GeV/c, c)if we know K_L energy in addition to gammas energy and position, K_L momentum $\geq$ 5GeV/c, and d)if we know K_L energy and decay vertex in addition to gammas energy and position, K_L momentum $\geq$ 500MeV/c.

Acknowledgement

I would like to show my gratitude to all the people who were associated with my two year study at Osaka University and completion of this thesis.

I am grateful to members of the KAMI collaboration, including Y.W.Wah and R.Kessler for their advice for my MC simulation.

I also owe a lot to the members of the Nagashima Group at Osaka University for the good companionship and encouragement. Katsumi Senyo, Satoshi Hidaka, Kazutaka Sumisawa, Makoto Yoshida, Jiro Ryuko, Takahiro Houjo, Kohji Hara, Hideki Miyake, and Kazunori Nitta, have given me great deal of help to proceed my research.

I would like to thank Ichiro Suzuki, Masahiro Sadamoto, Katsumi Senyo, Satoshi Hidaka, Koji Mori, and Keitaro Kurebayashi, who taught me physics and experiments as KTeV group in Osaka.

With Yuka Kajiyama, Mitsuhiro Matsumoto, and Hiroshi Tagomori, I shared good time on talking about physics and lead enjoyable research life.

Further gratitude is given to Akihiro Maki, Masato Takita, Masashi Hazumi, and Takanori Hara, for their kind instruction of the basics of physics as well as computer skills. Sachiko Tsuzuki's help and support for my research life must also be mentioned here.

I would like to give my profound thankfulness to the dedicated work of instruction and advice of Taku Yamanaka for the completion of this thesis. His deep concern on physics and keen eyes on everything he sees to seek the essential part of nature gave me a great amount of inspiration. Finally, I would like to thank my adviser, Professor Yorikiyo Nagashima, for giving me a chance to work on a research in high energy physics. From his devotion to physics I learned the attitude of professional researcher, which would certainly affects rest of my life.

Contents

1 Introduction **15**

1.1 Physics Interest in $K_L \to \pi^0\nu\bar{\nu}$ . . . 15

1.1.1 CP Violation . . . 15

1.1.2 CKM parameter η . . . 16

1.1.3 Decay of $K_L \to \pi^0\nu\bar{\nu}$ . . . 16

1.2 Experimental Challenges for Detecting $K_L \to \pi^0\nu\bar{\nu}$ . . . 18

1.3 Purpose and Overview . . . 19

2 Inefficiency of Photon Counter **20**

2.1 Photo-Nuclear Interaction . . . 20

2.2 Sampling Effect and Punch Through . . . 20

2.2.1 Geometry and Condition . . . 22

2.2.2 Calibration . . . 22

2.2.3 Inefficiency due to Sampling Effect and Punch Through . . . 23

2.2.4 Inefficiency of the Photon Counter . . . 23

3 Simulation using Ideal Model **29**

3.1 Condition and Geometry . . . 29

3.2 Simple Case . . . 31

3.2.1 Transverse momentum Cut . . . 31

3.2.2 Cut Criteria . . . 31

3.2.3 Background Level . . . 32

3.3 Case where Decay Vertex is known . . . 36

3.3.1 Mass Cut . . . 36

3.3.2 Transverse momentum Cut . . . 36

3.3.3 Background Level . . . 36

3.4 Case where K_L Energy is known . . . 40

3.4.1 Missing Mass Cut . . . 40

3.4.2 Missing mass VS. $E_{\gamma\gamma}$ Cut . . . 40

3.4.3 Background Level . . . 40

3.5 Case where Vertex and E_{K_L} are known . . . 46

3.5.1 Mass Cut . . . 46

3.5.2 Missing Mass Cut . . . 46

3.5.3 Missing mass VS. $E_{\gamma\gamma}$ Cut . . . 46

3.5.4 Background Level . . . 47

3.6 Summary . . . 52

4 Requirements on the Detector 53
4.1 Simple Case . . . 53
4.1.1 Smearing Gamma's Position . . . 53
4.1.2 Smearing Gamma's Energy . . . 54
4.1.3 Finite Detector Length . . . 54
4.1.4 Realistic model . . . 55
4.1.5 Summary . . . 55
4.2 Case where Decay Vertex is known . . . 60
4.2.1 Smearing Gamma's direction . . . 60
4.2.2 Smearing Gamma's Energy . . . 61
4.2.3 Finite Detector Length . . . 61
4.2.4 Realistic model . . . 61
4.2.5 Summary . . . 62
4.3 Case where E_{K_L} is known . . . 67
4.3.1 Smearing Kaons Energy . . . 67
4.3.2 Smearing Gammas Energy . . . 67
4.3.3 Smearing Gammas Position . . . 67
4.3.4 Finite Detector Length . . . 67
4.3.5 Realistic model . . . 68
4.3.6 Summary . . . 69
4.4 Case where Vertex and E_{K_L} are known . . . 75
4.4.1 Smearing Kaon energy . . . 75
4.4.2 Smearing the Gamma's energy . . . 75
4.4.3 Smearing Gamma's direction . . . 75
4.4.4 Finite Detector Length . . . 75
4.4.5 Realistic model . . . 76
4.4.6 Summary . . . 76

5 Discussion 83
5.1 Examination of Experiments . . . 83
5.1.1 BNL . . . 83
5.1.2 KAMI . . . 83
5.1.3 E391 . . . 84
5.2 Suggestions . . . 84

6 Conclusion 85

I CsI Photon Counter 86
I.1 Inefficiency of CsI photon counter . . . 86
I.2 Detector parameters . . . 87
I.3 Background Level . . . 87
I.4 Discussion . . . 87

II Reconstructed Decay Vertex Position 90

III Effect of the realistic K_L momentum 92
III.1 K_L momentum distribution . . . 92
III.2 Effect of the realistic K_L momentum . . . 92
III.3 $E_{\gamma\gamma}$ VS. M_{miss} Cut . . . 93

IV Threshold of Photon Counter **98**
IV.1 Inefficiency of Photon Counter 98
IV.2 Background Level 98
IV.3 Conclusion 98

A Contribution of Punch Through **101**

B Step in P_t distribution **103**

C Error on η **105**

D Dominant of Odd Pair Background **107**

List of Figures

1.1 The Z penguin and W-box diagrams which contribute to the decay $K_L \to \pi^0 \nu \bar{\nu}$ 17

1.2 (a)even pair background is caused by missing two gamma from one pion, and (b)odd pair is caused by missing two gamma from different pions 19

2.1 The detector geometry used in ES171 experiment. The detector(a) shows the 1mmPb/ 5mmScint calorimeter and the detector(b) shows the 0.5mm/ 5mmScint calorimeter and veto counter. 21

2.2 Photon detection inefficiency due to photo-nuclear interaction as a function of energy, measured by ES171 [10]. The open circles and the triangle show the inefficiency for 1mmPb/5mmScint calorimeter and 0.5mmPb/5mmScint calorimeter, respectively. . . . 21

2.3 The detector geometry used in EGS simulation. The detector(a) shows 1mmPb/5mmScint calorimeter, the detector(b) shows the 0.5mm/5mmScint calorimeter and the detector(c) shows the 0.1mm/5mmScint calorimeter. 22

2.4 Distribution of energy deposit in the scintillator in 1mmPb/ 5mmScint detector for the incident gamma energy of 20, 30, 40, 50, 70, and 100MeV. The distributions are fitted for a Gaussian. 24

2.5 Distribution of energy deposit in the scintillator in 0.5mmPb/ 5mmScint detector for the incident gamma energy of 20, 30, 40, 50, 70, and 100MeV. The distributions are fitted for a Gaussian. 24

2.6 Distribution of energy deposit in the scintillator in 0.1mmPb/ 5mmScint detector for the incident gamma energy of 20, 30, 40, 50, 70, and 100MeV. The distributions are fitted for a Gaussian. 25

2.7 Incident energy VS. deposit energy in scintillator for (a)1mmPb/ 5mmScint, (b)0.5mm/ 5mmScint, and (c)0.1mm/ 5mmScint 25

2.8 Distribution of energy deposit in the scintillator of 1mmPb/ 5mmScint detector for the incident energy of 20MeV, 30MeV, 40MeV, 50MeV, 70MeV, and 100MeV. The shadowed area below the threshold of 3.25MeV, which corresponds to 10MeV gamma, contributes to inefficiency. 26

2.9 Distribution of energy deposit in the scintillator of 0.5mmPb/ 5mmScint detector for the incident energy of 20MeV, 30MeV, 40MeV, 50MeV, 70MeV, and 100MeV. The shadowed area below the threshold of 5.02MeV, which corresponds to 10MeV gamma, contributes to inefficiency. 26

2.10 Distribution of energy deposit in the scintillator of 0.1mmPb/ 5mmScint detector for the incident energy of 20MeV, 30MeV, 40MeV, 50MeV, 70MeV, and 100MeV. The shadowed area below the threshold of 8.38MeV, which corresponds to 10MeV gamma, contributes to inefficiency. 27

2.11 Photon detection inefficiency due to the sampling effect and punch through as a function of incident energy of gamma. The open circles, the dot points, and the cross points show the 1mmPb/ 5mmScint, 0.5mmPb/ 5mmScint, and 0.1mmPb/ 5mmScint detector, respectively. 27
2.12 Total detection inefficiency as a function of the photon energy for (a)1mmPb/5mmScint and (b)0.5mmPb/5mmScint sampling calorimeters. The dashed line and dotted line show the inefficiency due to the photo-nuclear interaction and the sum of sampling effect and punch through, respectively. Above 1GeV, the inefficiency required by KAMI is used. . 28

3.1 The detection geometry used in simulation 29
3.2 Explanation of how to decide the cut region. (a)transverse momentum of $K_L \to \pi^0\nu\bar{\nu}$. (b)transverse momentum of $K_L \to \pi^0\pi^0$. (c)N/S ratio distribution that is (a) divided by (b). (d)The region with N/S ratio under this line is decided as signal region, and we take down this line. (e)When the error on η get down to 10%, this region is decided as signal region. 33
3.3 P_t distribution for $K_L \to \pi^0\pi^0$ are shown for the K_L momentum of 500MeV/c, 1GeV/c, 5GeV/c, 10GeV/c, and 50GeV/c in the simple case. The 1mmPb/5mmScint sampling calorimeter was used as the photon counter. The shadow area shows the signal region.(see 3.2.2) 34
3.4 P_t distribution for $K_L \to \pi^0\nu\bar{\nu}$ are shown for the K_L momentum of 500MeV/c, 1GeV/c, 5GeV/c, 10GeV/c, and 50GeV/c in the simple case. The 1mmPb/5mmScint sampling calorimeter was used as the photon counter. The shadow area shows the signal region.(see 3.2.2) 34
3.5 Background level in the Simple Case is shown as a function of K_L momentum. The solid line and the dashed line show background level for using 1mm Pb/5mm Scint and 0.5mm Pb/5mm Scint detector, respectively. 35
3.6 The distribution of two gammas mass for K_L momentum of 500MeV/c, 1GeV/c, 5GeV/c, 10GeV/c, and 50GeV/c. The 1mmPb/ 5mmSint calorimeter was used as the photon counter. The shadow area shows the signal region of $m_{\pi^0} \pm 10MeV/c^2$ 37
3.7 P_t distribution for $K_L \to \pi^0\pi^0$ are shown for the K_L momentum of 500MeV/c, 1GeV/c, 5GeV/c, 10GeV/c, and 50GeV/c in the case where vertex is known. The 1mmPb/5mmScint sampling calorimeter was used as the photon counter. The shadow area shows the signal region.(see 3.2.2) 38
3.8 P_t distribution for $K_L \to \pi^0\nu\bar{\nu}$ are shown for the K_L momentum of 500MeV/c, 1GeV/c, 5GeV/c, 10GeV/c, and 50GeV/c in the case where vertex is known. The 1mmPb/5mmScint sampling calorimeter was used as the photon counter. The shadow area shows the signal region.(see 3.2.2) 38
3.9 The background level as a function of K_L momentum is shown. The solid line and the dashed line show the background level for the case where vertex is known using 1mm Pb/5mm Scint and 0.5mm Pb/5mm Scint detector, respectively. The dotted line show the background level in simple case using 1mm Pb/5mm Scint. The background level at 1GeV/c is greater than that at 500MeV/c because the cut region and P_t distribution are different between them as shown in Fig.3.7. 39
3.10 Distribution of missing mass for $K_L \to \pi^0\pi^0$ for the K_L momentum of 500MeV/c, 1GeV/c, 5GeV/c, 10GeV/c, and 50GeV/c in the case where E_{K_L} is known. The 1mmPb/5mmScint sampling calorimeter was used as the photon counter. The shadow area shows the cut region. 42

3.11 Distribution of missing mass for $K_L \to \pi^0\nu\bar{\nu}$ for the K_L momentum of 500MeV/c, 1GeV/c, 5GeV/c, 10GeV/c, and 50GeV/c in the case where E_{K_L} is known. The 1mmPb/5mmScint sampling calorimeter was used as the photon counter. The shadow area shows the cut region. 42
3.12 Missing mass VS. $E_{\gamma\gamma}$ for the K_L momentum of 500MeV/c, 1GeV/c, and 5GeV/c in the case where E_{K_L} is known. The 1mmPb/5mmScint sampling calorimeter was used as the photon counter. The left row shows the distribution for the background, and the center row shows the distribution of signal. The right row shows the signal region selected by the method described in the text. 43
3.13 Missing mass VS. $E_{\gamma\gamma}$ for the K_L momentum of 10GeV/c, and 50GeV/c in the case where E_{K_L} is known. The 1mmPb/5mmScint sampling calorimeter was used as the photon counter. The left row shows the distribution for the background, and the center row shows the distribution of signal. The right row shows the signal region selected by the method described in the text. 44
3.14 The background level as a function of P_{K_L} is shown for the case where E_{K_L} is known. For comparison, simple case and the case where we know decay vertex are also shown. . 45
3.15 The distribution of missing mass for $K_L \to \pi^0\pi^0$ for the K_L momentum of 500MeV/c, 1GeV/c, 5GeV/c, 10GeV/c, and 50GeV/c in the case where the vertex and E_{K_L} are known. The 1mmPb/5mmScint sampling calorimeter was used as the photon counter. The shadow area shows the cut region. 48
3.16 The distribution of missing mass for $K_L \to \pi^0\nu\bar{\nu}$ for the K_L momentum of 500MeV/c, 1GeV/c, 5GeV/c, 10GeV/c, and 50GeV/c in the case where the vertex and E_{K_L} are known. The 1mmPb/5mmScint sampling calorimeter was used as the photon counter. The shadow area shows the cut region. 48
3.17 Missing mass VS. $E_{\gamma\gamma}$ for the K_L momentum of 500MeV/c, 1GeV/c, and 5GeV/c in the case where the vertex and E_{K_L} are known. The 1mmPb/5mmScint sampling calorimeter is used as the photon counter The left row shows the distribution for the background, and the center row shows the distribution for signal. The right row shows the signal region selected by the method described in the text. 49
3.18 Missing mass VS. $E_{\gamma\gamma}$ for the K_L momentum of 10GeV/c, and 50GeV/c in the case where the vertex and E_{K_L} are known. The 1mmPb/5mmScint sampling calorimeter is used as the photon counter The left row shows the distribution for the background, and the center row shows the distribution for signal. The right row shows the signal region selected by the method described in the text. 50
3.19 The background level as a function of P_{K_L} is shown for the case where the decay vertex and E_{K_L} are known. For comparison, other cases are also shown. 51

4.1 The detection geometry used in realistic model 54
4.2 P_t distribution after smearing gamma's hit position by ΔX=0.1 in the simple case. K_L momenta are 5GeV/c, 10GeV/c, and 50GeV/c from the top. The left row shows background and the right row shows the signal. The detector was assumed to be made of 1mmPb/ 5mmScint calorimeter. 57
4.3 The background level after smearing gamma's hit positions in the simple case is shown as a function of P_{K_L}. The detector was assumed to be made of 1mmPb/ 5mmScint calorimeter. 57
4.4 The background level after smearing gamma energies in the simple case is shown as a function of P_{K_L}. The detector was assumed to be made of 1mmPb/ 5mmScint calorimeter. 58

4.5 P_t distributions after using a finite detector length of L=1000 in the simple case. K_L momentums are 5GeV/c, 10GeV/c, and 50GeV/c from the top. The left row shows background and the right row shows the signal. The detector was assumed to be made of 1mmPb/ 5mmScint calorimeter. 58
4.6 The background level after using finite detector in the simple case is shown as a function of P_{K_L}. The detector was assumed to be made of 1mmPb/ 5mmScint calorimeter. . . . 59
4.7 The background level for a detector with finite resolutions and length is shown as a function of P_{K_L}. The used conditions are ΔX=0.01, $\Delta E/E = 1\%/\sqrt{E(GeV)}$, and L=P_{K_L}/10MeV/c. The detector was assumed to be made of 1mmPb/ 5mmScint calorimeter. 59
4.8 Schematic geometry for measuring the direction of gamma. We assumed to measure the direction of gammas by converting gamma to two electrons and measuring the direction of the electron track 60
4.9 Two gammas mass distribution after smearing gammas direction by b=5 for $K_L \to \pi^0\nu\bar{\nu}$ in the case vertex is known. K_L momenta are 500MeV/c, 1GeV/c, 5GeV/c, 10GeV/c, and 50GeV/c. The detector is assumed to be made of 1mmPb/ 5mmScint calorimeter. . 63
4.10 P_t distribution after smearing gammas direction by b=5 for $K_L \to \pi^0\pi^0$ in the case where vertex is known. K_L momenta are 500MeV/c, 1GeV/c, 5GeV/c, 10GeV/c, and 50GeV/c. The detector is assumed to be made of 1mmPb/ 5mmScint calorimeter. 64
4.11 The background level after smearing gammas direction in case where vertex is known. The detector was assumed to be made of 1mmPb/ 5mmScint calorimeter. The background level for 1GeV/c on b=5 does not exist, because $\Delta\eta/\eta$=10% was not achieved with any cuts. 64
4.12 The background level after smearing gammas energy in the case where vertex is known. The detector was assumed to be made of 1mmPb/ 5mmScint calorimeter. 65
4.13 The background level after using finite length detector in case where vertex is known. The detector was assumed to be made of 1mmPb/ 5mmScint calorimeter. 65
4.14 The background level for a realistic model in the case where vertex is known. The conditions are $\Delta E/E = 1\%/\sqrt{E(GeV)}$, $\Delta\theta = 1/E(MeV)$, and L=E_{K_L}/10MeV. The detector was assumed to be made of 1mmPb/ 5mmScint calorimeter. 66
4.15 Missing mass VS. $E_{\gamma\gamma}$ for the K_L momentum of 500MeV/c, 1GeV/c, and 5GeV/c in the case where E_{K_L} is known. The 1mmPb/5mmScint sampling calorimeter was used as the photon counter. We smeared the K_L energy by 1% in sigma. The left row shows the distribution for the background, and the center row shows the distribution for the signal. The right row shows the signal region selected by the method described in the text. . . 70
4.16 Missing mass VS. $E_{\gamma\gamma}$ for the K_L momentum of 10GeV/c, and 50GeV/c in the case where E_{K_L} is known. The 1mmPb/5mmScint sampling calorimeter was used as the photon counter. We smeared the K_L energy by 1% in sigma. The left row shows the distribution for the background, and the center row shows the distribution for the signal. The right row shows the signal region selected by the method described in the text. . . 71
4.17 Background level after smearing the K_L energy with $\Delta E_{K_L}/E_{K_L}$ = 1% and 10% in the case where E_{K_L} is known. The 1mmPb/5mmScint sampling calorimeter was used as the photon counter. 72
4.18 Background level after smearing gammas energy with a=1% and 10% in the case where E_{K_L} is known. The 1mmPb/5mmScint sampling calorimeter was used as the photon counter. The background level at 500MeV for a=0.1 does not exist, because $\Delta\eta/\eta$ can not reach 10% with any cut region. 72

4.19 Background level after smearing gammas position with ΔX=0.01 and 0.1 in the case where E_{K_L} are known. The 1mmPb/5mmScint sampling calorimeter was used as the photon counter. 73
4.20 Background level for a detector with a finite length(L =100 and 1000) in the case where E_{K_L} is known. The 1mmPb/5mmScint sampling calorimeter was used as the photon counter. The background level at 10GeV/c and 50GeV/c in L=100 are absent, because most of gammas escape the detector. 73
4.21 Background level for a realistic detector with a finite length and finite resolutions in the case where K_L energy are known. The conditions are $\Delta E_{K_L}/E_{K_L}$=5%, a=0.01, ΔX=0.01, and L=P_{K_L}/10MeV/c. The 1mmPb/5mmScint sampling calorimeter was used as the photon counter. 74
4.22 Missing mass VS. $E_{\gamma\gamma}$ for the K_L momentum of 500MeV/c, 1GeV/c, and 5GeV/c in the case where vertex and E_{K_L} are known. The 1mmPb/5mmScint sampling calorimeter was used as the photon counter. We smeared the K_L energy by 1% in sigma. The left row shows the distribution for the background, and the center row shows the distribution for the signal. The right row shows the signal region selected by the method described in the text. 78
4.23 Missing mass VS. $E_{\gamma\gamma}$ for the K_L momentum of 10GeV/c, and 50GeV/c in the case where vertex and E_{K_L} are known. The 1mmPb/5mmScint sampling calorimeter was used as the photon counter. We smeared the K_L energy by 1% in sigma. The left row shows the distribution for the background, and the center row shows the distribution for the signal. The right row shows the signal region selected by the method described in the text. . . 79
4.24 Background level after smearing the K_L energy with $\Delta E_{K_L}/E_{K_L}$ = 1% and 10% in the case where vertex and E_{K_L} are known. The 1mmPb/5mmScint sampling calorimeter was used as the photon counter. 80
4.25 Background level after smearing gammas energy with a=1% and 10% in the case where vertex and E_{K_L} are known. The 1mmPb/5mmScint sampling calorimeter was used as the photon counter. The background level at 500MeV for a=0.1 does not exist, because $\Delta\eta/\eta$ can not reach 10% with any cut region. 80
4.26 Background level after smearing gammas direction with b=1 and 5 in the case where vertex and E_{K_L} are known. The 1mmPb/5mmScint sampling calorimeter was used as the photon counter. 81
4.27 Background level for a detector with a finite length in the case where vertex and E_{K_L} are known. The 1mmPb/5mmScint sampling calorimeter was used as the photon counter. The background level at 50GeV in L=50 and L=100 are absent, because most of gammas escape the detector. 81
4.28 Background level for a realistic detector with a finite length and finite resolutions in the case where vertex and K_L energy are known. The conditions are $\Delta E_{K_L}/E_{K_L}$=5%, a=0.01, b=1, and L=P_{K_L}/10MeV. The 1mmPb/5mmScint sampling calorimeter was used as the photon counter. 82

I.1 Photon detection inefficiency for CsI photon counter as a function of gamma's energy, measured by ES171 [14]. The cross correspond to the data, and the solid line is the inefficiency which KAMI experiment required in EOI. 86
I.2 The background level for a realistic model in the simple case is shown. The solid line and the dashed line show the background level using CsI photon counter and 1mmPb/5mmScint sampling detector, respectively. 88
I.3 The background level for a realistic model in the case where vertex is known is shown. The solid line and the dashed line show the background level using CsI photon counter and 1mmPb/5mmScint sampling detector, respectively. 88

I.4 The background level for a realistic model in the case where K_L energy is known is shown. The solid line and the dashed line show the background level using CsI photon counter and 1mmPb/5mmScint sampling detector, respectively. 89

I.5 The background level for a realistic model in the case where vertex and K_L energy are known is shown. The solid line and the dashed line show the background level using CsI photon counter and 1mmPb/5mmScint sampling detector, respectively. 89

II.1 Distribution of reconstructed vertex position before cuts for a detector with finite resolutions and length. The real vertex position is zero. 91

III.1 The K_L momentum(GeV/c) distribution, measured in KAMI beam test. The dots and histogram correspond to the data and MC, respectively. 93

III.2 The background level as a function of the peak K_L momentum(P_{peak}) for the simple case. The solid line and dashed line show the case where realistic K_L momentum and a monochromatic K_L momentum are used, respectively. 95

III.3 The background level as a function of the peak K_L momentum(P_{peak}) for the case where vertex is known. The solid line and dashed line show the case where the realistic K_L momentum and a monochromatic K_L momentum are used, respectively. 95

III.4 M_{miss} VS. $E_{\gamma\gamma}$ for P_{peak} of 5GeV/c, 10GeV/c, and 50GeV/c in the simple case. The E_{K_L} which is necessary to calculate M_{miss} is assumed to be the K_L momentum at the peak of the distribution. The 1mmPb/5mmScint sampling calorimeter was used as the photon counter. The left row shows the distribution for the background, and the center row shows the distribution for the signal. The right row shows the signal region selected by the method described in Section3.4.2. 96

III.5 The background level as a function of P_{peak} for the simple case. The dotted line shows the case where transverse momentum cut is used and the lead/scint is used as detector. The solid line and dashed line show the cases where E_{K_L} VS. M_{miss} cut is used instead of transverse momentum cut, and for solid line the lead/scint is used as detector and for dashed line the CsI is used as detector. 97

III.6 The background level as a function of P_{peak} for the case where vertex is known. The dotted line shows the case where only $M_{\gamma\gamma}$ cut is used and the lead/scint is used as detector. The solid line and dashed line show the cases where E_{K_L} VS. M_{miss} cut is used in addition to $M_{\gamma\gamma}$ cut, and for solid line the lead/scint is used as detector and for dashed line the CsI is used as detector. 97

IV.1 Total detection inefficiency as a function of the photon energy for 1mmPb/5mmScint sampling calorimeters. The upper(lower) figure shows the inefficiency whose threshold is 1MeV(5MeV). The dashed line and dotted line show the inefficiency due to the photonuclear interaction and the sum of sampling effect and punch through, respectively. Above 1GeV, the inefficiency required by KAMI is used. 99

IV.2 The background level as a function of K_L momentum for simple case. The solid line shows the inefficiency using threshold of 10MeV, which was used in previous chapters. The dashed and dotted lines show the background levels using the threshold of 5MeV and 1MeV, respectively. The 1mm Pb/5mm Scint detector is used as photon counter. . 100

A.1 Total photon absorption cross section for lead 102

B.1 (a)transverse momentum for K_L momentum of 10GeV/c in 1mmPb/5mmScint detector. (b)Relation between P_t and energy of two missing gammas,$E_{miss\gamma\gamma}$ for even pair background. 104

D.1 Distribution of energies of two missing gammas. (a)even pair background from 500MeV/c K_L (b)odd pair background from 1GeV/c K_L (c)even pair background from 5GeV/c K_L (d)odd pair background from 50GeV/c K_L. The area below the solid line is forbidden for even pair background. The detector is assumed to be made of 1mmPb/5mmScint calorimeter. 108

List of Tables

2.1 Parameters of lead/scintillator sandwich detector used in EGS simulation 22

3.1 Acceptance after transverse momentum cut in the simple case. In the left(right) table, 1mmPb/5mmScint. (0.5mmPb/5mmScint.) detector was used. 32
3.2 Acceptance after the π^0 mass cut and the P_t cut for the case where decay vertex is known. In the left(right) table, 1mmPb/5mmScint.(0.5mmPb/5mmScint.) detector was used. . 37
3.3 Acceptance after the missing mass cut and the missing mass VS. $E_{\gamma\gamma}$ cut in the case where we know E_{K_L}. In the left(right) table, 1mmPb/5mmScint(0.5mmPb/5mmScint) detector was used. 41
3.4 Acceptance after the two gamma's mass cut, the missing mass cut, and the missing mass VS. $E_{\gamma\gamma}$ cut in the case where decay vertex and E_{K_L} are known. In the left(right) table, 1mmPb/5mmScint.(0.5mmPb/5mmScint.) detector was used. 46

4.1 Acceptance for the signal and background using a finite length detector in the simple case. The upper on left, lower on left, and right tables show the acceptances for K_L momentum of 5GeV/c, 10GeV/c, and 50GeV/c, respectively. The detector was assumed to be made of 1mmPb/ 5mmScint calorimeter. 55
4.2 Acceptances for the signal and background for the ideal and a realistic model in simple case. The realistic model uses a detector with $L = P_{K_L}/10MeV/c$, $\Delta X = 0.01$, and $\Delta E/E = 1\%/\sqrt{E(GeV)}$. The detector was assumed to be made of 1mmPb/ 5mmScint calorimeter. 56
4.3 Acceptance for signal and background using a finite length detector in the case where vertex is known. We used K_L momentum of 500MeV/c, 1GeV/c, 5GeV/c, 10GeV/c, and 50GeV/c, respectively. The detector was assumed to be made of 1mmPb/ 5mmScint calorimeter. 62
4.4 Acceptance for the signal and background for the ideal and realistic models in the case where vertex is known. The realistic model uses a detector with $L = P_{K_L}/10MeV/c$, $\Delta\theta = 1/E(MeV)$, and $\Delta E/E = 1\%/\sqrt{E(GeV)}$. We studied K_L momentum of 5GeV/c, 10GeV/c, and 50GeV/c. The detector was assumed to be made of 1mmPb/ 5mmScint calorimeter. 62
4.5 Acceptance for the signal and background using a finite length detector in the case where E_{K_L} are known. The 1mmPb/5mmScint sampling calorimeter was used as the photon counter. 68
4.6 Acceptance for the signal and background for the ideal and realistic models in the case where K_L energy are known. The realistic model uses a detector with $L = P_{K_L}/10MeV/c$, $\Delta E_{K_L}/E_{K_L} = 0.05$, $\Delta X = 0.01$, and $\Delta E/E = 1\%/\sqrt{1E(GeV)}$. The detector was assumed to be made of 1mmPb/ 5mmScint calorimeter. 69

4.7 Acceptance for the signal and background using a finite length detector in the case where vertex and E_{K_L} are known. The 1mmPb/5mmScint sampling calorimeter was used as the photon counter. 76
4.8 Acceptance for the signal and background for the ideal and realistic models in the case where vertex and K_L energy are known. The realistic model uses a detector with $L = P_{K_L}/10MeV/c$, $\Delta E_{K_L}/E_{K_L} = 0.05$, $\Delta\theta = 1/E(MeV)$, and $\Delta E/E = 1\%/\sqrt{1E(GeV)}$. We studied K_L momentum of 500MeV/c, 1GeV/c, 5GeV/c, 10GeV/c, and 50GeV/c. The detector was assumed to be made of 1mmPb/ 5mmScint calorimeter. 77

III.1 Acceptance for the simple case and the case where vertex is known with a realistic K_L momentum. For the simple case, $E_{\gamma\gamma}$ VS. M_{miss} cut is used to rejected backgrounds, and for the case where vertex is known, $M_{\gamma\gamma}$ cut and $E_{\gamma\gamma}$ VS. M_{miss} cut are used. The 1mmPb/5mmScint calorimeter was used as photon counter. 94

Chapter 1

Introduction

The existence of symmetry principles in physics had been speculated as a manifestation of underlying beauty of order of the universe. From Newtonian mechanics to quantum mechanics, symmetry principles, connected with conservation laws, have provided us economical but elegant ways of looking at the nature. The law of right-left symmetry, associated with parity conservation, and invariance in charge conjugation operation, the two discrete symmetry laws which gained importance in quantum mechanics, had also been assumed to hold in subatomic world of physics. In this context, the breakdown of the combination of charge and parity symmetry in kaon decay, following parity violation discovered in weak interactions, had given us great impact on our view of the nature. At the same time, however, the discovery opened our eyes toward a new framework of physics. Afterwards, efforts have been paid to establish a model which incorporates the CP violation.

After about three decades since the CP breaking observation, so called the Standard Model has become believed to be the most probable candidate for the full description of elementary particle physics. Recent attention has been focused upon the complete determination of the parameters introduced in this scheme. In this respect, the rare kaon decay, $K_L \to \pi^0 \nu\bar{\nu}$, has gained a key role for the determination of the parameters. We will observe the underlying physics and the purpose and overview of this study in this chapter.

1.1 Physics Interest in $K_L \to \pi^0 \nu\bar{\nu}$

1.1.1 CP Violation

The combination of charge conjugation and parity transformation changes K^0 into $\bar{K^0}$, and vice versa:

$$CP|K^0\rangle = |\bar{K^0}\rangle \,, \tag{1.1}$$

$$CP|\bar{K^0}\rangle = |K^0\rangle \,. \tag{1.2}$$

(We use a conventional phase definition, and currently neglect the small effect of CP violation.)

The eigenvalues and eigenstates of CP are described as:

$$|K_1\rangle = \frac{1}{\sqrt{2}}\left[|K^0\rangle + |\bar{K^0}\rangle\right] \qquad (CP = +1)\,, \tag{1.3}$$

$$|K_2\rangle = \frac{1}{\sqrt{2}}\left[|K^0\rangle - |\bar{K^0}\rangle\right] \qquad (CP = -1)\,. \tag{1.4}$$

K_2 is the longer-lived kaons, whose lifetime is 5.2×10^{-8} seconds, and K_1 is the shorter-lived kaons, whose lifetime is 0.89×10^{-10} seconds. It had been believed from CP consistency that $|K_2\rangle$ decays to the three pions, which form a CP odd state, while $|K_1\rangle$ decays to two pions in a CP even state.

In 1964, Cronin and Fitch, *et al.*, observed that the longer-lived kaons decayed to two pions [1]. This suggests that CP odd long-lived kaons, K_L, decays into CP even mode, and CP is not conserved in this decay.

This phenomenon can be explained if K_L is actually composed not only of $|K_2\rangle$ but also with a slight mixture of $|K_1\rangle$:

$$|K_L\rangle = \frac{1}{\sqrt{1+\epsilon^2}}\left[|K_2\rangle + \epsilon|K_1\rangle\right] \ , \tag{1.5}$$

and K_1 decays to two pions. Such a mechanism for causing K_L to decay to two pions is called indirect CP violation. However, CP can be violated if K_2 in equation (1.5) decays to two π^0's. If K_2 directly decays to two pions, we can say that the CP is directly violated.

1.1.2 CKM parameter η

Currently, the powerful framework to explain CP violation is the Standard Model, which incorporates electromagnetic, weak, and strong interactions into a single scheme. It has a mechanism to introduce CP violation, including the direct CP violation.

In the Standard Model picture, direct CP violation is connected to the framework of quark mixing presented by Cabbibo, Koboyashi, and Maskawa [2]. In this theory, direct CP violation stems from the consequence of a three generation model.

The charged current in weak interaction can be written as:

$$J^\mu = \begin{pmatrix} \bar{u} & \bar{c} & \bar{t} \end{pmatrix} \frac{\gamma^\mu(1-\gamma^5)}{2} U \begin{pmatrix} d \\ s \\ b \end{pmatrix} . \tag{1.6}$$

The matrix U, introduced by Kobayashi and Maskawa, tells us the coupling of up and down type quarks:

$$U = \begin{pmatrix} V_{ud} & V_{us} & V_{ub} \\ V_{cd} & V_{cs} & V_{cb} \\ V_{td} & V_{ts} & V_{tb} \end{pmatrix} . \tag{1.7}$$

The 3×3 unitary matrix U can be represented by 4 parameters, with 5 arbitrary phases left aside. Of 4 parameters, 3 are real parameters and 1 is complex phase factor which accounts for the CP violation.

Wolfenstein parameterized the matrix components as follows [3]:

$$U = \begin{pmatrix} 1-\frac{\lambda^2}{2} & \lambda & A\lambda^3(\rho - i\eta) \\ -\lambda & 1-\frac{\lambda^2}{2} & A\lambda^2 \\ A\lambda^3(1-\rho-i\eta) & -A\lambda^2 & 1 \end{pmatrix} . \tag{1.8}$$

The η parameter accounts for the CP violation, and the determination of the η parameter is one of the primary goals of particle physics of today. As we will see, measurement of the branching ratio of rare CP violating decays can determine the value of η.

1.1.3 Decay of $K_L \to \pi^0\nu\bar{\nu}$

The observation of a rare decay $K_L \to \pi^0\nu\bar{\nu}$ is a good window to determine the η parameter. As shown in Fig. 1.1, this decay is governed by short-distance transition current and occurs almost entirely from the direct CP violation, as described below.

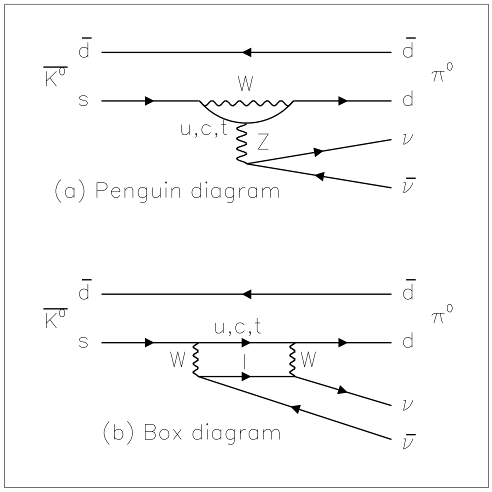

Figure 1.1: The Z penguin and W-box diagrams which contribute to the decay $K_L \to \pi^0 \nu \bar{\nu}$

The amplitude for $K_L \to \pi^0 \nu \bar{\nu}$ can be written as

$$A(K_L \to \pi^0 \nu \bar{\nu}) = \frac{1}{\sqrt{1+\epsilon^2}} \left[A(K_2 \to \pi^0 \nu \bar{\nu}) + \epsilon A(K_1 \to \pi^0 \nu \bar{\nu}) \right] , \tag{1.9}$$

or

$$A(K_L \to \pi^0 \nu \bar{\nu}) = \frac{1}{\sqrt{2(1+\epsilon^2)}} \left[(1+\epsilon) A(K^0 \to \pi^0 \nu \bar{\nu}) - (1-\epsilon) A(\bar{K^0} \to \pi^0 \nu \bar{\nu}) \right] , \tag{1.10}$$

using equations (1.3) and (1.4). Since top quark can be in medium state(Fig. 1.1), this decay involves to the V_{td} and V_{ts}. Using the Wolfenstein's parameterization (1.8),

$$A(K_L \to \pi^0 \nu \bar{\nu}) \propto V_{td}^* V_{ts} - V_{ts}^* V_{td} \sim 2i\eta \, . \tag{1.11}$$

Thus, we can see that the branching ratio of $K_L \to \pi^0 \nu \bar{\nu}$ is proportional to η^2, and determines the η parameter.

The branching ratio can be calculated [4, 5] as

$$BR(K_L \to \pi^0 \nu \bar{\nu}) = 1.94 \times 10^{-10} \eta^2 A^4 \chi^2(x) \tag{1.12}$$

where $x = m_t/m_W$, $\chi \sim x^{1.2}$, and A is a CKM parameter in Wolfenstien parameterization of equation (1.8). The theoretical estimate of this branching ratio is $\cong 3.0 \times 10^{-11}$ based on the current knowledge of CKM parameters [4, 5]. Due to the uncertainties on the CKM parameters, these predictions still contain an error of $\cong 2 \times 10^{-11}$. The best published limit to data for the $K_L \to \pi^0 \nu \bar{\nu}$ decay is 5.9×10^{-7} (90%CL) from E799-I at Fermi National Accelerator Laboratory (FNAL)[6]. The theoretical uncertainty on the relation between $BR(K_L \to \pi^0 \nu \bar{\nu})$ and η, that is uncertainty of $A^4\chi^2(x)$ in equation (1.12), has a magnitude of a few percent[4]. Therefore, by measuring the branching ratio of $K_L \to \pi^0 \nu \bar{\nu}$, we can directly determine CKM parameter η with a high accuracy.

1.2 Experimental Challenges for Detecting $K_L \to \pi^0\nu\bar{\nu}$

In this section, we will describe the experimental challenges for detecting $K_L \to \pi^0\nu\bar{\nu}$ and possible kinematic variables that we could use.

Since almost 99 % of π^0's decay into two γ's, the detection of $K_L \to \pi^0\nu\bar{\nu}$ means finding 2γ's originating from a π^0 decay. This raises some difficulties for observing $K_L \to \pi^0\nu\bar{\nu}$.

First difficulty is the measurement of the vertex position. With an orthodox photon detector which can only detect energy and position of gammas, we cannot measure the vertex position, because we do not know the direction of gamma. However, if we know the vertex position, we can reconstruct gamma's momentum and thus invariant mass of two gammas. With this mass distribution, some backgrounds can be rejected very effectively. Therefore we should find out whether we really need a detector which can measure direction of the gamma or not.[1]

Second difficulty is the existence of many difficult backgrounds sources. The decay modes which can be background are $K_L \to \pi^0\pi^0$, $K_L \to \pi^0\pi^0\pi^0$, $K_L \to \gamma\gamma$, $K_L \to \pi^0\gamma\gamma$, $\Lambda \to n\pi^0$, etc.. Of these backgrounds, the dominant and the most severe background is $K_L \to \pi^0\pi^0 \to 4\gamma$(BR=$9.36\times10^{-4}$) where two gammas were missed. There are following two cases for missing two gammas. One is that gamma miss photon counter, either by going between photon counters or going through a beam hole in a detector. Therefore, it is important to have a hermetic coverage around the decay region and minimize the beam hole size. Another reason is that photon counter misses detection although gamma hits the photon counter. This effect depends on the inefficiency of photon counter, and this inefficiency is very sensitive to energy of the gamma. Therefore, the energy of incident K_L is an important factor.

Moreover, there are two kinds of backgrounds from $K_L \to \pi^0\pi^0$; (a)even pair background which is caused by missing two gammas originating from the same pion, and (b)odd pair background caused by missing two photons from different pions(Fig 1.2). Of these backgrounds, even pair background has a similar property as signal because observed two gammas come from one pion. Therefore, the suppression of even pair background is more difficult than that of odd pair background. To suppress even pair background, we should measure all kinematics of this decay, so E_{K_L} is an important variable. Therefore, we should find out whether we should measure E_{K_L} or not.

Now, various experiments are approaching these problems with several different methods.

For example, BNL (Brookhaven National Laboratory) is proposing to completely measure the kinematics of the gammas including position, angle, energy, and the time of flight (TOF) of K_L to measure the K_L momentum, and reconstruct π^0 momentum in K_L center of mass system [8]. In order to measure the K_L momentum by TOF, they plan to use a K_L beam with low momentum around 700 MeV/c. Further, they are planing to use photon veto surrounding the decay region.

At FNAL, the KAMI (Kaons At the Main Injector) experiment is planning to use high intensity proton beam at 120 GeV to reduce the gammas missed by photon veto. [9] The typical momentum of K_L is 13 GeV/c.

At KEK (High Energy Accelerator Research Organization in Japan), E391 is planning to use typically 2 GeV/c K_L beam. This beam energy is selected to avoid the background due to hyperons which are potential problems at high K_L energy, but to keep the gammas energy high enough to achieve enough veto power. The detector is surrounded by a hermetic veto counter to reduce the $K_L \to \pi^0\pi^0$ background[7]. In future, this experiments will move to JHF(Japan Hadron Facility) and is planning to collect about one thousand $K_L \to \pi^0\nu\bar{\nu}$ events.

[1] The KTeV experiment at FNAL set an upper limit on branching ratio of less than 5.8×10^{-5} with the 90 % confidence level [6] by using $\pi \to e^+e^-\gamma$(Dalitz decay). This method has an advantage that one can detect the electron and positron tracks found by tracking chambers and use them to fully reconstruct the π^0 mass and decay vertex. However, the trade-off here is its small branching fraction (1.2 %) of the Dalitz decay and a low acceptance to collect low mass e^+e^- tracks. Currently, since the expected number of signal itself is small, this method is not useful to observe $K_L \to \pi^0\nu\bar{\nu}$.

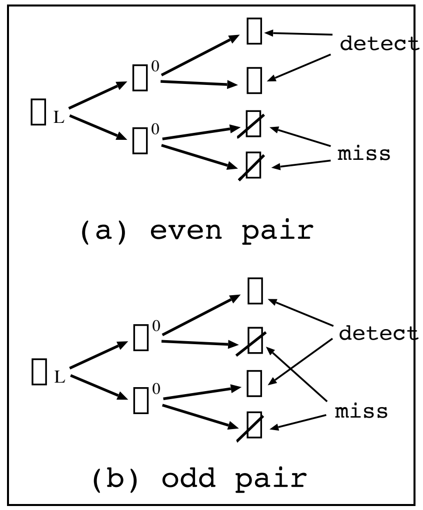

Figure 1.2: (a)even pair background is caused by missing two gamma from one pion, and (b)odd pair is caused by missing two gamma from different pions

1.3 Purpose and Overview

Now, as described above, several experiments using different methods are being planned, but we do not know which method is the best. In this thesis, we will go back to the basics and study the necessary conditions to detect the branching ratio of $K_L \to \pi^0 \nu \bar{\nu}$ and measure η parameter.

The goal of this study is to establish the necessary conditions for measuring η with a 10% error while keeping the number of background events below the number of signal events.

In order to achieve this goal, we ran simple Monte Carlo. For different E_{K_L}, we studied whether we need to measure K_L decay vertex, and E_{K_L}. We also studied required performance and geometry of the detector.

In this study, we considered only $K_L \to \pi^0 \pi^0$ as background, because this background is expected to be dominant and difficult to suppress.

In the next chapter, we will describe the inefficiency of photon counter which has very important role in this experiment. In Chapter 3, we assumed a perfect detector and studied the best limit on the background for different E_{K_L} and methods. In Chapter 4, we introduced detector resolution and geometry, and studied the required specification on the detector. In Chapter 5, we will examine the currently planned experiments based on the results obtained by this study, and give suggestions for further study. At last, in Chapter 6, we will give the conclusion of this study.

Chapter 2

Inefficiency of Photon Counter

As we described in the previous chapter, the major background to $K_L \to \pi^0 \nu \bar{\nu}$ is $K_L \to \pi^0 \pi^0$ decay where two gammas were not detected. It is therefore very important to have a good understanding of the inefficiency of photon counter. In this chapter, we will estimate the photon counter inefficiency.

In this study, we used the lead/scintillator sandwich sampling calorimeter as the photon counter. This is because this type is less expensive than fully active calorimeter such as CsI and has a good performance. For the sampling calorimeter, the dominant components of inefficiencies are due to photo-nuclear interaction, sampling effect and punch through. These effects will be explained in the following section in detail.

2.1 Photo-Nuclear Interaction

In this section, we will describe the detection inefficiency due to photo-nuclear interaction.

The photo-nuclear interaction is a reaction that an incident gamma is absorbed by the nucleus and this nucleus emits protons, neutrons, or photons. If the nucleus emits protons or high energy photon, it is easy to detect. On the other hand, if the nucleus emits only neutrons or low energy photons, it is difficult to detect, because neutrons have no charge and do not react by electro-magnetic interaction. In this case, the incident photon will not be detected.

This inefficiency was studied by ES171 experiment at KEK Tanashi [10]. In this experiment, two types of sampling calorimeters were tested. One was a sandwich of 1mm lead and 5mm scintillator, with a total thickness of 18.2 radiation length. We will call this detector '1mmPb/5mmScint' for short (Fig. 2.1(a)). The other was a 6.8 radiation lengths long sandwich of 0.5mm lead and 5mm scintillator, followed by 18.2 radiation lengths long 1mmPb/5mmScint to veto the punch through events. We will call the front detector '0.5mmPb/5mmScint' (Fig. 2.1(b)). Both detectors had a cross section of 15cm$\times$15cm. The energy threshold for both detectors was set to 10MeV.

Figure 2.2 shows the inefficiency of Pb/Scint calorimeter due to photo-nuclear interaction measured by ES171.

2.2 Sampling Effect and Punch Through

Besides the photo-nuclear interaction, there are two kinds of electro-magnetic interactions which causes inefficiency. They are sampling effect and punch through.

In the case of sampling calorimeters, if an incident photon deposits most of its energy into lead layers, and deposits energy below a detection threshold into the scintillator, the photon will not be detected. This is called sampling effect.

If a photon goes through the detector without reaction, the photon will not be detected. This is called punch through.

We estimated these inefficiencies using the EGS [1] Monte Carlo simulation.

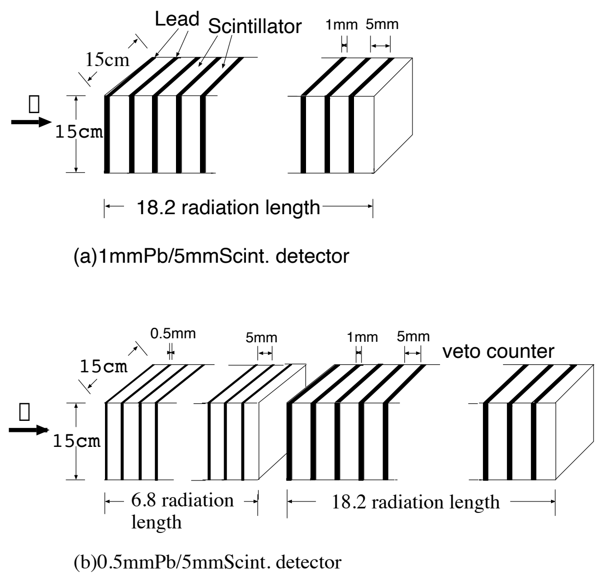

Figure 2.1: The detector geometry used in ES171 experiment. The detector(a) shows the 1mmPb/ 5mmScint calorimeter and the detector(b) shows the 0.5mm/ 5mmScint calorimeter and veto counter.

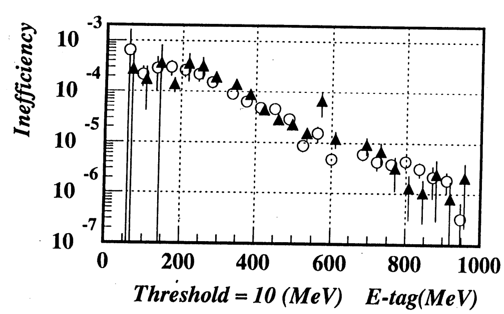

Figure 2.2: Photon detection inefficiency due to photo-nuclear interaction as a function of energy, measured by ES171 [10]. The open circles and the triangle show the inefficiency for 1mmPb/5mmScint calorimeter and 0.5mmPb/5mmScint calorimeter, respectively.

[1]Electron Gamma Shower

2.2.1 Geometry and Condition

In this simulation, to investigate the effect of sampling effect and punch through, lead/scintillator sandwich detectors with three different lead thicknesses(0.1mm, 0.5mm, and 1mm) were used. The parameters of these detectors are shown in Table 2.1

Detector	thickness of lead	thickness of scint.	number of Pb/Scint layer	radiation length
1mmPb/5mmScint	1mm	5mm	96pairs	18.2
0.5mmPb/5mmScint	0.5mm	5mm	187pairs	18.8
0.1mmPb/5mmScint	0.1mm	5mm	620pairs	18.3

Table 2.1: Parameters of lead/scintillator sandwich detector used in EGS simulation

In this simulation, the detectors were assumed to be infinitely wide, because in real experiment, a hermetic photon detector will be used. A schematic geometry of the detector is shown in Fig. 2.3.

Photons with a monochromatic energy was injected vertically to the plane.

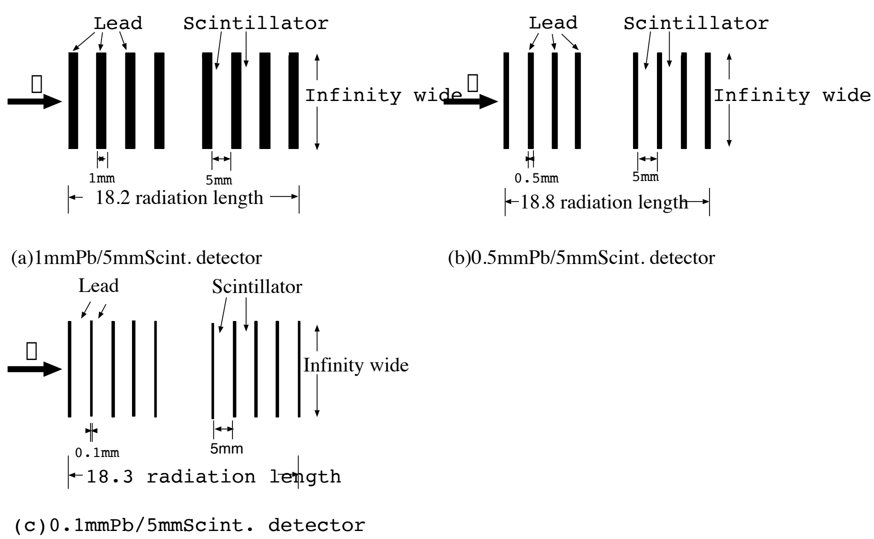

Figure 2.3: The detector geometry used in EGS simulation. The detector(a) shows 1mmPb/5mmScint calorimeter, the detector(b) shows the 0.5mm/5mmScint calorimeter and the detector(c) shows the 0.1mm/5mmScint calorimeter.

2.2.2 Calibration

The observable in these sampling detectors is the energy deposit in scintillator, but what we really want is the incident energy of gamma. Therefore in this section, we will estimate the relation between incident photon energy and the energy deposit in scintillator.

Figures 2.4, 2.5, and 2.6 show the energy deposit in the scintillator in 1mmPb/5mmScint, 0.5mmPb/5mmScint, and 0.1mmPb/5mmScint detector, respectively for several different gammas energy. These distributions were fitted for a Gaussian to obtain the mean energy deposit for each incident energy. Figure 2.7 shows the mean energy deposit as a function of incident energy. The correlation is given by

$$E_{dep} = 0.3381E_{inc} - 0.1491MeV \qquad for\ 1mmPb/5mmScint. \tag{2.1}$$
$$E_{dep} = 0.5141E_{inc} - 0.1309MeV \qquad for\ 0.5mmPb/5mmScint. \tag{2.2}$$
$$E_{dep} = 0.8475E_{inc} - 0.1138MeV \qquad for\ 0.1mmPb/5mmScint. \tag{2.3}$$

where E_{dep} is the energy deposit in the scintillator, and E_{inc} is the incident energy.

2.2.3 Inefficiency due to Sampling Effect and Punch Through

In this section, we will estimate the inefficiency due to sampling effect and punch through. The inefficiency is defined as the probability of having the observed energy deposit below a given threshold. To compare our results with ES171 results, the threshold was set to 10MeV in incident gammas energy. Based on Equations (2.1), (2.2), and (2.3), this threshold corresponds to 3.25MeV, 5.02MeV, and 8.38MeV for 1mmPb/5mmScint, 0.5mmPb/5mmScint, and 0.1mmPb/5mmScint, respectively.

Strictly speaking, a threshold is decided by the number of photo-electrons, but not gamma's energy. Therefore the gamma energy corresponding to the threshold is smeared by a statistical fluctuation of the number photo-electrons. However, the threshold of 10 MeV corresponds to about 20 photo-electrons, and the statistical effect on the gammas energy is about $10/\sqrt{20}$MeV($\cong$ 2.2MeV). This has little influence on the results (see Fig.2.8, 2.9, and 2.10), so it appropriates to use deposit energy to decide the threshold.

In Figures 2.8, 2.9, and 2.10, the distribution of energy deposit in the scintillator is shown for three sampling calorimeters. The shadowed area contributes to the inefficiency. The peak at 0MeV has two components; the dominant component is punch through, and another component is due to a backward scattering of the incident photon in the first lead layer. These are described in Appendix A.

Figure 2.11 shows the inefficiency due to the sampling effect and punch through for 1mmPb/5mmSinti, 0.5mmPb/5mmSinti, and 0.1mmPb/5mmSinti calorimeters. As shown in this figure, the inefficiency is higher for low energy gammas and for the calorimeter with thicker lead, and as the energy grow up, this effect reduces rapidly.

2.2.4 Inefficiency of the Photon Counter

The total inefficiency of photon counter is the sum of inefficiencies due to photo-nuclear interaction(Fig. 2.2), sampling effect, and punch through(Fig. 2.11). Since ES171 experiment has no data above 1GeV, we will assume the inefficiency that KAMI requires for this region [9].

As a result, figure 2.12 show the detection inefficiency of (a)1mmPb/ 5mmSinti and (b)0.5mmPb/ 5mmSinti calorimeter, respectively.

In the following studies, we will assume that photon counters have the inefficiency shown in Figure 2.12.

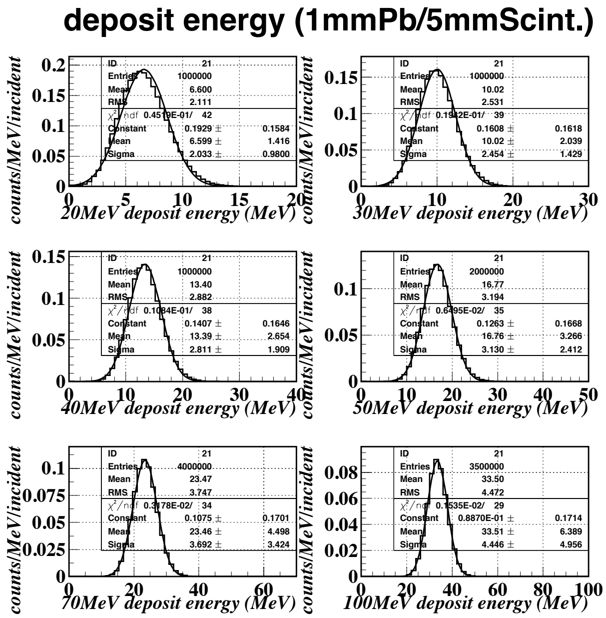

Figure 2.4: Distribution of energy deposit in the scintillator in 1mmPb/ 5mmScint detector for the incident gamma energy of 20, 30, 40, 50, 70, and 100MeV. The distributions are fitted for a Gaussian.

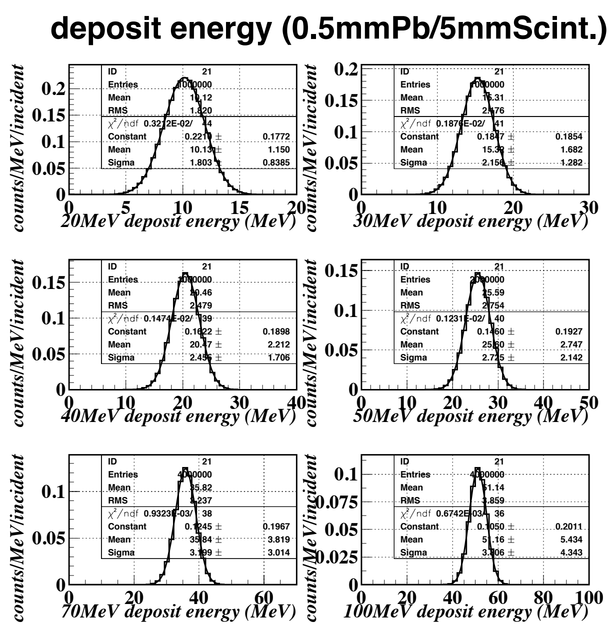

Figure 2.5: Distribution of energy deposit in the scintillator in 0.5mmPb/ 5mmScint detector for the incident gamma energy of 20, 30, 40, 50, 70, and 100MeV. The distributions are fitted for a Gaussian.

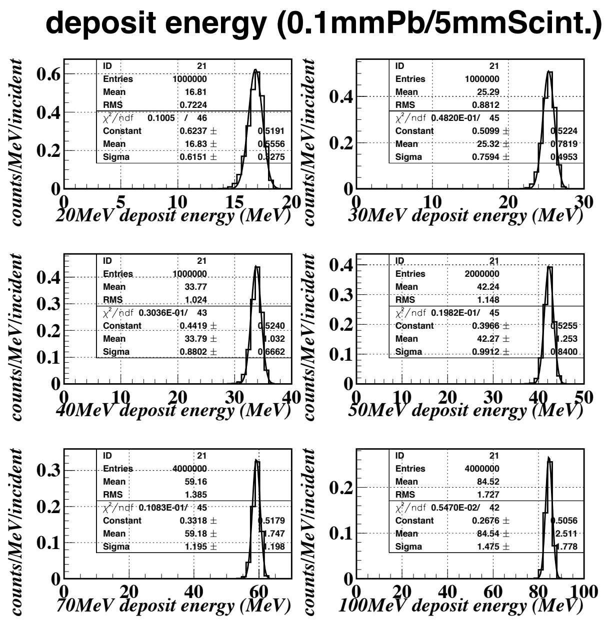

Figure 2.6: Distribution of energy deposit in the scintillator in 0.1mmPb/ 5mmScint detector for the incident gamma energy of 20, 30, 40, 50, 70, and 100MeV. The distributions are fitted for a Gaussian.

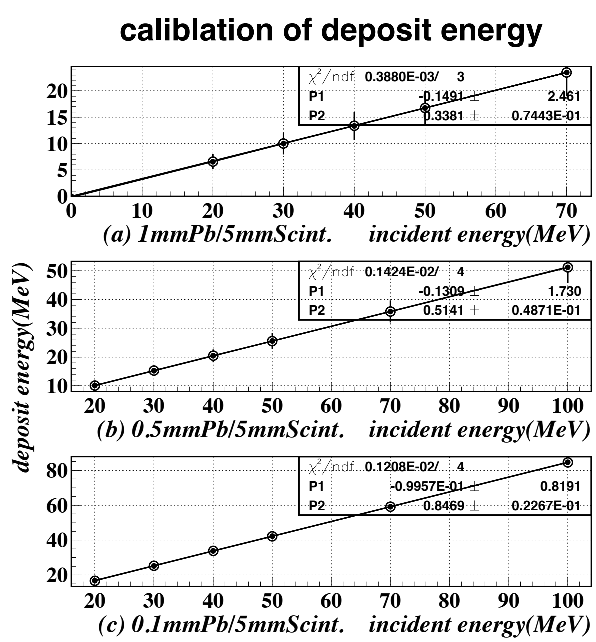

Figure 2.7: Incident energy VS. deposit energy in scintillator for (a)1mmPb/ 5mmScint, (b)0.5mm/ 5mmScint, and (c)0.1mm/ 5mmScint

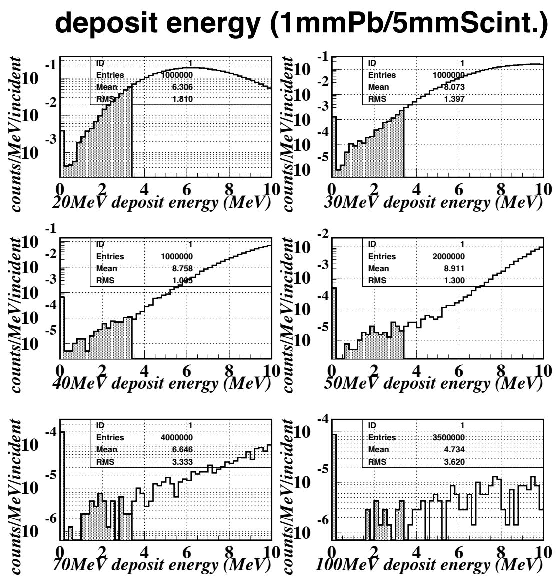

Figure 2.8: Distribution of energy deposit in the scintillator of 1mmPb/ 5mmScint detector for the incident energy of 20MeV, 30MeV, 40MeV, 50MeV, 70MeV, and 100MeV. The shadowed area below the threshold of 3.25MeV, which corresponds to 10MeV gamma, contributes to inefficiency.

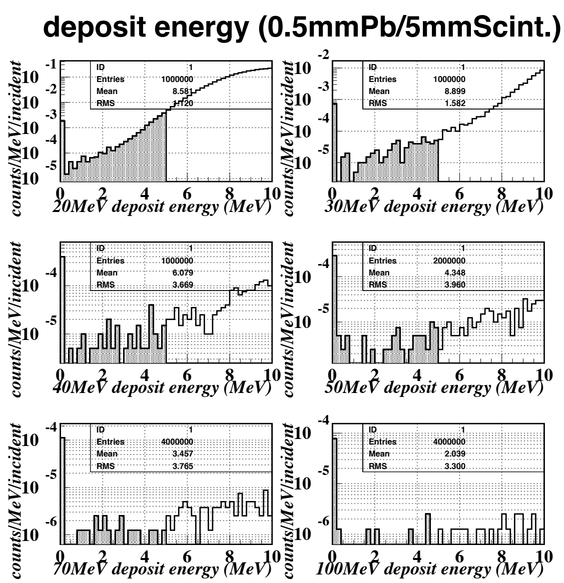

Figure 2.9: Distribution of energy deposit in the scintillator of 0.5mmPb/ 5mmScint detector for the incident energy of 20MeV, 30MeV, 40MeV, 50MeV, 70MeV, and 100MeV. The shadowed area below the threshold of 5.02MeV, which corresponds to 10MeV gamma, contributes to inefficiency.

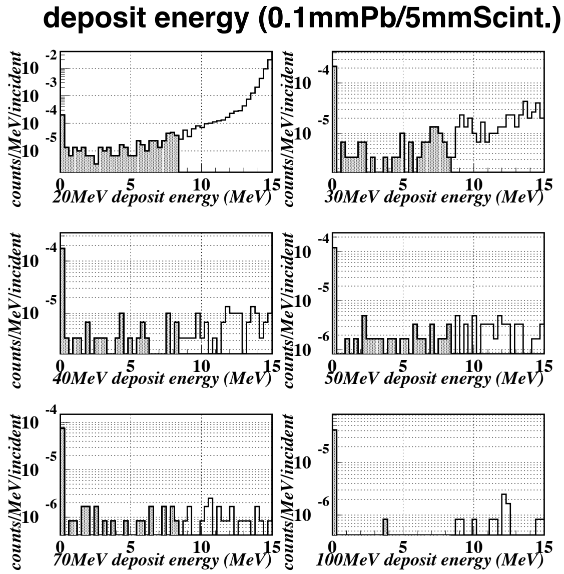

Figure 2.10: Distribution of energy deposit in the scintillator of 0.1mmPb/ 5mmScint detector for the incident energy of 20MeV, 30MeV, 40MeV, 50MeV, 70MeV, and 100MeV. The shadowed area below the threshold of 8.38MeV, which corresponds to 10MeV gamma, contributes to inefficiency.

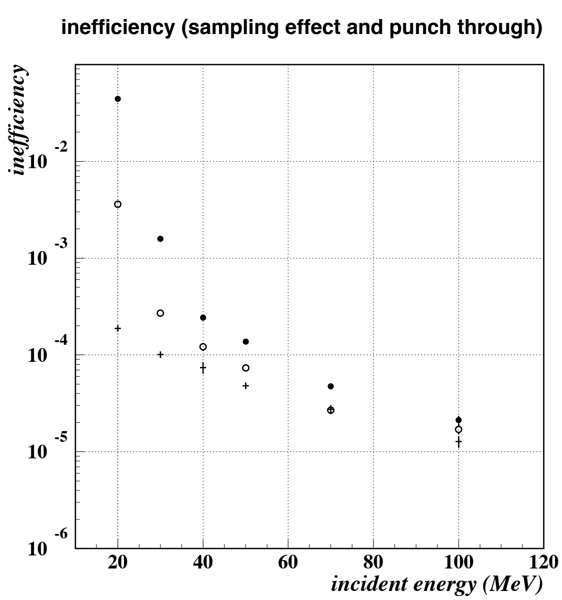

Figure 2.11: Photon detection inefficiency due to the sampling effect and punch through as a function of incident energy of gamma. The open circles, the dot points, and the cross points show the 1mmPb/ 5mmScint, 0.5mmPb/ 5mmScint, and 0.1mmPb/ 5mmScint detector, respectively.

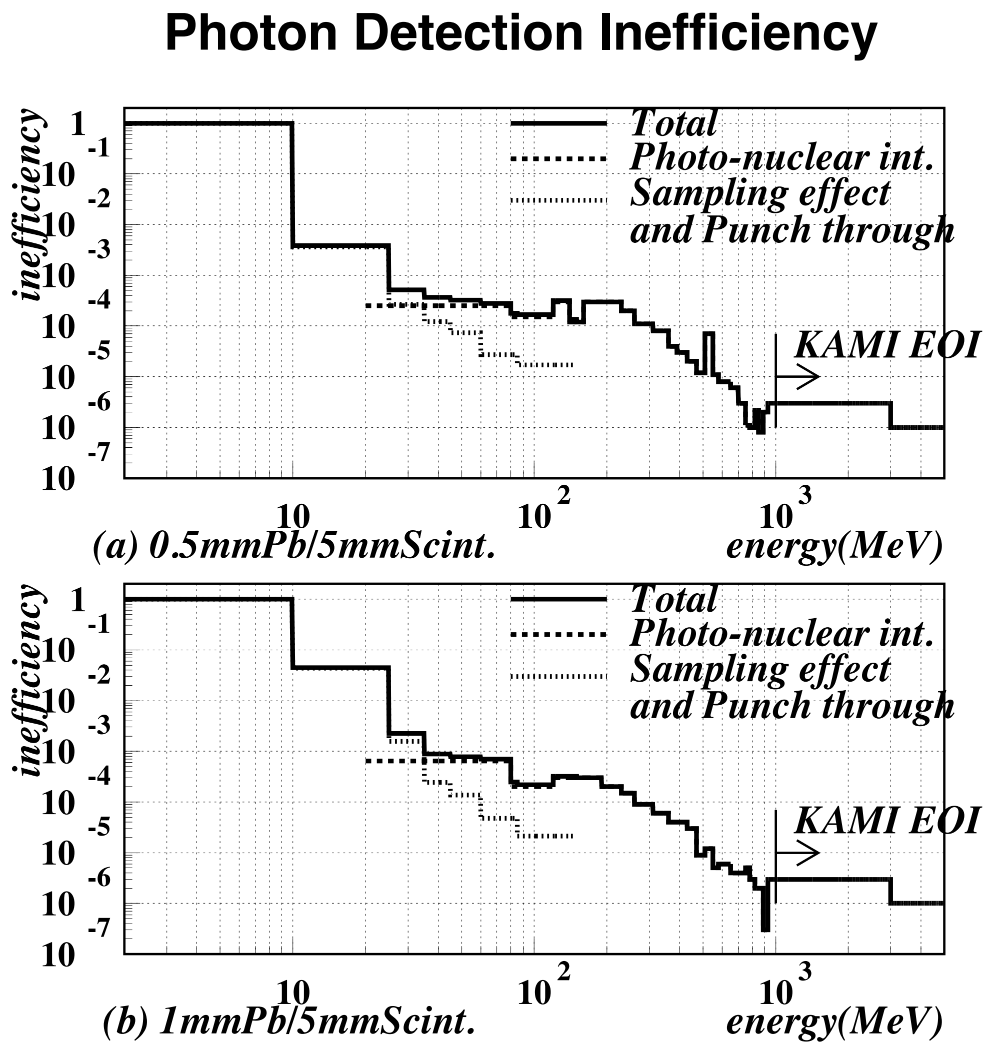

Figure 2.12: Total detection inefficiency as a function of the photon energy for (a)1mmPb/5mmScint and (b)0.5mmPb/5mmScint sampling calorimeters. The dashed line and dotted line show the inefficiency due to the photo-nuclear interaction and the sum of sampling effect and punch through, respectively. Above 1GeV, the inefficiency required by KAMI is used.

Chapter 3

Simulation using Ideal Model

To satisfy the purpose described in the introduction, we studied the best way to suppress background event ($K_L \to \pi^0\pi^0 \to \gamma\gamma$) from signal event ($K_L \to \pi^0\nu\bar{\nu} \to \gamma\gamma$) and the level of background in $K_L \to \pi^0\nu\bar{\nu}$. For this study, we generated $K_L \to \pi^0\nu\bar{\nu}$ events and $K_L \to \pi^0\pi^0$ events with Monte Carlo simulation. In this chapter and the next chapter, we will describe the results of this simulation.

In this chapter, we will describe the results of the study in an ideal condition where the detector covers all the solid angle (4π detector) and has perfect energy and position resolutions. There are two reasons why we studied this ideal model; one is to understand the feature of $K_L \to \pi^0\nu\bar{\nu}$ and $K_L \to \pi^0\pi^0$, and the second is to know the ultimate limit of background suppression.

3.1 Condition and Geometry

In this section, we will explain the condition of this ideal model in detail.

We generated events in the following way. At first, K_L beam with a monochromatic energy and an infinitely small beam size came along the Z axis. All the K_L's decayed at Z=0 to $\pi^0\nu\bar{\nu}$ or $\pi^0\pi^0$, which decayed immediately to photons. The photons were detected by an infinitely long cylindrical detector surrounding the Z axis. The detector was made of lead/scintillator sandwich, and assumed to have the inefficiency described in Chapter2. The detector measured the energy and position of photons with a perfect resolution. The detector design is shown in Fig. 3.1.

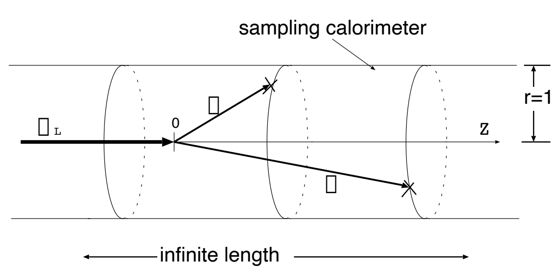

Figure 3.1: The detection geometry used in simulation

In this simulation, to take the effect of the photon counter into account, we assigned the weight to each events which is the probability for observing the event. For $K_L \to \pi^0\nu\bar{\nu}$, by using photon detection inefficiency $\bar{\epsilon}(E)$(Fig.2.12) which depended on gammas energy E, weight is expressed simply as

$$weight = (1 - \bar{\epsilon}(E_1))(1 - \bar{\epsilon}(E_2)), \tag{3.1}$$

where E_1 and E_2 are energies of two gammas. Since inefficiency is far smaller than '1', this weight is almost '1'. On the other hand, for $K_L \to \pi^0\pi^0$, we considered all combinations of choosing two detected gammas from four gammas. For each combination, we assigned a weight as shown in following table.

detected gammas energy	missing gammas energy	weight
E_1, E_2	E_3, E_4	$(1 - \bar{\epsilon}(E_1))(1 - \bar{\epsilon}(E_2))\bar{\epsilon}(E_3)\bar{\epsilon}(E_4)$
E_1, E_3	E_2, E_4	$(1 - \bar{\epsilon}(E_1))(1 - \bar{\epsilon}(E_3))\bar{\epsilon}(E_2)\bar{\epsilon}(E_4)$
E_1, E_4	E_2, E_3	$(1 - \bar{\epsilon}(E_1))(1 - \bar{\epsilon}(E_4))\bar{\epsilon}(E_2)\bar{\epsilon}(E_3)$
E_2, E_3	E_1, E_4	$(1 - \bar{\epsilon}(E_2))(1 - \bar{\epsilon}(E_3))\bar{\epsilon}(E_1)\bar{\epsilon}(E_4)$
E_2, E_4	E_1, E_3	$(1 - \bar{\epsilon}(E_2))(1 - \bar{\epsilon}(E_4))\bar{\epsilon}(E_1)\bar{\epsilon}(E_3)$
E_3, E_4	E_1, E_2	$(1 - \bar{\epsilon}(E_3))(1 - \bar{\epsilon}(E_4))\bar{\epsilon}(E_1)\bar{\epsilon}(E_2)$

The sum of these six weights was used as the weight for the event. [1] Since inefficiency is very small, these weights are far smaller than '1'. The acceptance is calculated by dividing the sum of weight by the number of events.

We ran simulations at five different K_L momenta, 500MeV/c, 1GeV/c, 5GeV/c, 10GeV/c, and 50GeV/c. The number of generated signal events was 10^7 $K_L \to \pi^0\pi^0$ for each K_L momentum. The number of generated background $K_L \to \pi^0\pi^0$ events are shown below.

P_{K_L}	500MeV/c	1GeV/c	5GeV/c	10GeV/c	50GeV/c
number of events	$\cong 4 \times 10^7$	$\cong 1.6 \times 10^8$	$\cong 1.1 \times 10^9$	$\cong 3.3 \times 10^9$	$\cong 7.4 \times 10^9$

Higher statistics was required for higher P_{K_L}, because the event weights from high P_{K_L} varied in many orders of magnitude due to a wider gamma energy range.

Besides the conditions described above, we considered the following four cases.

- [**Simple Case**] In this case, the sampling calorimeter is assumed to measure only the gammas energy and hit position in the calorimeter.
- [**A case where vertex is known**] In this case, we assumed that we know K_L decay vertex position in addition to the energy and position of gammas.
- [**A case where E_{K_L} is known**] In this case, we assumed that we know the energy of K_L in addition to the energy and position of gammas.
- [**A case where vertex and E_{K_L} are known**] In this case, we assumed that we know the K_L decay vertex position and the energy of K_L in addition to the energy and position of gammas.

In following, we will describe these four cases.

[1] Actually in this simulation, we treated each combinations as a separate event.

3.2 Simple Case

In this section, we will consider a simple case where we only use the gamma's energy and hit position in the calorimeter. This is a very orthodox case, and this detector can be made by using the existing technology.

3.2.1 Transverse momentum Cut

In the simple case, the effective way to suppress the $K_L \to \pi^0\pi^0$ background is to cut on the transverse momentum of π^0. In this subsection, we will explain the method to reconstruct the transverse momentum and show the transverse momentum distribution.

First, in order to calculate the decay vertex position, we assumed that two detected gammas came from one π^0. We can then calculate the angle between the two gammas, θ, by

$$cos\theta = 1 - \frac{m_{\pi^0}^2}{2E_{\gamma 1}E_{\gamma 2}}, \tag{3.2}$$

where m_{π^0} is the mass of π^0, and $E_{\gamma 1}$ and $E_{\gamma 2}$ are the energy of two detected gammas. Using this θ and the gammas hit position, we can calculate the decay position on the Z axis. There are however, two candidate decay positions, typically in the upstream and downstream of the detected positions. In this simulation, we chose the one in the upstream, because most of the gammas fly downstream in this energy. Here, notice that this method gives the correct decay position only for the signal events and the even pair background events, but not for the odd pair background events.

Using this decay vertex position and the gamma's energies, we can calculate the two gamma's momentum, and the transverse momentum of pion. In Figure 3.2, (a) shows the transverse momentum for background, and (b) shows the one for signal at K_L momentum of 50GeV/c. The peak around 205MeV/c in the P_t distribution for the background (Fig. 3.2(a)) is due to the even pair background, and the rest is due to the odd pair background. Comparing the transverse momentum distribution for $K_L \to \pi^0\nu\bar{\nu}$ with that for $K_L \to \pi^0\pi^0$, it is obvious that a cut on transverse momentum is very effective.

3.2.2 Cut Criteria

Next, we need to decide a cut region. We considered the following two criteria for deciding the cut region.

First, we should select the cut region which can determine η with an accuracy of 10%. Since $|\eta|^2$ is in proportional to signal branching ratio, we need to measure the branching ratio within 20%. We considered statistic error of signal and background events as the sole source of the error on branching ratio. Consequently, the $\Delta\eta/\eta$ depends on the number of signal and background events, which depends on the signal region. As described in Appendix C, the $\Delta\eta/\eta$ is expressed as:

$$\Delta\eta/\eta = \frac{\sqrt{BR_{sig} \times A_{sig} + BR_{bkg} \times A_{bkg}}}{2 \times \sqrt{N_{decay}} \times BR_{sig} \times A_{sig}} \tag{3.3}$$

where BR_{sig}, BR_{bkg}, A_{sig}, A_{bkg}, and N_{decay} mean the branching ratio of signal, branching ratio of background, acceptance of signal, acceptance of background, and the number of K_L decays, respectively. In this study we assumed N_{decay} to be 1.4×10^{13} which is the number suggested in KAMI, and BR_{sig} of 3×10^{-11}, so unknown parameters are only A_{sig} and A_{bkg} which depends on the signal region.

Second, among all the possible signal regions which satisfy the first criterion, we chose the region which gives the lowest background to signal ratio(N/S). In order to do so, we first made the N/S ratio distribution(Fig. 3.2(c)) by dividing the background P_t distribution(Fig. 3.2(a)) by the signal P_t distribution(Fig. 3.2(b)).

Next, we selected a high N/S ratio shown as a horizontal line in Fig. 3.2(d), and removed the events in the region where N/S ratio is above this line (shown in white in Figure 3.2(d)). We then lowered this N/S ratio line to reduce more background events until $\Delta\eta/\eta$ reaches 10% as shown in Fig. 3.2(e). The region where the N/S is below the line is defined as the signal region.

Figure 3.3 and 3.4 show the transverse momentum of π^0 for K_L momentum of 500MeV/c, 1GeV/c, 5GeV/c, 10GeV/c, and 50GeV/c. The cut regions for each K_L momentum are shown as shadow area. For K_L momentum of 500MeV/c and 1GeV/c, $\Delta\eta/\eta$ could not reach 10% or below with any cut region, so the signal region does not exist. As shown in these figures, in typical, the signal region exists above even pair background peak ($\geq$ 215MeV/c) and some area below 215 MeV/c. The step at about 180MeV/c for the K_L momentum of 10GeV/c is an artifact of a step in the photon detection inefficiency we used (Fig. 2.12). More detailed description on this is written in Appendix B.

3.2.3 Background Level

In the following studies, we will describe the amount of background in terms of background level which is described next.

The background level can be expressed as

$$\frac{\#background}{\#signal} = \frac{background\ level}{signal\ B.R.} \tag{3.4}$$

In this study, the signal branching ratio is expected to be $\cong 3 \times 10^{-11}$. For example, if the background level is 3×10^{-11}, it means that the expected number of background events is the same as the number of signal events, and if the background level is 3×10^{-12}, it means that the expected number of background events is tenth of the signal. To satisfy the purpose described in the introduction, in the following studies we will demand the background level to be less than the signal branching ratio (3×10^{-11}).

In actual calculation, we used the following equation.

$$background\ level = BR_{bkg} \times \frac{A_{bkg}}{A_{sig}} \tag{3.5}$$

Figure 3.5 shows the background level for the 1mmPb/5mmScint and 0.5mmPb/5mmScint detectors. The background levels for 500MeV/c and 1GeV/c do not exist because $\Delta\eta/\eta$ could not reach 10% or below with any cut region. As shown in this figure, below the $\simeq$ 6GeV/c, we can not get background level under 3×10^{-11} even with this ideal model, because this is in ideal model. The difference between 1mmPb/ 5mmScint and 0.5mmPb/ 5mmScint is small. The acceptances at different K_L momenta are shown in Table 3.1.

Based on this background level, if we only cut on P_t, the K_L momentum has to be at least 5GeV/c.

1mmPb/5mmScint. detector

Momentum of K_L (GeV)	Acceptance of signal	Acceptance of background
5	0.14	6.6×10^{-9}
10	0.080	8.5×10^{-10}
50	0.064	8.5×10^{-11}

0.5mmPb/5mmScint. detector

Momentum of K_L (GeV)	Acceptance of signal	Acceptance of background
5	0.14	6.3×10^{-9}
10	0.080	7.7×10^{-10}
50	0.064	7.7×10^{-11}

Table 3.1: Acceptance after transverse momentum cut in the simple case. In the left(right) table, 1mmPb/5mmScint. (0.5mmPb/5mmScint.) detector was used.

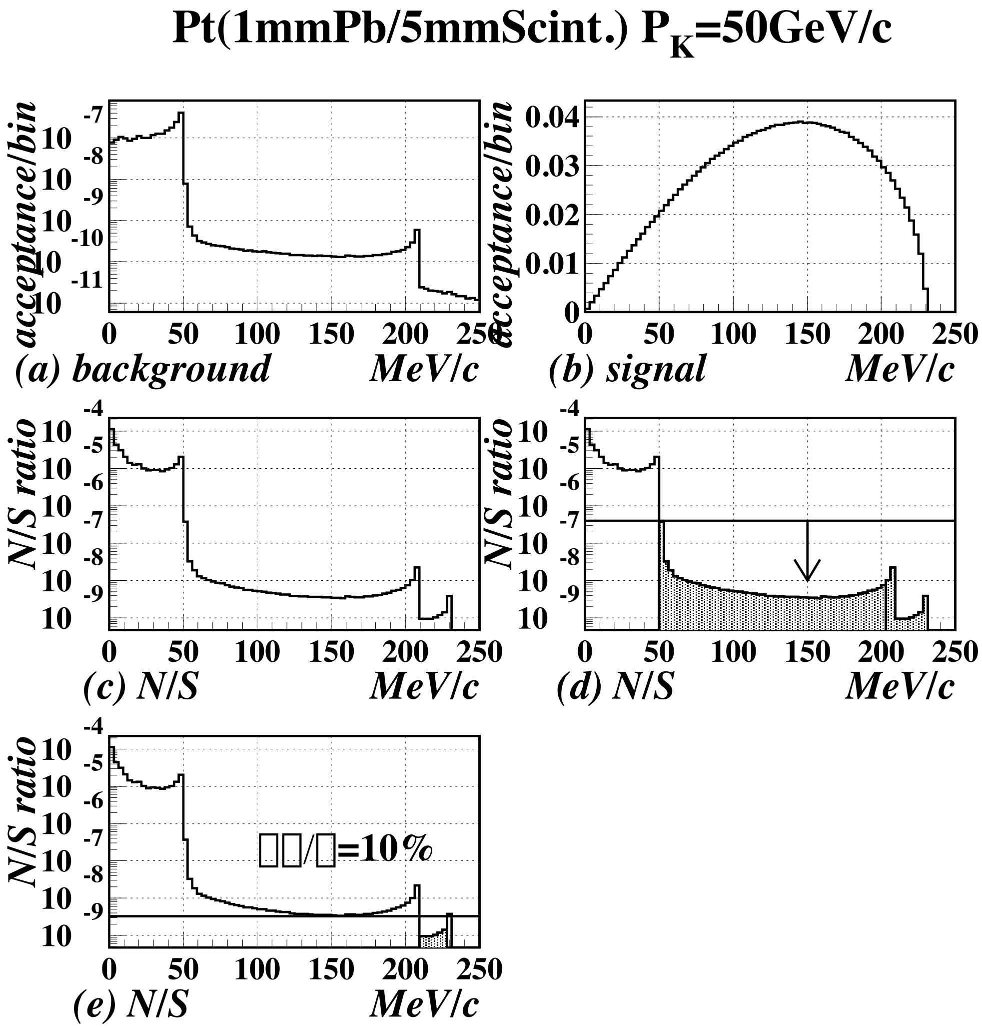

Figure 3.2: Explanation of how to decide the cut region. (a)transverse momentum of $K_L \to \pi^0\nu\bar{\nu}$. (b)transverse momentum of $K_L \to \pi^0\pi^0$. (c)N/S ratio distribution that is (a) divided by (b). (d)The region with N/S ratio under this line is decided as signal region, and we take down this line. (e)When the error on η get down to 10%, this region is decided as signal region.

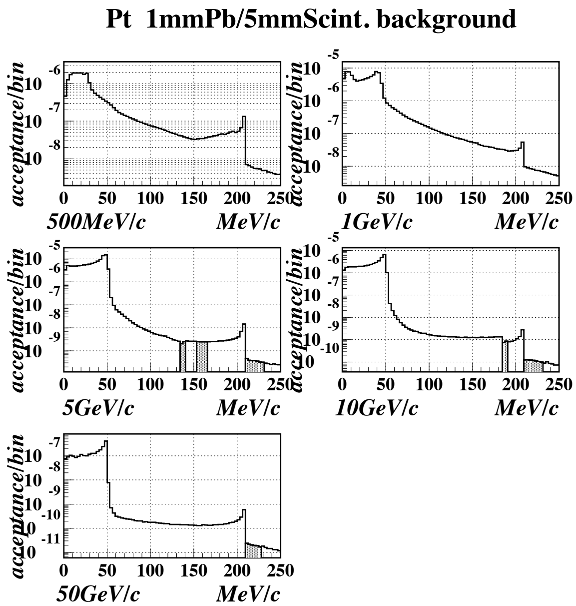

Figure 3.3: P_t distribution for $K_L \to \pi^0\pi^0$ are shown for the K_L momentum of 500MeV/c, 1GeV/c, 5GeV/c, 10GeV/c, and 50GeV/c in the simple case. The 1mmPb/5mmScint sampling calorimeter was used as the photon counter. The shadow area shows the signal region.(see 3.2.2)

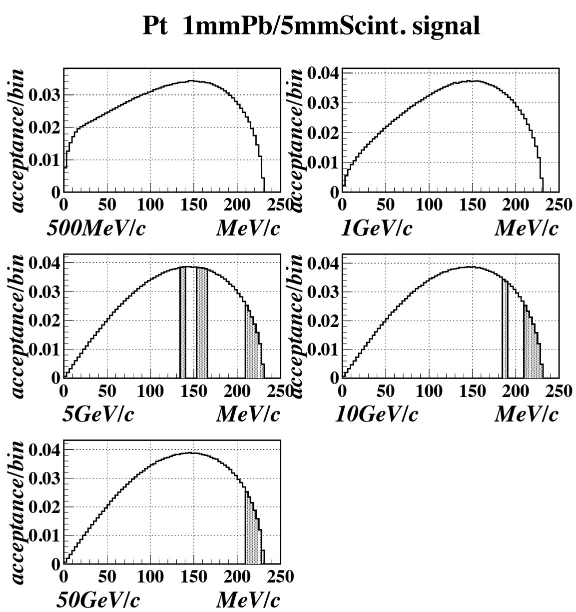

Figure 3.4: P_t distribution for $K_L \to \pi^0\nu\bar{\nu}$ are shown for the K_L momentum of 500MeV/c, 1GeV/c, 5GeV/c, 10GeV/c, and 50GeV/c in the simple case. The 1mmPb/5mmScint sampling calorimeter was used as the photon counter. The shadow area shows the signal region.(see 3.2.2)

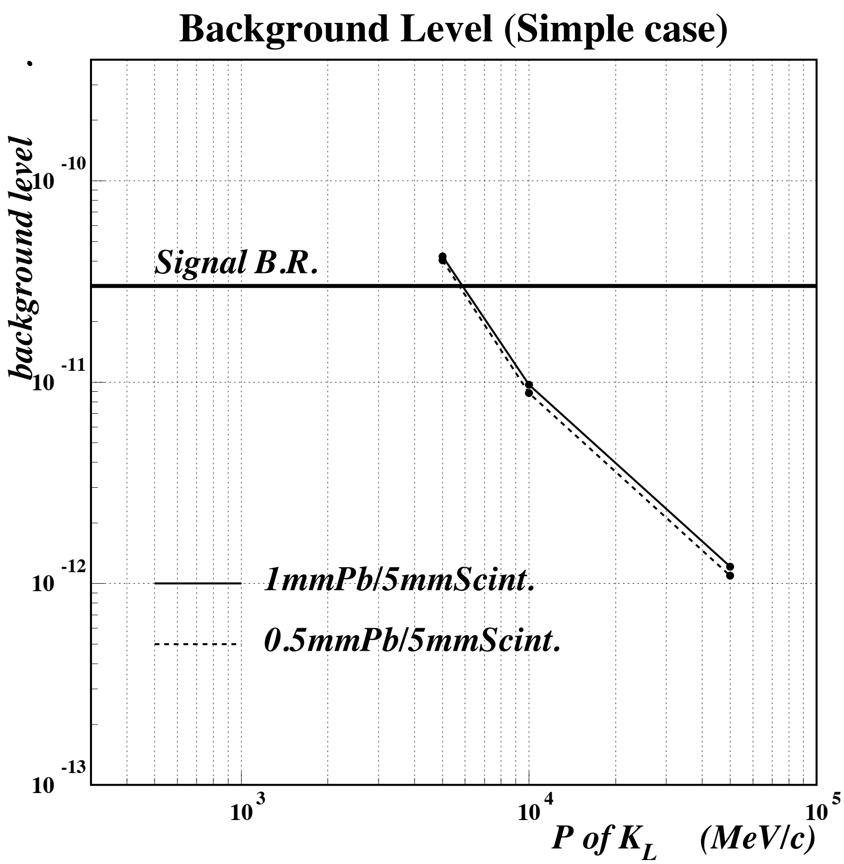

Figure 3.5: Background level in the Simple Case is shown as a function of K_L momentum. The solid line and the dashed line show background level for using 1mm Pb/5mm Scint and 0.5mm Pb/5mm Scint detector, respectively.

3.3 Case where Decay Vertex is known

In this section, we assumed that in addition to the gamma's energy and hit position in calorimeter, we can measure the decay vertex. This can be realized, for example, by measuring the direction of gamma's. Actually an experiment proposed at Brookhaven [8] is planing to use this new technique.

In this case, once we know the decay vertex, by requiring two gamma's mass to be consistent with the pions mass, we can reject the odd pair background events. We can further reduce background by using P_t cut described in the previous section.

3.3.1 Mass Cut

In this case where we know the decay vertex position, we can calculate the momentum of the detected two gammas. Using these momenta and the gamma's energies, we can reconstruct the invariant mass of the two gamma's($m_{\gamma\gamma}$) as shown in Figure 3.6. If these two gammas come from the same pion(as for even pair background and signal events), the reconstructed mass should be the pion's mass ($\simeq$135MeV/c^2). On the other hand, if two gammas come from different pions(odd pair background), the mass is usually different from the pion's mass. So we can remove the most of the odd pair background from $K_L \to \pi^0\pi^0$ by requiring the two gammas mass to be the pion's mass. Here, since we assumed that the detector has the perfect energy and position resolutions, the two gammas mass will be exactly the pions mass. We could then set the mass window to be infinitely small and reject all the odd pair background events. However, this is not realistic, so we set the signal region as $m_{\pi^0} \pm 10MeV/c^2$. This width is based on the pions mass width observed in the CsI calorimeter by KTeV experiment. [11]

As shown in Figure 3.6 and 3.3, the number of odd pair background events is much larger than the number of even pair background events. Especially at high K_L momentum the difference is enhanced. This is because even pair background is suppressed with a kinematic constraint as explained in Appendix D.

3.3.2 Transverse momentum Cut

To suppress background remaining in the signal region in mass distribution, we applied a cut on the transverse momentum of π^0. Since we know the decay vertex, we can reconstruct the transverse momentum without assuming the pion mass as in the simple case. Figure 3.7 and 3.8 show the distributions of P_t after the mass cut. The signal region in P_t was defined by the same method as in the simple case. At higher K_L momentum, the number of events in low transverse momentum region increases because the remaining events after the π^0 mass cut are dominated by odd pair background events. More detail we described in Appendix D. In result, at low K_L momentum(500MeV/c and 1GeV/c) the signal region also increase the low P_t regions. The step in these figures are caused by step in photon detection inefficiency(Fig. 2.12), as similarly to the simple case(3.2.1). More detailed description on this is given in Appendix B.

3.3.3 Background Level

Figure 3.9 shows the background level for 1mmPb/ 5mmScint and 0.5mmPb/ 5mmScint detector. These background levels are about 5$\sim$10 times lower than those for the simple case, and η can be measured to 10% of itself at all K_L momentum.

To make background level below the signal branching ratio(3×10^{-11}), the K_L momentum has to be at least $\simeq$2GeV/c.

The acceptance after this cut is shown in Table 3.2.

1mmPb/5mmScint. detector

Momentum of K_L (GeV)	Acceptance of signal	Acceptance of background
0.5	0.36	5.9×10^{-8}
1	0.44	9.2×10^{-8}
5	0.070	2.8×10^{-10}
10	0.064	1.2×10^{-10}
50	0.064	1.6×10^{-11}

0.5mmPb/5mmScint. detector

Momentum of K_L (GeV)	Acceptance of signal	Acceptance of background
0.5	0.22	2.0×10^{-8}
1	0.19	1.4×10^{-8}
5	0.070	3.0×10^{-10}
10	0.064	9.6×10^{-11}
50	0.064	1.4×10^{-11}

Table 3.2: Acceptance after the π^0 mass cut and the P_t cut for the case where decay vertex is known. In the left(right) table, 1mmPb/5mmScint.(0.5mmPb/5mmScint.) detector was used.

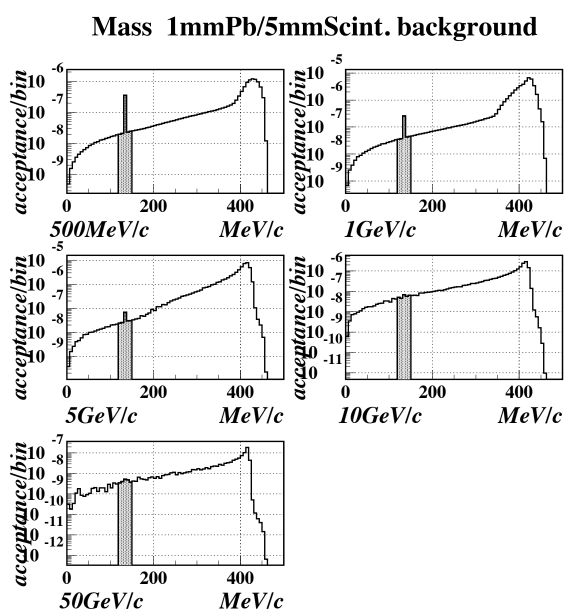

Figure 3.6: The distribution of two gammas mass for K_L momentum of 500MeV/c, 1GeV/c, 5GeV/c, 10GeV/c, and 50GeV/c. The 1mmPb/ 5mmSint calorimeter was used as the photon counter. The shadow area shows the signal region of $m_{\pi^0} \pm 10MeV/c^2$

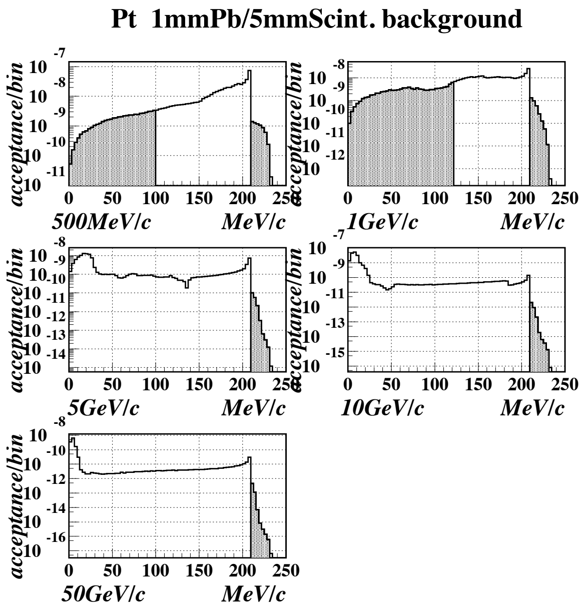

Figure 3.7: P_t distribution for $K_L \to \pi^0\pi^0$ are shown for the K_L momentum of 500MeV/c, 1GeV/c, 5GeV/c, 10GeV/c, and 50GeV/c in the case where vertex is known. The 1mmPb/5mmScint sampling calorimeter was used as the photon counter. The shadow area shows the signal region.(see 3.2.2)

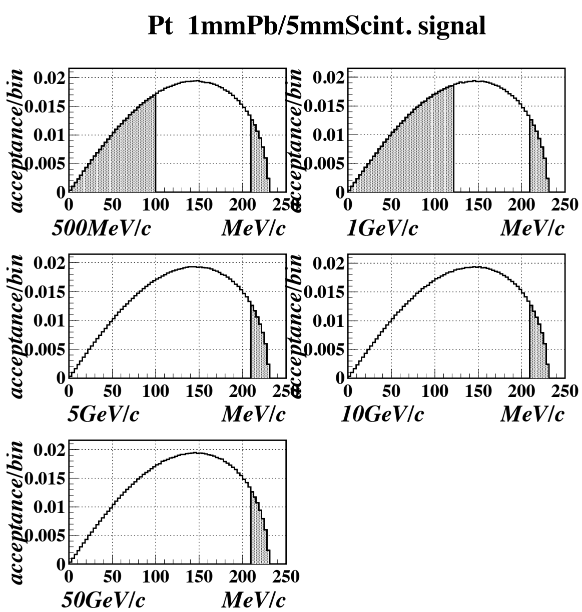

Figure 3.8: P_t distribution for $K_L \to \pi^0\nu\bar{\nu}$ are shown for the K_L momentum of 500MeV/c, 1GeV/c, 5GeV/c, 10GeV/c, and 50GeV/c in the case where vertex is known. The 1mmPb/5mmScint sampling calorimeter was used as the photon counter. The shadow area shows the signal region.(see 3.2.2)

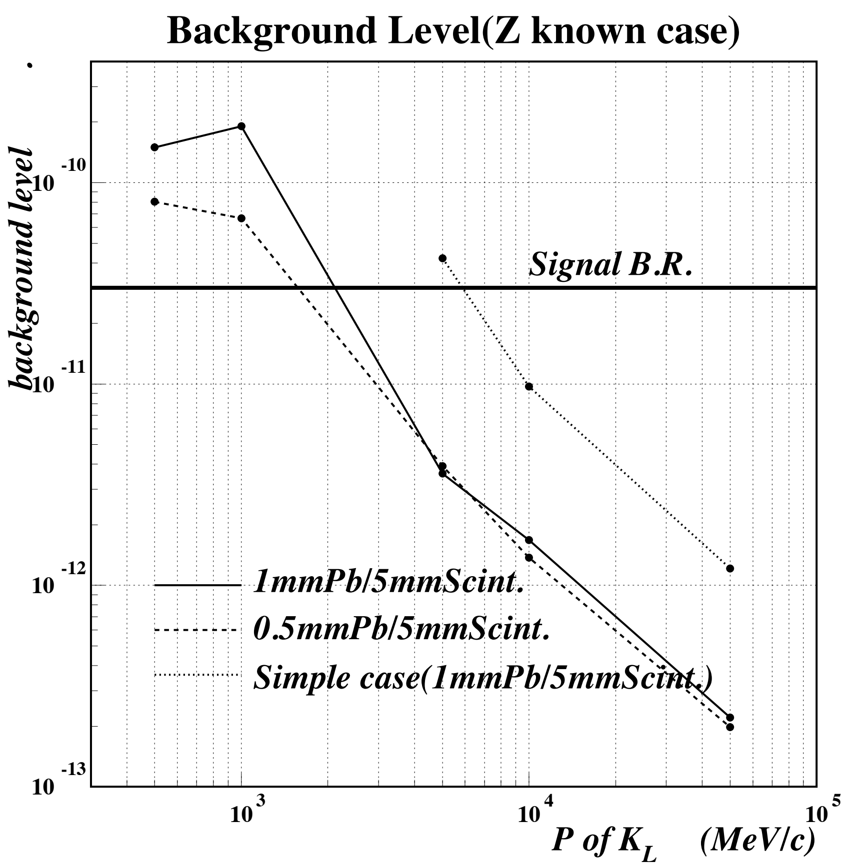

Figure 3.9: The background level as a function of K_L momentum is shown. The solid line and the dashed line show the background level for the case where vertex is known using 1mm Pb/5mm Scint and 0.5mm Pb/5mm Scint detector, respectively. The dotted line show the background level in simple case using 1mm Pb/5mm Scint. The background level at 1GeV/c is greater than that at 500MeV/c because the cut region and P_t distribution are different between them as shown in Fig.3.7.

3.4 Case where K_L Energy is known

In this section, we will assume that we know the K_L energy besides the gamma's energy and hit position in the calorimeter. This may be a very difficult technique to realize, because K_L is a neutral particle. However, an experiment at BNL is planning to measure K_L energy by using TOF, and one could consider producing K_L with a known energy by using $K^+ + n \to p + K^0$ charge exchange interaction.

In this case, the even pair background can be reduced effectively by cutting on a missing mass. We can further cut the odd pair background by using correlation between the missing mass and energy of two gammas.

3.4.1 Missing Mass Cut

In this case where we know the K_L energy, we can calculate missing mass, which is the invariant mass of the unobserved particles.

Assuming that the two observed gammas come from one pion, the missing mass is written as

$$M_{miss}^2 \equiv (E_{K_L} - E_{\gamma\gamma})^2 - (\overrightarrow{P_{K_L}} - \overrightarrow{P_{\gamma\gamma}})^2 \tag{3.6}$$

$$= m_{K_L}^2 + m_{\pi^0}^2 - 2E_{K_L}E_{\gamma\gamma} + 2P_{zK_L}Pz\gamma\gamma \tag{3.7}$$

where E_{K_L} and $E_{\gamma\gamma}$ are energy of K_L and two observed gammas, $\overrightarrow{P_{K_L}}$ and $\overrightarrow{P_{\gamma\gamma}}$ are momentum of K_L and two observed gammas, m_{K_L} and m_{π^0} are mass of K_L and π^0, and P_{zK_L} and $P_{z\gamma\gamma}$ are Z momentum of K_L and two gammas. Here, we assumed that K_L's come along the Z axis. In the case of even pair background, the missing mass should be a pion's mass. Therefore we can reject most of even pair background from $K_L \to \pi^0\pi^0$ by cutting events around the pion's mass.

Figure 3.10 and 3.11 show the distribution of the square of the the missing mass. Pion's mass corresponds to $\simeq$18225(MeV/c^2)^2.

Since the perfect resolution model was assumed, the peak at the pion's mass has no width. To be more realistic, we assumed that the M_{miss} has the same resolution as $m_{\gamma\gamma}$.

The cut region is defined as

$$(m_{\pi^0} - 10MeV/c^2)^2 \leq M_{miss}^2 \leq (m_{\pi^0} + 10MeV/c^2)^2. \tag{3.8}$$

This cut region is shown in Fig. 3.10 and 3.11 as shadow region.

3.4.2 Missing mass VS. $E_{\gamma\gamma}$ Cut

In order to suppress the remaining odd pair background, we cut on the correlation between missing mass and two gamma's energy($E_{\gamma\gamma}$). Figure 3.12 and 3.13 show the M_{miss} VS. $E_{\gamma\gamma}$ distributions before cutting on the missing mass.

The signal region was decided basically with the same method as in the simple case, but applied in two dimensions. At first, we made the N/S ratio distribution in the two dimensional plot which is the background distribution divided by the signal distribution. We then lowered a threshold on N/S ratio until the events in the region below the threshold achieves $\Delta\eta/\eta$ of 10%. The signal regions are shown in right row of Figure 3.12 and 3.13. The acceptance after this cut is shown in Table 3.3.

3.4.3 Background Level

Figure 3.14 shows the background level for 1mmPb/5mmScint and 0.5mmPb/5mmScint detector. This background level is about 5$\sim$100 times lower than the simple case. This background level is also lower than the background for the case where we know the decay vertex at low K_L momentum.

1mmPb/5mmScint. detector

Momentum of K_L (GeV)	Acceptance of signal	Acceptance of background
0.5	0.14	6.2×10^{-9}
1	0.066	2.3×10^{-10}
5	0.061	3.2×10^{-11}
10	0.061	5.7×10^{-11}
50	0.060	1.4×10^{-11}

0.5mmPb/5mmScint. detector

Momentum of K_L (GeV)	Acceptance of signal	Acceptance of background
0.5	0.083	1.0×10^{-9}
1	0.063	1.2×10^{-10}
5	0.060	1.9×10^{-11}
10	0.060	5.0×10^{-11}
50	0.060	1.3×10^{-11}

Table 3.3: Acceptance after the missing mass cut and the missing mass VS. $E_{\gamma\gamma}$ cut in the case where we know E_{K_L}. In the left(right) table, 1mmPb/5mmScint(0.5mmPb/5mmScint) detector was used.

From this background level, to get background level below the signal branching ratio(3×10^{-11}) , we need to use K_L with momentum greater than 600MeV/c for 1mmPb/5mmScinti detector, and at least 500MeV/c for 0.5mmPb/5mmScint detector.

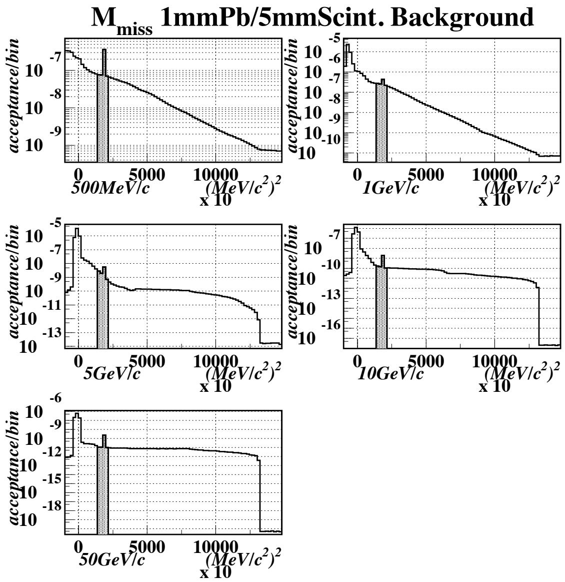

Figure 3.10: Distribution of missing mass for $K_L \to \pi^0\pi^0$ for the K_L momentum of 500MeV/c, 1GeV/c, 5GeV/c, 10GeV/c, and 50GeV/c in the case where E_{K_L} is known. The 1mmPb/5mmScint sampling calorimeter was used as the photon counter. The shadow area shows the cut region.

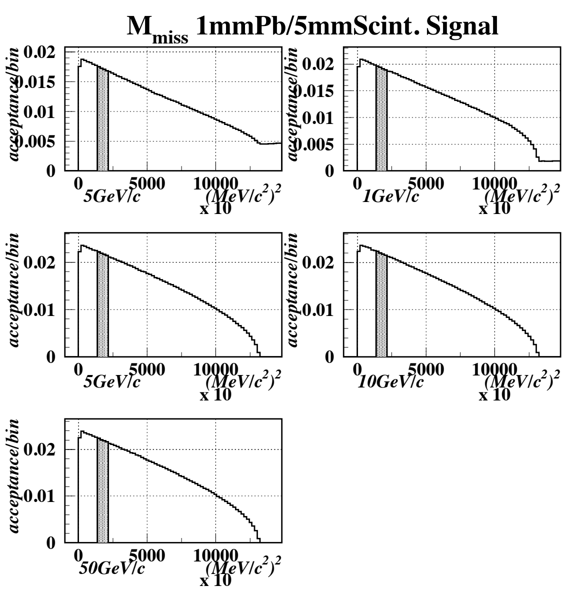

Figure 3.11: Distribution of missing mass for $K_L \to \pi^0\nu\bar{\nu}$ for the K_L momentum of 500MeV/c, 1GeV/c, 5GeV/c, 10GeV/c, and 50GeV/c in the case where E_{K_L} is known. The 1mmPb/5mmScint sampling calorimeter was used as the photon counter. The shadow area shows the cut region.

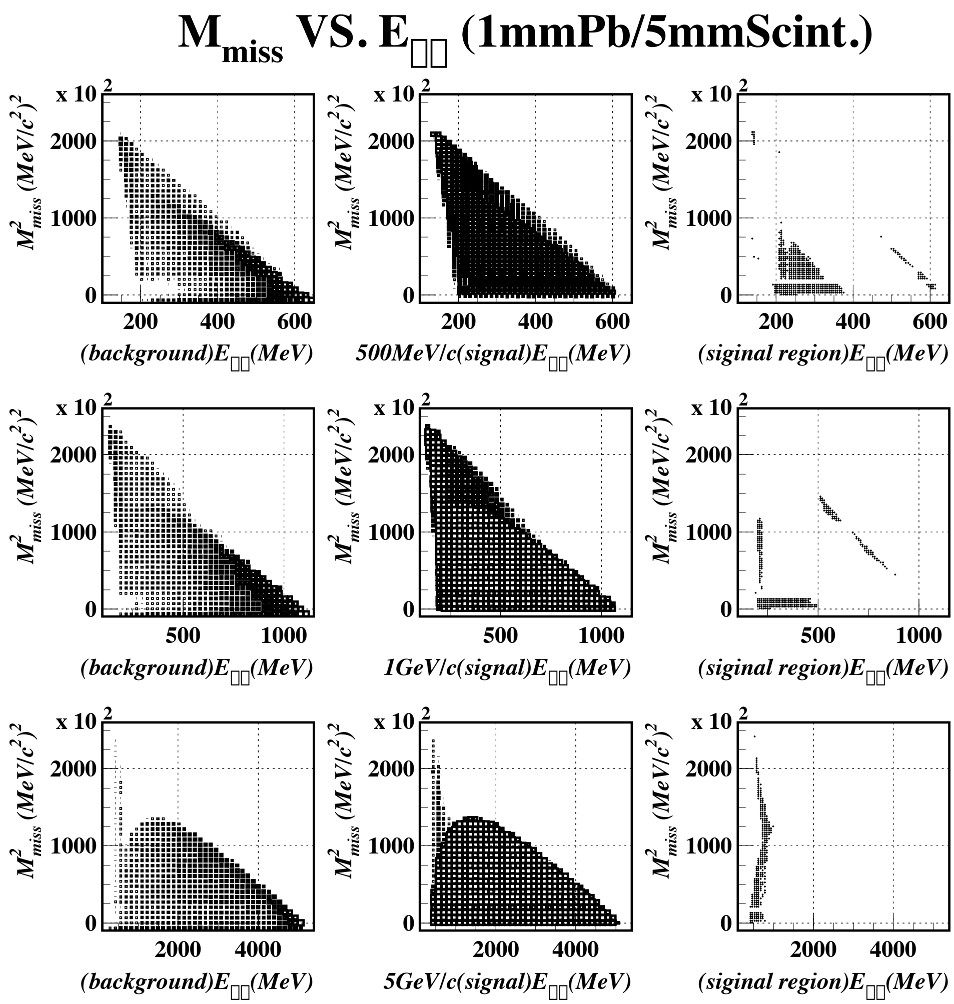

Figure 3.12: Missing mass VS. $E_{\gamma\gamma}$ for the K_L momentum of 500MeV/c, 1GeV/c, and 5GeV/c in the case where E_{K_L} is known. The 1mmPb/5mmScint sampling calorimeter was used as the photon counter. The left row shows the distribution for the background, and the center row shows the distribution of signal. The right row shows the signal region selected by the method described in the text.

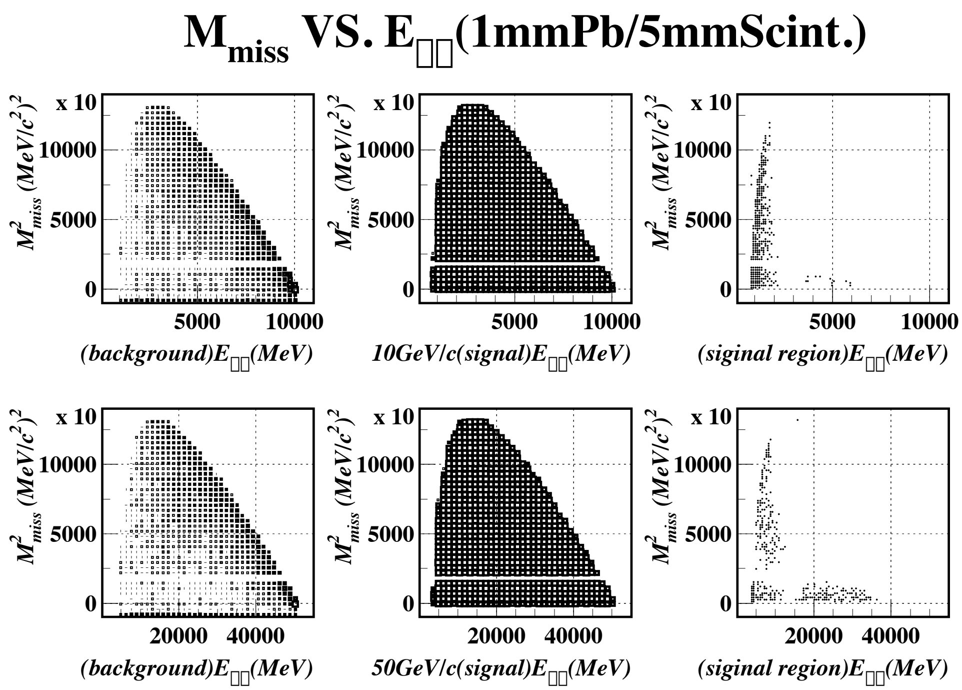

Figure 3.13: Missing mass VS. $E_{\gamma\gamma}$ for the K_L momentum of 10GeV/c, and 50GeV/c in the case where E_{K_L} is known. The 1mmPb/5mmScint sampling calorimeter was used as the photon counter. The left row shows the distribution for the background, and the center row shows the distribution of signal. The right row shows the signal region selected by the method described in the text.

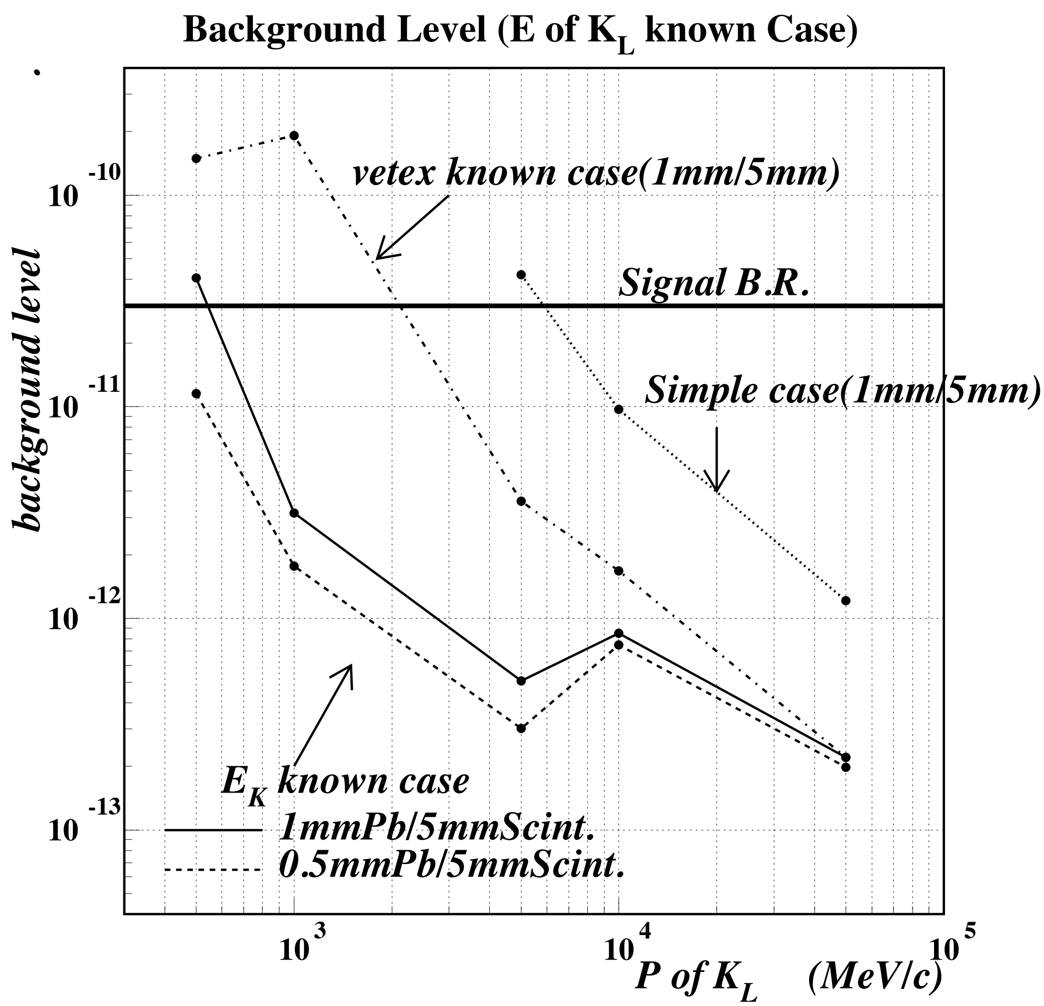

Figure 3.14: The background level as a function of P_{K_L} is shown for the case where E_{K_L} is known. For comparison, simple case and the case where we know decay vertex are also shown.

3.5 Case where Vertex and E_{K_L} are known

In this section, we will assume that we know the decay vertex and K_L energy besides the gamma's energy and hit position in the calorimeter.

In this case, the most of odd pair background can be reduced by using two gammas mass cut, and the even pair background can be reduced very effectively by using the missing mass cut described in Section 3.4. We can further cut the odd pair background by using correlation between the missing mass and energy of two gammas.

3.5.1 Mass Cut

Since we know the vertex position, we can suppress the odd pair background by requiring the two gammas mass to be consistent with pions mass. At this point, the mass distribution is the same as Fig. 3.6, so we chose the same cut required as in the case where vertex is known ($m_{\pi^0} \pm 10MeV/c^2$).

3.5.2 Missing Mass Cut

In this case where we know the K_L energy, we can calculate missing mass described in the previous section.

Figure 3.15 and 3.16 show the distribution of the square of the the missing mass after cutting on the two gammas mass. Pion's mass corresponds to $\simeq$18225(MeV/c^2)^2. As similar to the previous section, the cut region is defined as

$$(m_{\pi^0} - 10MeV/c^2)^2 \leq M_{miss}^2 \leq (m_{\pi^0} + 10MeV/c^2)^2. \tag{3.9}$$

This cut region is shown in Fig. 3.15 and 3.16 as shadow region.

3.5.3 Missing mass VS. $E_{\gamma\gamma}$ Cut

In order to suppress the remaining odd pair background, we cut on the correlation between missing mass and two gamma's energy. Figure 3.17 and 3.18 show the M_{miss} VS. $E_{\gamma\gamma}$ distributions after cutting on the two gammas mass and missing mass. The signal regions are shown in right row of Figure 3.17 and 3.18. The acceptance after this cut is shown in Table 3.4.

1mmPb/5mmScint. detector

Momentum of K_L (GeV)	Acceptance of signal	Acceptance of background
0.5	0.062	7.5×10^{-11}
1	0.060	6.8×10^{-12}
5	0.060	2.7×10^{-13}
10	0.060	3.7×10^{-14}
50	0.060	8.4×10^{-15}

0.5mmPb/5mmScint. detector

Momentum of K_L (GeV)	Acceptance of signal	Acceptance of background
0.5	0.061	3.3×10^{-11}
1	0.060	2.3×10^{-12}
5	0.060	3.4×10^{-13}
10	0.060	4.9×10^{-14}
50	0.060	8.4×10^{-15}

Table 3.4: Acceptance after the two gamma's mass cut, the missing mass cut, and the missing mass VS. $E_{\gamma\gamma}$ cut in the case where decay vertex and E_{K_L} are known. In the left(right) table, 1mmPb/5mmScint.(0.5mmPb/5mmScint.) detector was used.

3.5.4 Background Level

Figure 3.19 shows the background level for 1mmPb/5mmScint and 0.5mmPb/5mmScint detector.

In this case, the background level is lower than the signal branching ratio at the K_L momentum between 500MeV/c and 50GeV/c.

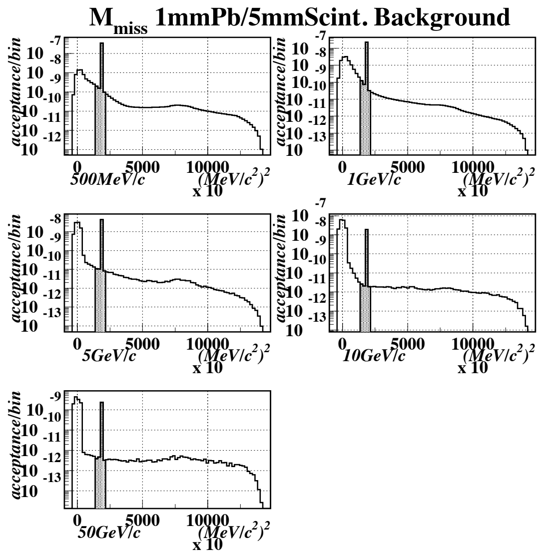

Figure 3.15: The distribution of missing mass for $K_L \to \pi^0\pi^0$ for the K_L momentum of 500MeV/c, 1GeV/c, 5GeV/c, 10GeV/c, and 50GeV/c in the case where the vertex and E_{K_L} are known. The 1mmPb/5mmScint sampling calorimeter was used as the photon counter. The shadow area shows the cut region.

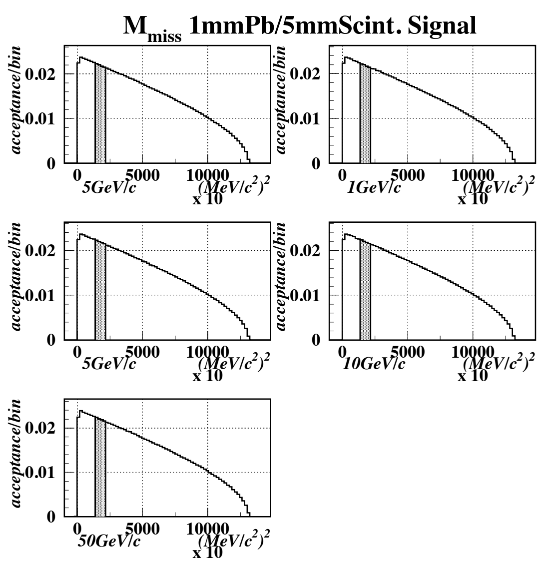

Figure 3.16: The distribution of missing mass for $K_L \to \pi^0\nu\bar{\nu}$ for the K_L momentum of 500MeV/c, 1GeV/c, 5GeV/c, 10GeV/c, and 50GeV/c in the case where the vertex and E_{K_L} are known. The 1mmPb/5mmScint sampling calorimeter was used as the photon counter. The shadow area shows the cut region.

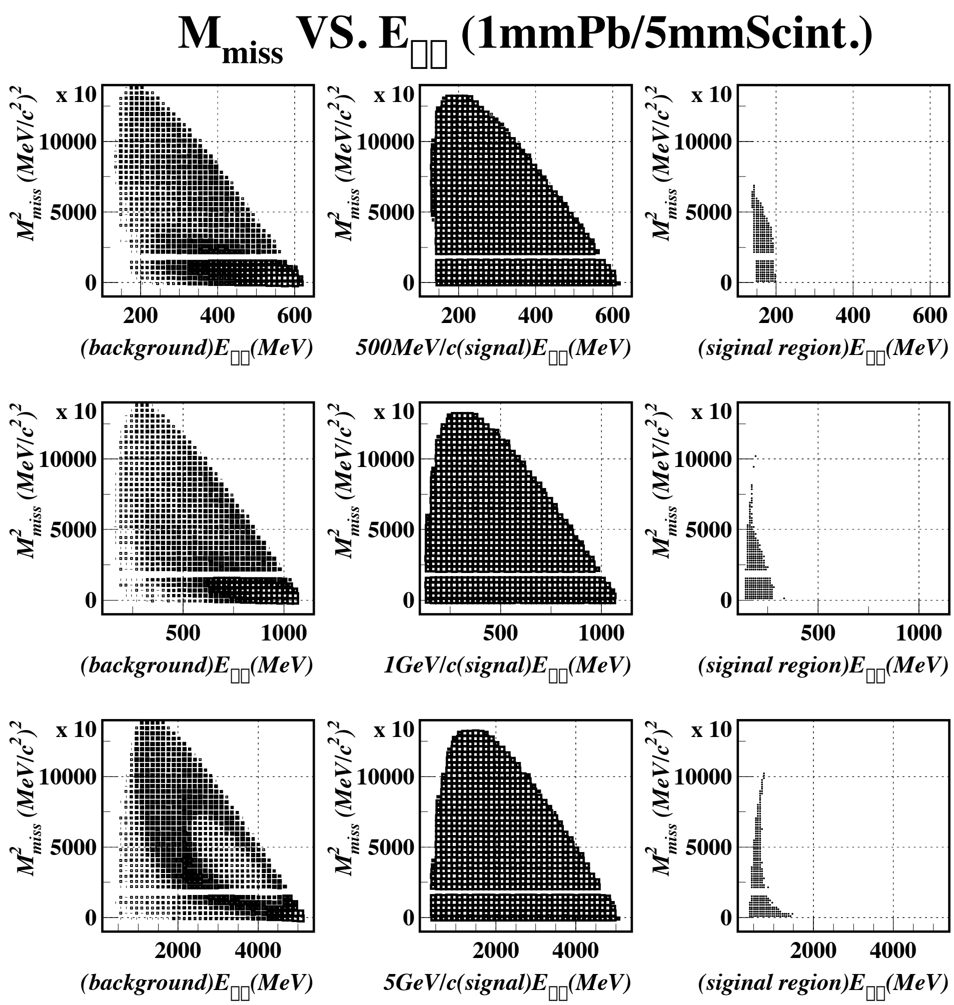

Figure 3.17: Missing mass VS. $E_{\gamma\gamma}$ for the K_L momentum of 500MeV/c, 1GeV/c, and 5GeV/c in the case where the vertex and E_{K_L} are known. The 1mmPb/5mmScint sampling calorimeter is used as the photon counter The left row shows the distribution for the background, and the center row shows the distribution for signal. The right row shows the signal region selected by the method described in the text.

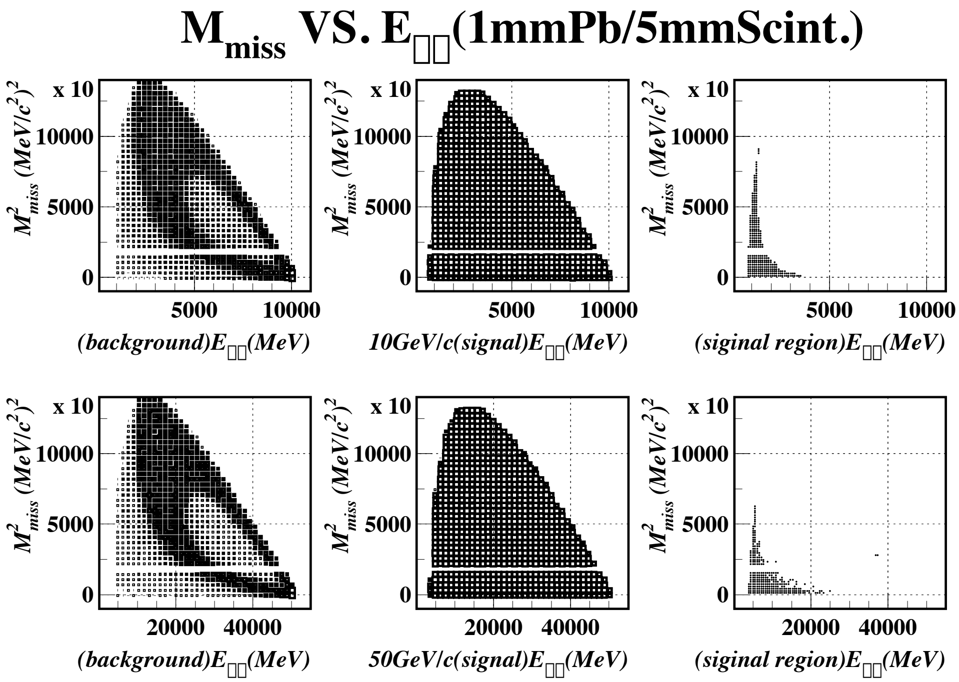

Figure 3.18: Missing mass VS. $E_{\gamma\gamma}$ for the K_L momentum of 10GeV/c, and 50GeV/c in the case where the vertex and E_{K_L} are known. The 1mmPb/5mmScint sampling calorimeter is used as the photon counter The left row shows the distribution for the background, and the center row shows the distribution for signal. The right row shows the signal region selected by the method described in the text.

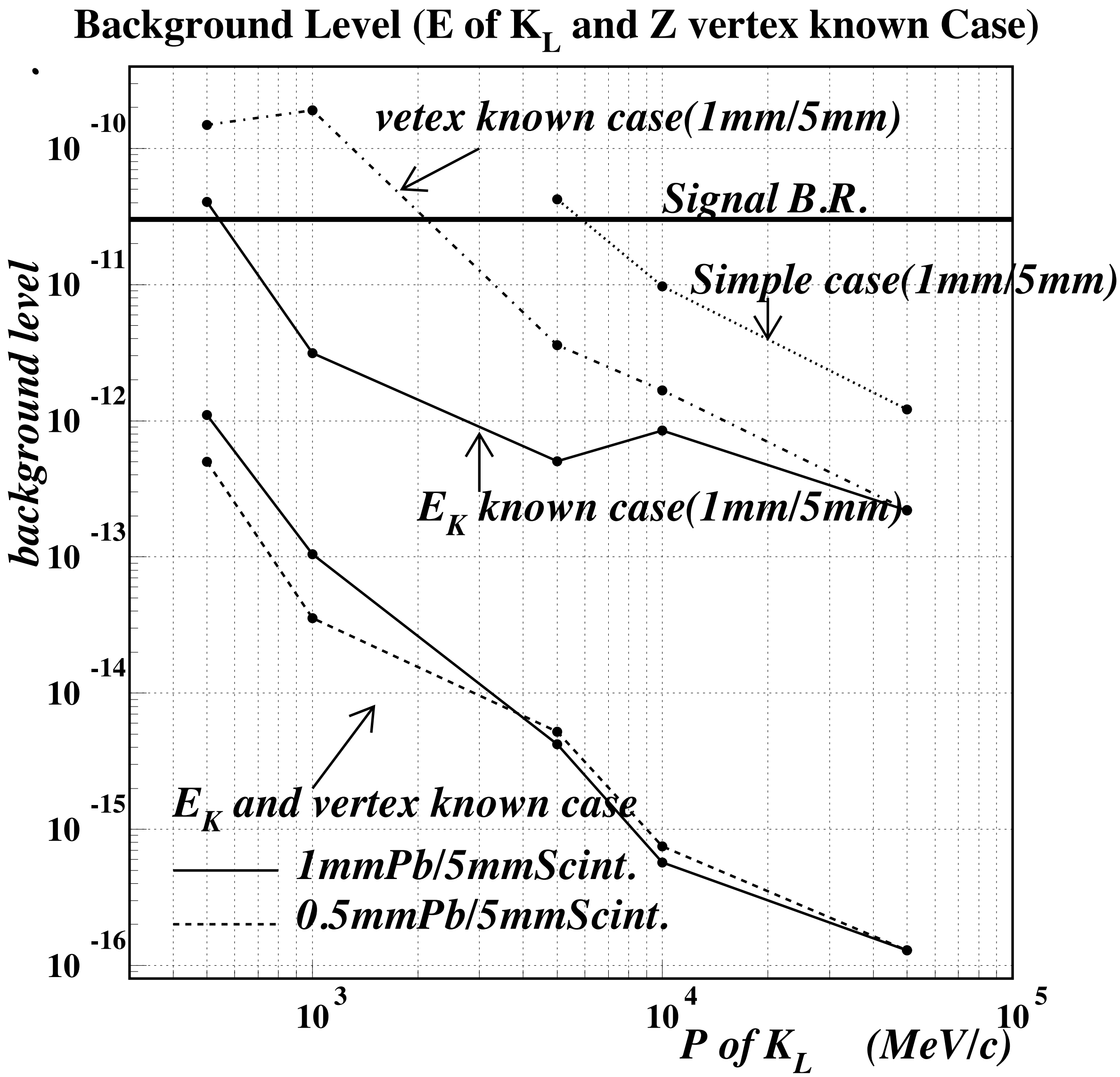

Figure 3.19: The background level as a function of P_{K_L} is shown for the case where the decay vertex and E_{K_L} are known. For comparison, other cases are also shown.

3.6 Summary

In this ideal model, to measure η with a 10% error and to make the background level below signal branching ratio(3×10^{-11}), we need following conditions.

- At K_L momentum of 500MeV/c, if we use 1mmPb/5mmScint detector, we need to know both K_L energy and vertex position. If we use 0.5mmPb/5mmScint detector, we need to know K_L energy, or both K_L energy and vertex position.
- At K_L momentum of 1GeV/c, we need to know K_L energy, or both K_L energy and vertex position.
- At K_L momentum of 5GeV/c, we need to know K_L energy, or vertex position, or both.
- At K_L momentum of 10GeV/c and 50GeV/c, we do not need to know K_L energy and vertex position.

The background level becomes lower in the order of simple case, case where the vertex is known, case where E_{K_L} are known, and case where the vertex and E_{K_L} are known.

Chapter 4

Requirements on the Detector

In the previous chapter, we assumed the ideal model, but in reality, the detector has finite resolutions and does not cover 4π solid angle. Therefore in this chapter, we will study the requirements on the detector for measuring the η to 10% of itself while keeping the background level below the signal branching ratio (3×10^{-11}).

The specifications that we considered are detector length, and resolution of observed variables such as gamma energy, gamma's hit position in the calorimeter, gamma's direction, and kaon energy. In this study, we will use only 1mmPb/5mmScint detector, because the difference between 1mmPb/ 5mmScint detector and 0.5mmPb/5mmScint detector is small as shown in Chapter 3.

In the following sections, we will study the requirements on detector in four cases described in Chapter 3.

4.1 Simple Case

In this section, we will consider the simple case where we only measure gamma's energy and the hit position in the calorimeter. Therefore we will study the effect of a finite resolution of gamma's energy and hit position, and an effect of having a finite detector length. In order to understand the each effect, we first varied resolutions of gamma energy and hit position, and the detector length one at a time, leaving the remaining conditions still perfect. At the end, we chose a set of realistic parameters and studied the background level.

4.1.1 Smearing Gamma's Position

In here, we only smeared gamma's hit position in the calorimeter with a Gaussian. The energy resolution was kept zero, and detector length was still kept infinite. We used the same position resolution ΔX to the Z direction and ϕ(polar angle) direction.

We studied three cases for ΔX, ΔX =0.001, 0.01, and 0.1 for the detector radius of '1'. This corresponds to ΔX=0.1mm, 1mm, and 1cm for a detector radius of 10cm.

Figure 4.2 shows the P_t distribution after smearing the hit positions. Compared to Fig. 3.3, we can see that the edge at 210MeV/c due to even pair background is smeared. Consequently, the signal region above the even pair peak in the ideal model(Fig. 3.3) is affected, and signal region moved to include the P_t region below the even pair peak.

Figure 4.3 shows the influence on the background levels by smearing the hit positions. As shown in this figure, for ΔX=0.001, there is no difference from the ideal model (section 3.2). However for

ΔX=0.01 and 0.1, background levels go up by a factor 1.1$\sim$1.3 and 0.5$\sim$2.5 from those for the ideal model, respectively.

4.1.2 Smearing Gamma's Energy

Here, we smeared only gamma's energy with a Gaussian, while keeping the other parameters perfect as in the ideal case. The energy resolution was parameterized as

$$\frac{\Delta E}{E} = \frac{a}{\sqrt{E}}, \tag{4.1}$$

where E is energy of gamma in GeV and a is a resolution constant. This is a general expression for calorimeters, and for the CsI calorimeter in KTeV [12] a is 2% and for a typical Lead-scintillator sandwich [13] a is about 9%.

The finite energy resolution affects the P_t distribution by smearing the edge at 210MeV/c, and signal region tends to move below the even pair peak.

We studied with two energy resolutions, a =0.01 and 0.1. Figure 4.4 shows the background levels. As shown in this figure, with a=0.01 there is no difference from the ideal model, but with a=0.1 the background level goes up by a factor 1.5$\sim$2 than in the ideal case.

4.1.3 Finite Detector Length

Here, we assumed that the detector has a finite length, instead of an infinite length. This means that the gammas near the beam line are not detected, which is equivalent to not using a veto counter in the beam. The resolutions of energy and hit position are assumed to be perfect.

A schematic geometry of the detector is shown in Fig. 4.1. As shown in this figure, we fixed the vertex position at Z = 0 and assumed that the detector ends at $Z = L$. We still assumed that the detector is infinitely long in the upstream direction. The latter assumption is not far from reality, because in these K_L energies, most of the gammas go downstream.

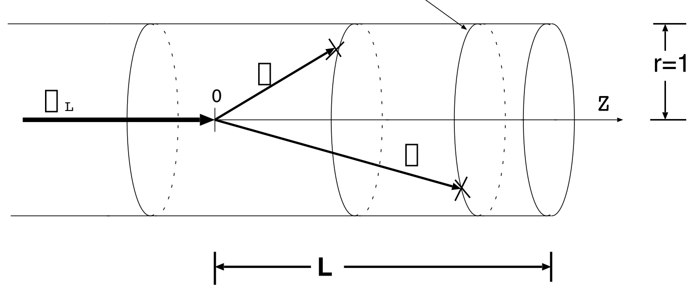

Figure 4.1: The detection geometry used in realistic model

Figure 4.5 shows the P_t distribution using a detector with L=1000. The finite detector length affects the P_t distribution for 50GeV/c, but not for 5GeV/c and 10GeV/c. This is because at high E_{K_L} most of gammas escape the detector and the shape of P_t distribution for the detected two gammas varies. Consequently, $\Delta\eta/\eta$ cannot reach 10% with any signal region.

We prepared three types of detectors, L=100, 1000 and 5000 for the detector radius of '1'. Figure 4.6 shows the background levels for the three different detector lengths. We cannot achieve $\Delta\eta/\eta$ of 10% with any cut, if L=100 and 500MeV/c$\leq E_{K_L} \leq$50GeV/c, or L=1000 and 50GeV/c$\leq E_{K_L}$. Since the gammas from high momentum K_L is boosted more forward than those from low momentum K_L, the detected position of the gamma moves towards downstream and escape from the detector as the K_L momentum goes higher. This is why in Figure 4.6, the background level jumps up or vanishes at higher E_{K_L}.

Intuitively, the hit position of gamma scales with Lorentz factor, γ, thus with E_{K_L}. Therefore the influence on background level by the detector length depends approximately on L/P_{K_L}. In Figure 4.6, we can see that the background level increases by a similar factor for P_{K_L}=50GeV/c and L=5000, and P_{K_L}=10GeV/c and L=1000 which both have $L/P_{K_L} = 10(MeV/c)^{-1}$.

The acceptances after using a detector with a finite length is shown in Table 4.1.

K_L momentum =5GeV/c

L	Acceptance for signal	Acceptance for background
ideal model	0.14	6.6×10^{-9}
5000	0.14	6.5×10^{-9}
1000	0.18	1.2×10^{-8}

K_L momentum =10GeV/c

L	Acceptance for signal	Acceptance for background
ideal model	0.080	8.5×10^{-10}
5000	0.079	8.6×10^{-10}
1000	0.12	3.9×10^{-9}

K_L momentum =50GeV/c

L	Acceptance for signal	Acceptance for background
ideal model	0.064	8.5×10^{-11}
5000	0.070	2.0×10^{-10}

Table 4.1: Acceptance for the signal and background using a finite length detector in the simple case. The upper on left, lower on left, and right tables show the acceptances for K_L momentum of 5GeV/c, 10GeV/c, and 50GeV/c, respectively. The detector was assumed to be made of 1mmPb/ 5mmScint calorimeter.

4.1.4 Realistic model

At the end, we simulated a realistic experiment by choosing a set of detector resolutions and a length.

As described above, the average hit position of gammas in Z is proportional to the K_L energy, so the detector length used in practice is tuned for $L \propto P_{K_L}$. In this study, from Figure 4.6, we chose $L = P_{K_L}/10MeV/c$ as the detector length. (The detector length at 5GeV/c, 10GeV/c, and 50GeV/c corresponds 500, 1000, and 5000 for detector radius of '1', respectively.) We chose position resolution of ΔX=0.01 and the energy resolution of $\Delta E/E = 1\%/\sqrt{E(GeV)}$.

Figure 4.7 shows the background levels for the realistic model. The background level for the realistic model is larger than that of ideal model by a factor three. With this condition, we must use K_L momentum of 10GeV/c or higher to satisfy our goal. At the K_L momentum of 10GeV/c, the signal to noise ratio is 1.

The acceptances for the realistic model are shown in Table 4.2.

4.1.5 Summary

We have studied the effect of finite detector resolutions and length in the simple case where we only measure the gamma's energy and position.

Finite resolutions on gamma's energy and hit position measurements smears the P_t distribution (Fig. 4.2). Since the smearing causes the even pair backgrounds below the edge at the 210MeV/c in

K_L momentum =5GeV/c

case	Acceptance for signal	Acceptance for background
ideal model	0.14	6.6×10^{-9}
realistic model	0.28	3.5×10^{-8}

K_L momentum =10GeV/c

case	Acceptance for signal	Acceptance for background
ideal model	0.080	8.5×10^{-10}
realistic model	0.12	4.4×10^{-9}

K_L momentum =50GeV/c

case	Acceptance for signal	Acceptance for background
ideal model	0.064	8.5×10^{-11}
realistic model	0.071	2.5×10^{-10}

Table 4.2: Acceptances for the signal and background for the ideal and a realistic model in simple case. The realistic model uses a detector with $L = P_{K_L}/10MeV/c$, $\Delta X = 0.01$, and $\Delta E/E = 1\%/\sqrt{E(GeV)}$. The detector was assumed to be made of 1mmPb/ 5mmScint calorimeter.

P_t to flow into the region above the edge, it directly affects the background level. Smearing gamma's position with ΔX=0.01 increases the background level by a factor 1.1 $\sim$ 1.3 from the ideal model. Smearing gamma's energy with $\Delta E/E = 1\%/\sqrt{E(GeV)}$ does not change the background level from the ideal model.

With a finite length detector, gammas of high momentum K_L go out detector, so the background level at high K_L momentum is affected. Therefore to compare between different K_L momentum similarly, we used a variable of L/P_{K_L}. Using the detection length with $L = P_{K_L}/10MeV/c$ increases the background level by a factor 2$\sim$3 from the ideal model.

As shown in Figure 4.7, if we prepared a detector with the following specifications, we can achieve our goal of measuring η with a 10% error while keeping the background level below 3×10^{-11}.

- K_L momentum: $P_{K_L} \geq$ 10GeV/c
- position resolution: ΔX=0.01 for a detector radius of '1'
- energy resolution: $\Delta E/E = 1\%/\sqrt{E(GeV)}$,
- Detector length: $L = P_{K_L}/10MeV/c$ for a detector radius of '1'

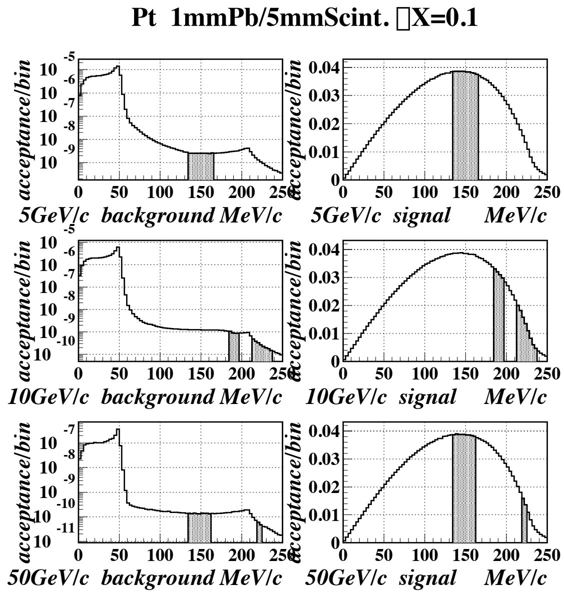

Figure 4.2: P_t distribution after smearing gamma's hit position by ΔX=0.1 in the simple case. K_L momenta are 5GeV/c, 10GeV/c, and 50GeV/c from the top. The left row shows background and the right row shows the signal. The detector was assumed to be made of 1mmPb/ 5mmScint calorimeter.

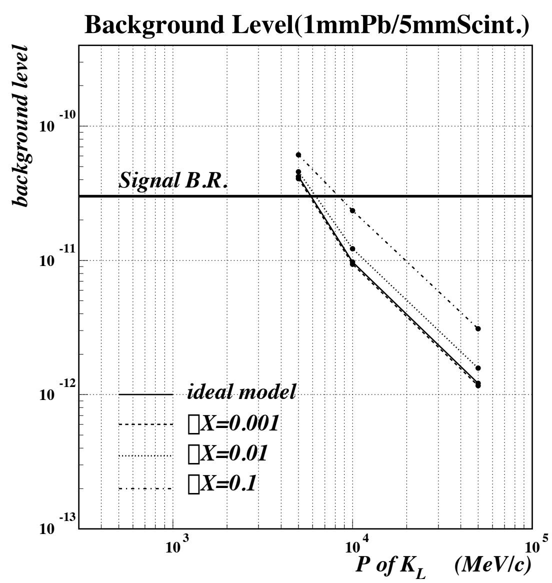

Figure 4.3: The background level after smearing gamma's hit positions in the simple case is shown as a function of P_{K_L}. The detector was assumed to be made of 1mmPb/ 5mmScint calorimeter.

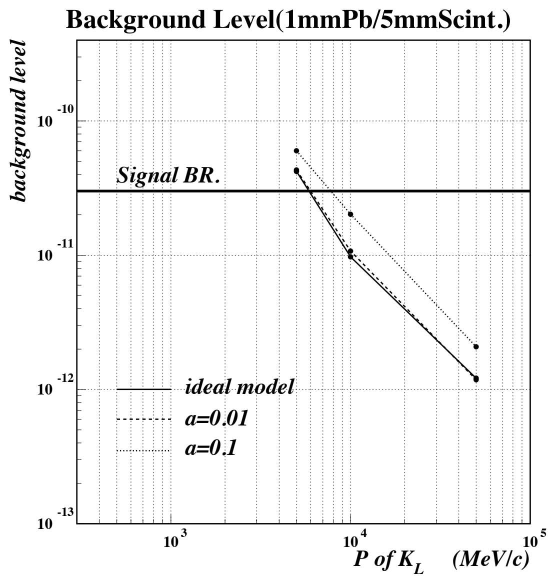

Figure 4.4: The background level after smearing gamma energies in the simple case is shown as a function of P_{K_L}. The detector was assumed to be made of 1mmPb/ 5mmScint calorimeter.

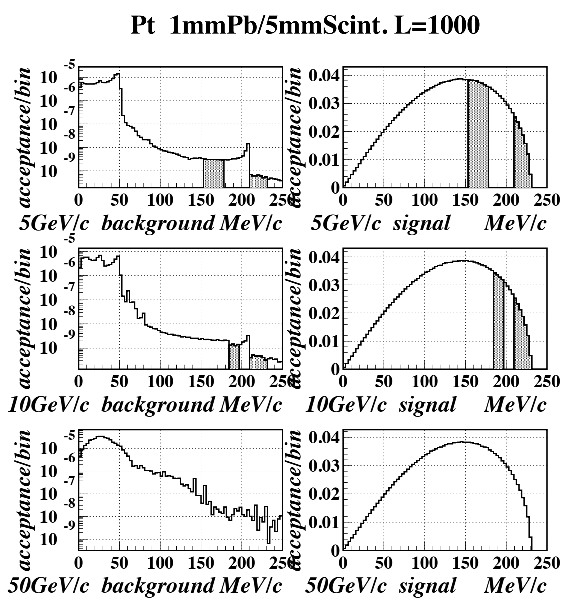

Figure 4.5: P_t distributions after using a finite detector length of L=1000 in the simple case. K_L momentums are 5GeV/c, 10GeV/c, and 50GeV/c from the top. The left row shows background and the right row shows the signal. The detector was assumed to be made of 1mmPb/ 5mmScint calorimeter.

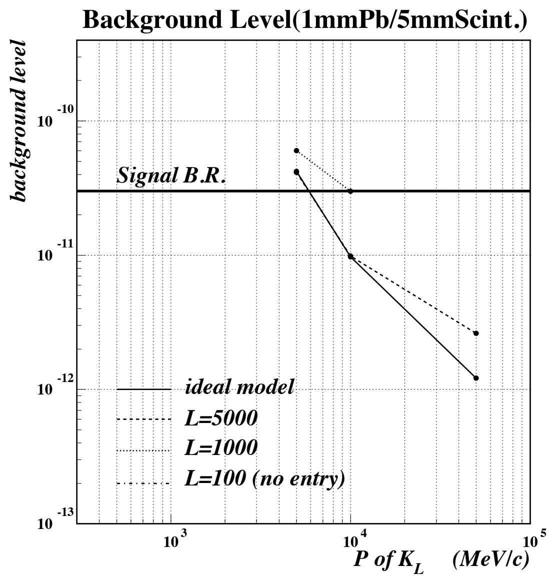

Figure 4.6: The background level after using finite detector in the simple case is shown as a function of P_{K_L}. The detector was assumed to be made of 1mmPb/ 5mmScint calorimeter.

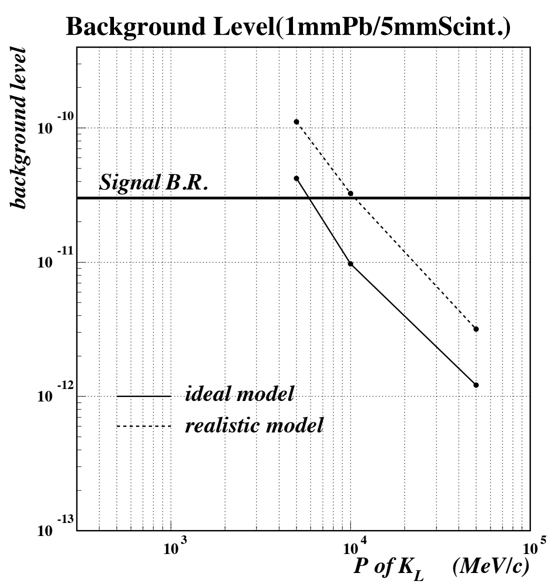

Figure 4.7: The background level for a detector with finite resolutions and length is shown as a function of P_{K_L}. The used conditions are ΔX=0.01, $\Delta E/E = 1\%/\sqrt{E(GeV)}$, and L=P_{K_L}/10MeV/c. The detector was assumed to be made of 1mmPb/ 5mmScint calorimeter.

4.2 Case where Decay Vertex is known

In this section, we will consider the case where we know the decay vertex in addition to gamma's energy and hit position in the calorimeter. Here, we assumed that we measure the decay vertex position by measuring the gamma's direction. Therefore, we studied the effect of the resolutions of gammas direction and energy, and the effect of having a finite detector length.

4.2.1 Smearing Gamma's direction

Here, we only smeared gamma's direction, while keeping the resolution of position to zero, and the detector length to infinite.

In order to measure the direction of gammas, we assumed a detector made of thin slabs as shown in Figure 4.8. In one of these slabs, the incident gamma converts into two electrons by a pair production. By measuring the direction of these electrons track, we can measure the direction of the incident gamma.

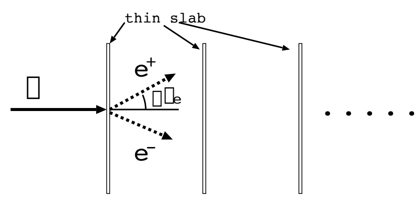

Figure 4.8: Schematic geometry for measuring the direction of gamma. We assumed to measure the direction of gammas by converting gamma to two electrons and measuring the direction of the electron track

The main contribution to the resolution of the direction of gamma is the multiple scattering of electrons in the first slab. The R.M.S. of multiple scattering angle of an electron converted half way into the slab, $\Delta\theta_e$, (Fig. 4.8) can be expressed as:

$$\Delta\theta_e \cong \frac{14MeV/c}{P_e}\sqrt{\frac{d}{2}} \tag{4.2}$$

where P_e is the momentum of electron in MeV/c and d is the thickness of the slab in radiation lengths. Since the direction of gamma is an average of the direction of two electrons, the error on the gammas direction, $\Delta\theta_\gamma$, can be written as

$$\begin{aligned}\Delta\theta_\gamma &= \frac{1}{\sqrt{2}}\Delta\theta_e && (4.3)\\ &\cong \frac{14MeV/c}{2\frac{E_\gamma}{2}}\sqrt{d} && (4.4)\\ &= \frac{14MeV/c}{E_\gamma}\sqrt{d} && (4.5)\end{aligned}$$

where E_γ is the energy of gamma in MeV, and we used the approximation of $E_\gamma \cong 2P_e$.

For θ(zenith angle) component of gammas direction, we smeared with following resolution,

$$\Delta\theta = \frac{b}{E_\gamma}, \tag{4.6}$$

where b is constant and corresponds to $14MeV/c \times \sqrt{d}$ in Equation(4.5).

On the other hand, the polar angle of gamma, ϕ, is measured by connecting the Z axis and the hit position in the calorimeter. Therefore the resolution of ϕ component is much smaller than θ resolution in general. We neglected ϕ component and considered θ components only.

Figure 4.9 shows the $m_{\gamma\gamma}$ distribution for signal events for b=5. As shown in this figure, by smearing gamma's direction, the mass peak of signal is also smeared. However, even if we used large b such as b=5, most of the signal events are within signal region.

Figure 4.10 shows the P_t distribution for background events for b=5. Similarly with the simple case, the edge at about 210MeV/c is smeared, affecting the signal region. This is the main reason why background level increases with a finite angular resolution for gamma.

Here, we studied two cases, b=1 and 5. These correspond to a slab thickness of 0.005 and 0.13 radiation lengths, respectively. Figure 4.11 shows the background level after smearing the direction of gammas. As shown in this figure, for K_L momentum of 5GeV/c $\sim$ 50GeV/c, the background levels for b=1 and b=5 are higher than the ideal model by a factor 1.7 $\sim$ 2.2 and 5.3 $\sim$ 7.4, respectively.

4.2.2 Smearing Gamma's Energy

Here, we smeared only gamma's energy, while keeping the resolution of gamma's direction to zero, and detector length to infinite.

A finite energy resolution affects the P_t distribution by smearing the edge at 210 MeV/c, and affects the invariant mass of two gammas by smearing the peak at pion mass.

Figure 4.12 shows the background levels for two cases, a=0.01 and 0.1. As shown in this figure, there is no difference between a=0.01 and ideal model, but a=0.1 increases the background levels by a factor 4$\sim$10 times from the ideal model.

4.2.3 Finite Detector Length

Here, we assumed that the detector has a finite length, instead of an infinite length. The resolutions of energy and direction of gamma are assumed to be perfect.

We used the two types of detectors, L=100, and 1000. Figure 4.13 shows the background levels for the two different detector lengths. If L=100, we cannot achieve $\Delta\eta/\eta$=10% with any cut for 500MeV/c $\leq P_{K_L} \leq$ 10GeV/c and 50GeV/c. For L=1000, we can see that at high K_L momentum the background level jumps up. This is because most of gammas escape the detector.

The acceptances for a detector with a finite length is shows in Table 4.3.

4.2.4 Realistic model

At the end, we simulated a realistic experiment by choosing a set of detector resolutions and length.

From the same reason as in the simple case, we chose $L = P_{K_L}/10MeV/c$ as detector length. We chose direction resolution of $\Delta\theta = 1/E$ and the energy resolution of $\Delta E/E = 1\%/\sqrt{E(GeV)}$.

Figure 4.14 shows the background levels for the realistic model. The background level for the realistic model is 2.7$\sim$3.3 larger than that of ideal model. With this condition, we can achieve our goal if K_L momentum is greater than 5GeV/c. If K_L momentum is 10GeV/c, the number of signal events is 4.7 times greater than that of background events.

The acceptances for the realistic model are shows in Table 4.4.

K_L momentum =500MeV/c

L	Acceptance for signal	Acceptance for background
ideal model	0.36	5.9×10^{-8}
1000	0.37	6.1×10^{-8}

K_L momentum =1GeV/c

L	Acceptance for signal	Acceptance for background
ideal model	0.44	9.2×10^{-8}
1000	0.45	9.5×10^{-8}

K_L momentum =5GeV/c

L	Acceptance for signal	Acceptance for background
ideal model	0.070	2.8×10^{-10}
1000	0.070	2.8×10^{-10}
100	0.26	2.8×10^{-8}

K_L momentum =10GeV/c

L	Acceptance for signal	Acceptance for background
ideal model	0.064	1.2×10^{-10}
1000	0.064	1.3×10^{-10}

K_L momentum =50GeV/c

L	Acceptance for signal	Acceptance for background
ideal model	0.064	1.6×10^{-11}
1000	0.076	6.2×10^{-10}

Table 4.3: Acceptance for signal and background using a finite length detector in the case where vertex is known. We used K_L momentum of 500MeV/c, 1GeV/c, 5GeV/c, 10GeV/c, and 50GeV/c, respectively. The detector was assumed to be made of 1mmPb/ 5mmScint calorimeter.

K_L momentum =5GeV/c

case	Acceptance for signal	Acceptance for background
ideal model	0.070	2.8×10^{-10}
realistic model	0.082	8.7×10^{-10}

K_L momentum =10GeV/c

case	Acceptance for signal	Acceptance for background
ideal model	0.064	1.2×10^{-10}
realistic model	0.075	5.3×10^{-10}

K_L momentum =50GeV/c

case	Acceptance for signal	Acceptance for background
ideal model	0.064	1.6×10^{-11}
realistic model	0.065	5.2×10^{-11}

Table 4.4: Acceptance for the signal and background for the ideal and realistic models in the case where vertex is known. The realistic model uses a detector with $L = P_{K_L}/10MeV/c$, $\Delta\theta = 1/E(MeV)$, and $\Delta E/E = 1\%/\sqrt{E(GeV)}$. We studied K_L momentum of 5GeV/c, 10GeV/c, and 50GeV/c. The detector was assumed to be made of 1mmPb/ 5mmScint calorimeter.

4.2.5 Summary

We have studied the effect of finite detector resolutions and length in the case where we know decay vertex in addition to the gamma's energy and position.

Finite resolutions on gamma energy and direction measurements smears P_t and $m_{\gamma\gamma}$ distributions.

Smearing gammas direction with $\Delta\theta = 1/E$ increases the background level by a factor $1.7 \sim 2.2$ from the ideal model. Smearing gammas energy with $\Delta E/E = 1\%/\sqrt{E(GeV)}$ dose not change the background level from the ideal model. Using finite detection length with $L = P_{K_L}/10MeV/c$ dose not change the background level from the ideal model.

As shown in Figure 4.14, if we prepared a detector with the following specifications, we can achieve our goal of measuring η with a 10% error with S/N$\geq$1.

- K_L momentum: $P_{K_L} \geq$5GeV/c
- gammas energy resolution: $\Delta E/E = 1\%/\sqrt{E(GeV))}$
- gammas direction resolution: $\Delta\theta = 1/E(MeV)$ (corresponding to using the thin slab of 0.005 radiation lengths)
- Detector length: $L = P_{K_L}/$10MeV/c for a detector radius of '1'

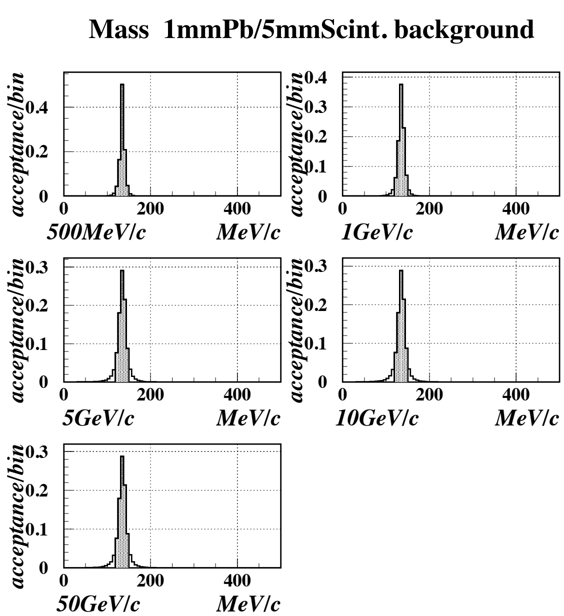

Figure 4.9: Two gammas mass distribution after smearing gammas direction by b=5 for $K_L \rightarrow \pi^0\nu\bar{\nu}$ in the case vertex is known. K_L momenta are 500MeV/c, 1GeV/c, 5GeV/c, 10GeV/c, and 50GeV/c. The detector is assumed to be made of 1mmPb/ 5mmScint calorimeter.

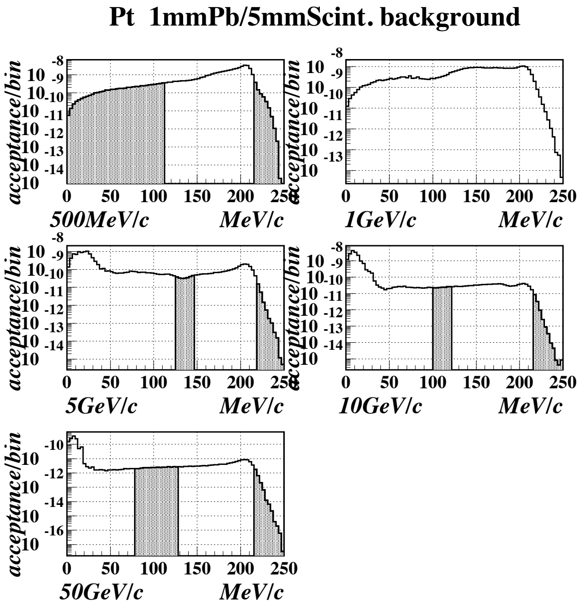

Figure 4.10: P_t distribution after smearing gammas direction by b=5 for $K_L \rightarrow \pi^0\pi^0$ in the case where vertex is known. K_L momenta are 500MeV/c, 1GeV/c, 5GeV/c, 10GeV/c, and 50GeV/c. The detector is assumed to be made of 1mmPb/ 5mmScint calorimeter.

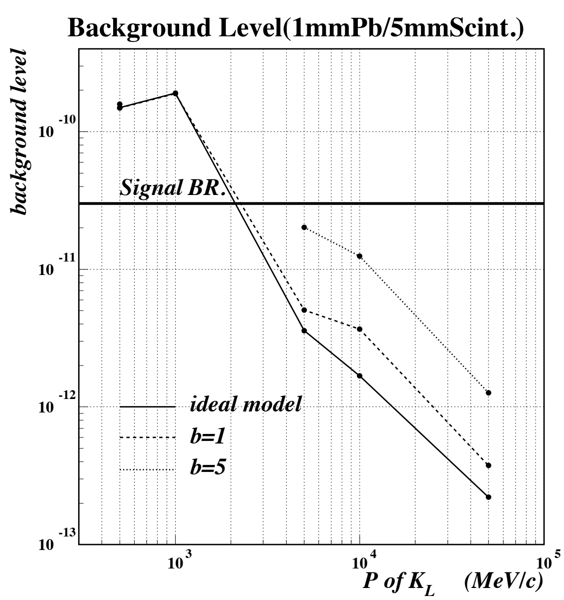

Figure 4.11: The background level after smearing gammas direction in case where vertex is known. The detector was assumed to be made of 1mmPb/ 5mmScint calorimeter. The background level for 1GeV/c on b=5 does not exist, because $\Delta\eta/\eta$=10% was not achieved with any cuts.

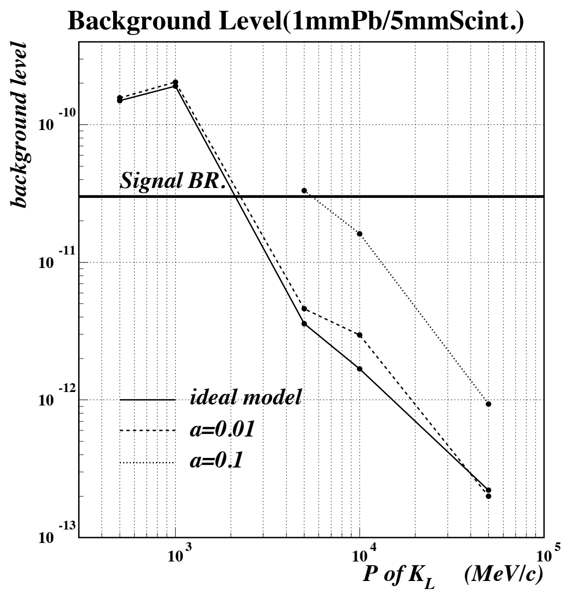

Figure 4.12: The background level after smearing gammas energy in the case where vertex is known. The detector was assumed to be made of 1mmPb/ 5mmScint calorimeter.

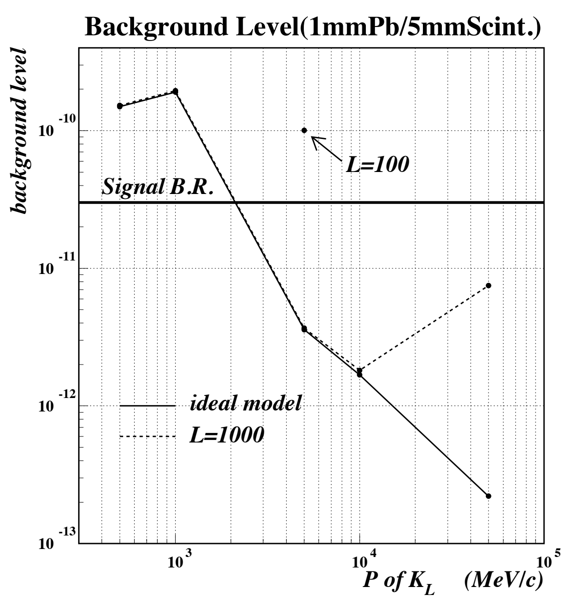

Figure 4.13: The background level after using finite length detector in case where vertex is known. The detector was assumed to be made of 1mmPb/ 5mmScint calorimeter.

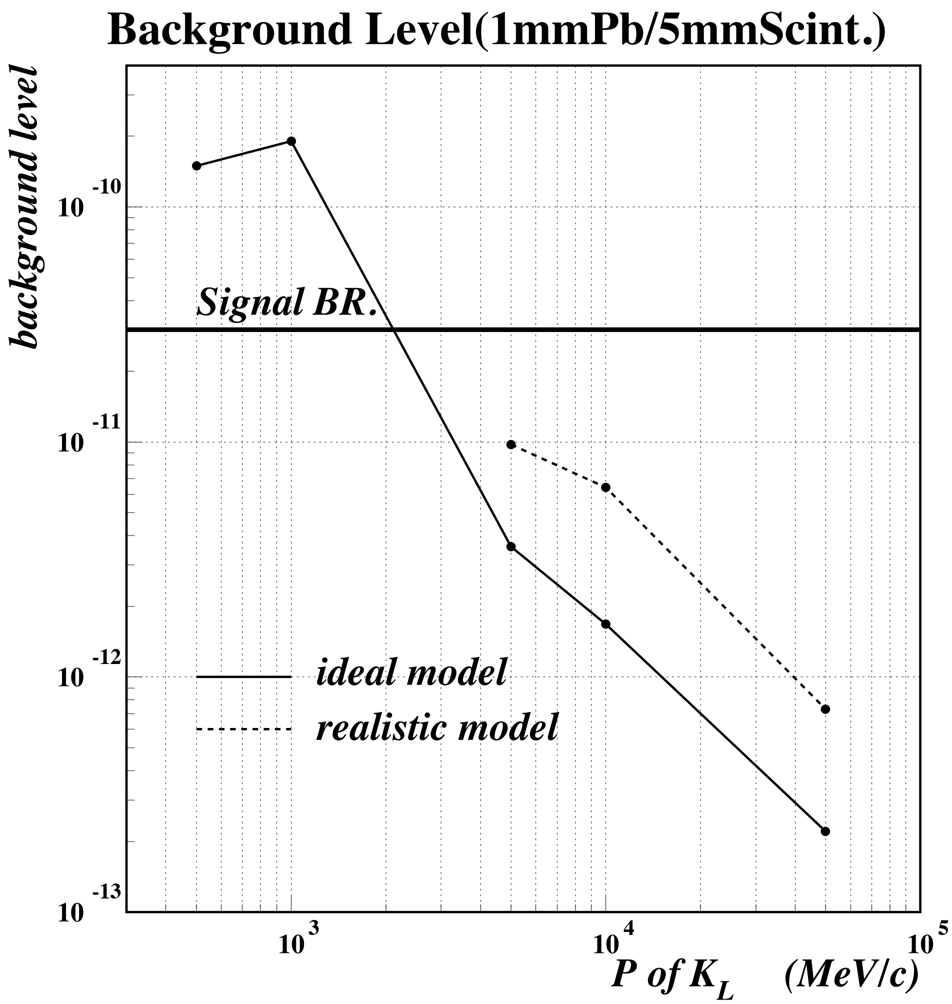

Figure 4.14: The background level for a realistic model in the case where vertex is known. The conditions are $\Delta E/E = 1\%/\sqrt{E(GeV)}$, $\Delta\theta = 1/E(MeV)$, and $L{=}E_{K_L}/10\text{MeV}$. The detector was assumed to be made of 1mmPb/ 5mmScint calorimeter.

4.3 Case where E_{K_L} is known

In this section, we will considered the case where we know the K_L energy in addition to the gamma's energy and hit position in the calorimeter. Therefore we studied the effect of the resolutions of kaon energy, gammas position and energy, and an effect of having a finite detector length.

In the ideal case, since the peak of even pair background is monochromatic, we made a universal cut on the missing mass ($M_{\pi^0} \pm 10MeV/c^2$), and further we used 'missing mass VS. $E_{\gamma\gamma}$' cut whose signal region was optimized. However, with a realistic model, the missing mass for the even pair background is smeared, so we unified the both cuts, and simply cut on the missing mass VS.$E_{\gamma\gamma}$. However, when we only varied the detector length, missing mass peak was not smeared, so we use the cut on the missing mass as in the simple case.

4.3.1 Smearing Kaons Energy

We only smeared the K_L energy with a Gaussian, while the resolutions of gamma's position and energy were kept zero, and the detector length was still kept infinite. Here we simply examined $\Delta E_{K_L}/E_{K_L}=$ 10% and 1%.

Figure 4.15 and 4.16 show the correlation between the missing mass and two gamma's energy for $\Delta E_{K_L}/E_{K_L}=$ 1%. As shown in these figures (especially 500MeV/c), the optimized cut removes the even pair background events in the region around $M_{\pi^0}^2 \cong 18225(\text{MeV}/c^2)^2$.

Figure 4.17 shows these background levels after smearing K_L energy. With $\Delta E_{K_L}/E_{K_L}=$ 1%, there is no difference from the ideal model, but with $\Delta E_{K_L}/E_{K_L}=$ 10%, the background levels increases by a factor 1.6$\sim$2.3 from the ideal model.

4.3.2 Smearing Gammas Energy

Here, we only smeared gamma's energy with a Gaussian, while the resolutions of kaon energy and gamma's position were kept zero, and the detector length was still kept infinite.

We studied two energy resolutions for gamma, a=0.01 and 0.1(Equation(4.1)). Figure 4.18 shows the background levels after smearing gamma's energy.

For a=0.01 and 0.1, the background levels increase by a factor $\sim$2.2 and 1.5$\sim$5.2, respectively. This factor is larger for lower K_L momentum.

4.3.3 Smearing Gammas Position

Here, we only smeared gamma's position with a Gaussian, while the resolutions of kaon energy and gamma's energy were kept zero, and the detector length was still kept infinite.

We studied two energy resolutions for gamma, ΔX=0.01 and 0.1. Figure 4.19 shows the background levels after smearing gamma's position.

For ΔX=0.01 and 0.1, the background levels increase by a factor $\sim$1.5 and 1.5$\sim$2.4, respectively.

4.3.4 Finite Detector Length

Here, we assumed that the detector has a finite length, instead of an infinite length. The resolutions of energies and position are assumed to be perfect.

We prepared two types of detectors, L=100, 1000. Figure 4.20 shows the background levels for two difference detector lengths. The acceptances for different detector lengths are shown in Table 4.5.

K_L momentum =500MeV/c

L	Acceptance for signal	Acceptance for background
ideal model	0.14	6.2×10^{-9}
1000	0.14	6.4×10^{-9}
100	0.24	2.4×10^{-8}

K_L momentum =1GeV/c

L	Acceptance for signal	Acceptance for background
ideal model	0.066	2.3×10^{-10}
1000	0.067	2.7×10^{-10}
100	0.26	2.9×10^{-8}

K_L momentum =5GeV/c

L	Acceptance for signal	Acceptance for background
ideal model	0.061	3.4×10^{-11}
1000	0.070	4.1×10^{-10}
100	0.14	6.0×10^{-9}

K_L momentum =10GeV/c

L	Acceptance for signal	Acceptance for background
ideal model	0.061	5.7×10^{-11}
1000	0.064	1.6×10^{-10}

K_L momentum =50GeV/c

L	Acceptance for signal	Acceptance for background
ideal model	0.060	1.4×10^{-11}
1000	0.061	5.2×10^{-11}

Table 4.5: Acceptance for the signal and background using a finite length detector in the case where E_{K_L} are known. The 1mmPb/5mmScint sampling calorimeter was used as the photon counter.

4.3.5 Realistic model

At the end, we simulated a realistic experiment by choosing a set of detector resolutions and a length.

For the reason explained in Section 4.1.4, we chose $L = P_{K_L}/10MeV/c$ as the detector length. The resolution of K_L energy was chosen to be $\Delta E_{K_L}/E_{K_L}$=5%, since BNL [8] is planing to measure E_{K_L} with an error of a few percent. We chose a direction resolution of $\Delta X = 0.01$ and the energy resolution of $\Delta E/E = 1\%/\sqrt{E(GeV)}$.

Figure 4.21 shows the background levels for the realistic model. The background levels for a realistic model is lager than those for the ideal model by a factor 3.5~31. With this condition, we can achieve our goal even if K_L momentum is greater than 5GeV/c. This background level is almost the same as the background in the case where decay vertex is known.

The acceptances for these realistic cases are shown in Table 4.6.

K_L momentum =5GeV/c

L	Acceptance of signal	Acceptance of background
ideal model	0.061	3.4×10^{-11}
realistic model	0.091	1.6×10^{-9}

K_L momentum =10GeV/c

L	Acceptance of signal	Acceptance of background
ideal model	0.061	5.7×10^{-11}
realistic model	0.067	2.6×10^{-10}

K_L momentum =50GeV/c

L	Acceptance of signal	Acceptance of background
ideal model	0.060	1.4×10^{-11}
realistic model	0.061	5.1×10^{-11}

Table 4.6: Acceptance for the signal and background for the ideal and realistic models in the case where K_L energy are known. The realistic model uses a detector with $L = P_{K_L}/10MeV/c$, $\Delta E_{K_L}/E_{K_L} = 0.05$, $\Delta X = 0.01$, and $\Delta E/E = 1\%/\sqrt{1E(GeV)}$. The detector was assumed to be made of 1mmPb/ 5mmScint calorimeter.

4.3.6 Summary

We have studied the effect of finite detector resolutions and length in the case where we know K_L energy in addition to the gamma's energy and position.

Smearing the K_L energy with $\Delta E_{K_L}/E_{K_L}$=10% increases the background level by a factor 1.6∼2.3 from the ideal model. Smearing gamma's energy with $\Delta E/E = 1\%/\sqrt{E(GeV)}$ increases the background level by a factor ∼2.2 from the ideal model. Smearing gamma's position with $\Delta X = 0.01$ increases the background level by a factor ∼1.5 from the ideal model.

As shown in Figure 4.21, if we prepared a detector with the following specifications, we can achieve our goal of measuring η with a 10% error with S/N≥1.

- K_L momentum: $P_{K_L} \geq$5GeV/c
- K_L energy resolution: $\Delta E_{K_L}/E_{K_L} = 0.05$
- gammas energy resolution: $\Delta E/E = 1\%/\sqrt{E(GeV))}$
- gammas position resolution: $\Delta X = 0.01$ for a detector radius of '1'.
- Detector length: $L = P_{K_L}/$10MeV/c for a detector radius of '1'.

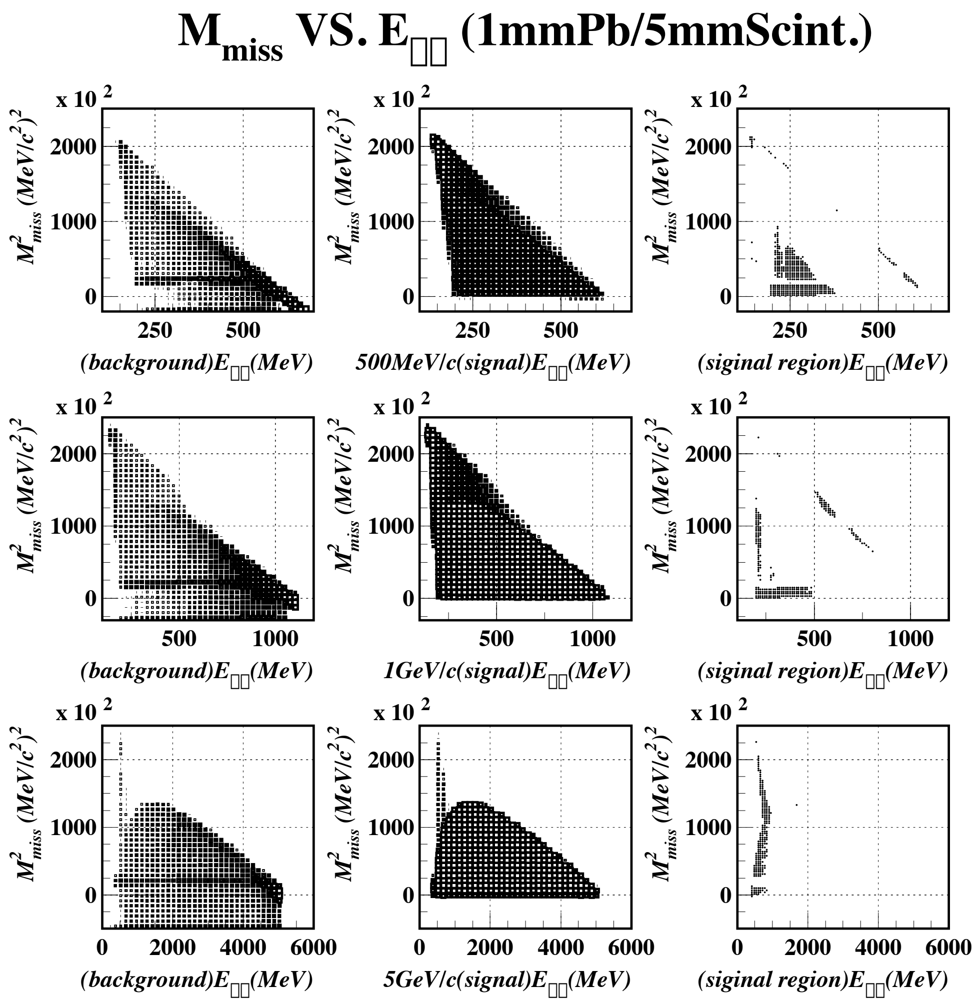

Figure 4.15: Missing mass VS. $E_{\gamma\gamma}$ for the K_L momentum of 500MeV/c, 1GeV/c, and 5GeV/c in the case where E_{K_L} is known. The 1mmPb/5mmScint sampling calorimeter was used as the photon counter. We smeared the K_L energy by 1% in sigma. The left row shows the distribution for the background, and the center row shows the distribution for the signal. The right row shows the signal region selected by the method described in the text.

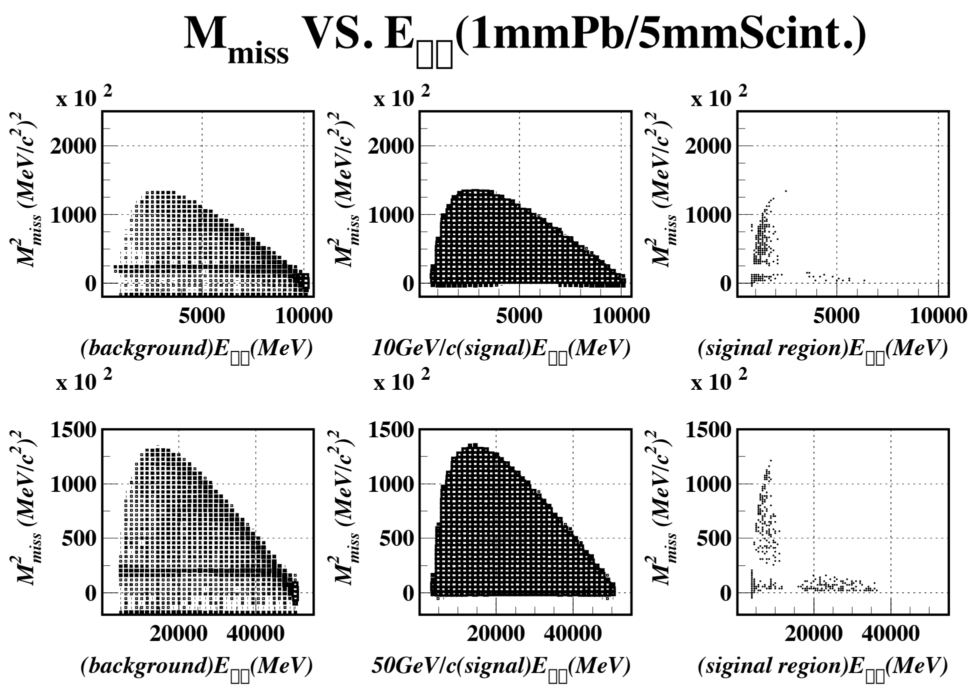

Figure 4.16: Missing mass VS. $E_{\gamma\gamma}$ for the K_L momentum of 10GeV/c, and 50GeV/c in the case where E_{K_L} is known. The 1mmPb/5mmScint sampling calorimeter was used as the photon counter. We smeared the K_L energy by 1% in sigma. The left row shows the distribution for the background, and the center row shows the distribution for the signal. The right row shows the signal region selected by the method described in the text.

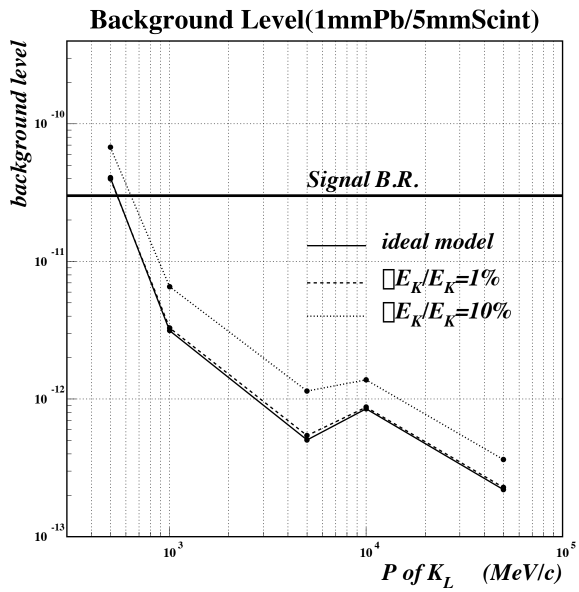

Figure 4.17: Background level after smearing the K_L energy with $\Delta E_{K_L}/E_{K_L} = 1\%$ and 10% in the case where E_{K_L} is known. The 1mmPb/5mmScint sampling calorimeter was used as the photon counter.

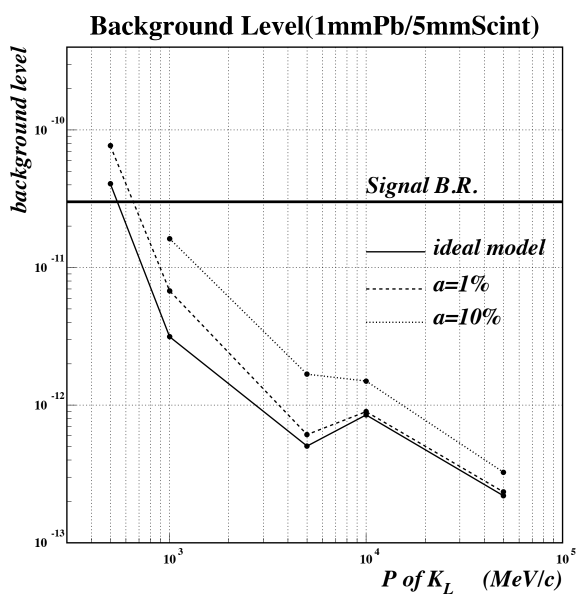

Figure 4.18: Background level after smearing gammas energy with a=1% and 10% in the case where E_{K_L} is known. The 1mmPb/5mmScint sampling calorimeter was used as the photon counter. The background level at 500MeV for a=0.1 does not exist, because $\Delta\eta/\eta$ can not reach 10% with any cut region.

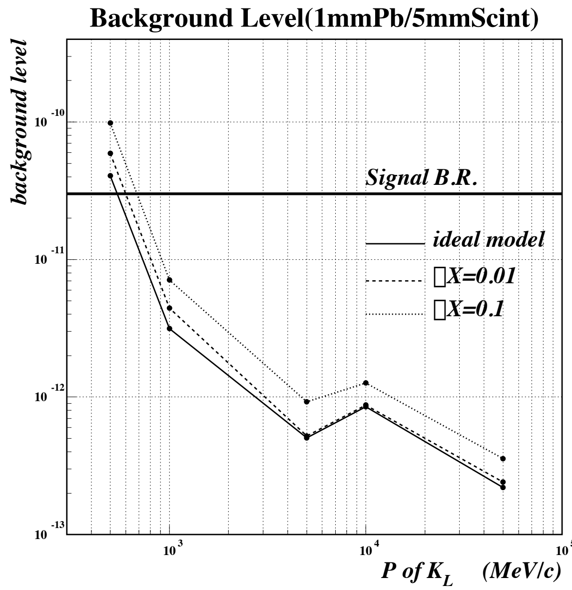

Figure 4.19: Background level after smearing gammas position with ΔX=0.01 and 0.1 in the case where E_{K_L} are known. The 1mmPb/5mmScint sampling calorimeter was used as the photon counter.

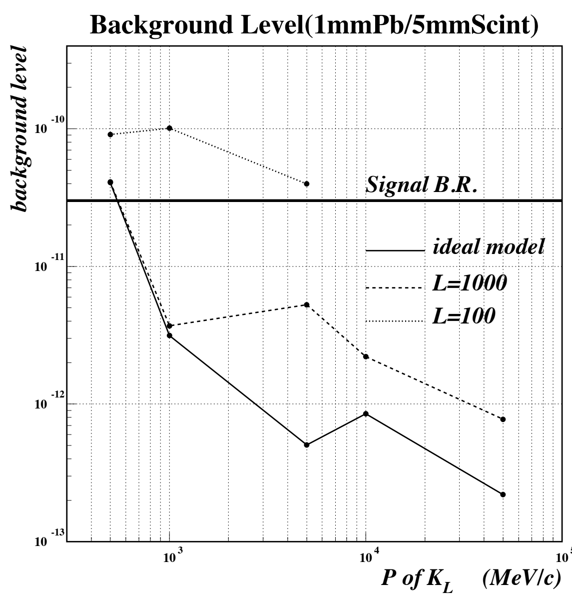

Figure 4.20: Background level for a detector with a finite length(L =100 and 1000) in the case where E_{K_L} is known. The 1mmPb/5mmScint sampling calorimeter was used as the photon counter. The background level at 10GeV/c and 50GeV/c in L=100 are absent, because most of gammas escape the detector.

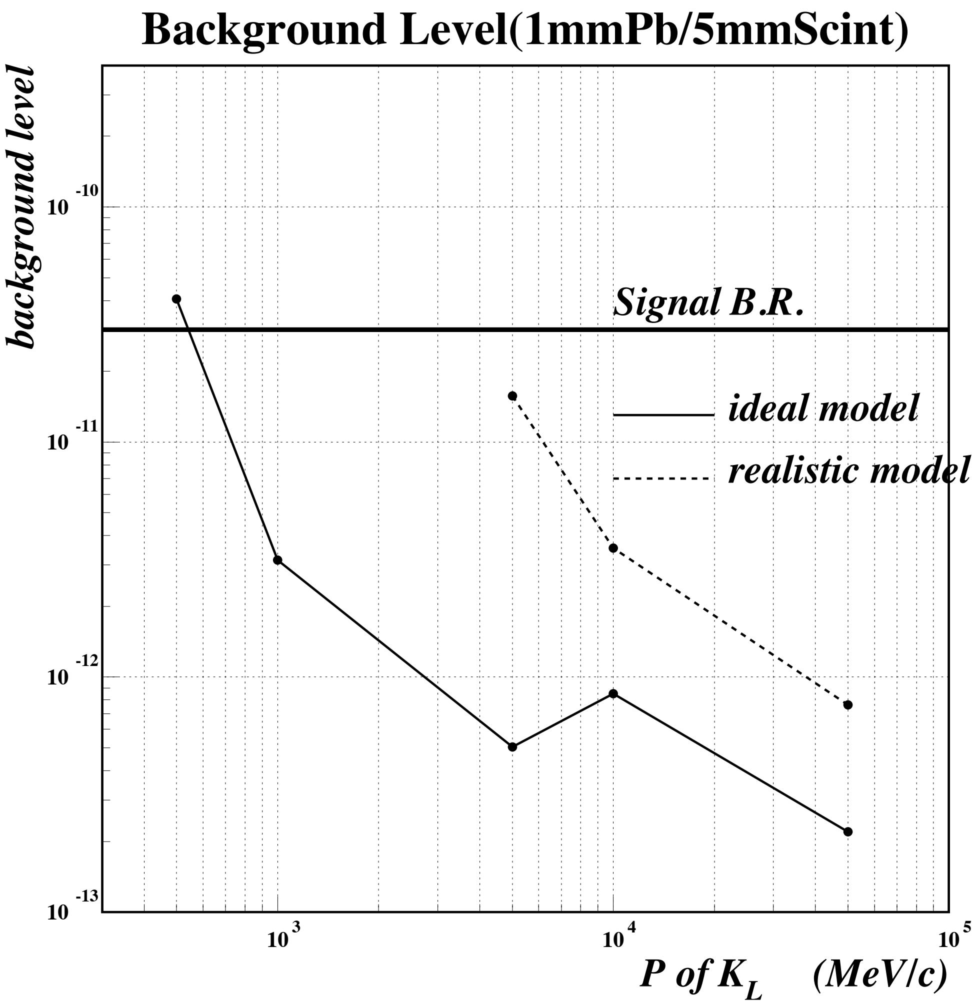

Figure 4.21: Background level for a realistic detector with a finite length and finite resolutions in the case where K_L energy are known. The conditions are $\Delta E_{K_L}/E_{K_L}$=5%, a=0.01, ΔX=0.01, and L=P_{K_L}/10MeV/c. The 1mmPb/5mmScint sampling calorimeter was used as the photon counter.

4.4 Case where Vertex and E_{K_L} are known

In this section, we will consider the case where we know decay vertex and K_L energy in addition to the gamma's energy and hit position in the calorimeter. Therefore we studied the effect of the resolutions of kaon energy, gammas direction and energy, and an effect of having a finite detector length.

For the reason described in the previous section, we unified the cut on missing mass and the cut on missing mass VS. $E_{\gamma\gamma}$, and simply cut on the missing mass VS. $E_{\gamma\gamma}$ besides two gammas mass. When we varied the detector length only, we use the cut on the missing mass as in the simple case.

4.4.1 Smearing Kaon energy

Here, we only smeared the K_L energy with a Gaussian, while the resolutions of gamma's direction and energy were kept zero, and the detector length was still kept infinite. Here we simply examined $\Delta E_{K_L}/E_{K_L}$= 10% and 1%.

Figure 4.22 and 4.23 show the correlation between the missing mass and two gamma's energy for $\Delta E_{K_L}/E_{K_L}$= 1%. As shown in these figures, the optimized cut removes the even pair background events in the region around $M^2_{\pi^0} \cong 18225(\mathrm{MeV}/c^2)^2$. By smearing the K_L energy, some events flow into $M^2_{miss} < 0$ region.

Figure 4.24 shows the background levels after smearing K_L energy. With $\Delta E_{K_L}/E_{K_L}$= 1%, there is no difference from the ideal model, but with $\Delta E_{K_L}/E_{K_L}$= 10%, the background levels increase by a factor 3.2$\sim$20.6 from the ideal model.

4.4.2 Smearing the Gamma's energy

Here, we only smeared gamma's energy with a Gaussian, while the resolutions of kaon energy and gamma's direction were kept zero, and the detector length was still kept infinite.

We studied two energy resolutions for gamma, a=0.01 and 0.1(Equation(4.1)). Figure 4.25 shows the background levels after smearing gamma's energy.

For a=0.01 and 0.1, the background levels increase by a factor 1.4$\sim$2.9 and 2$\sim$100, respectively. This factor is larger for lower K_L momentum.

4.4.3 Smearing Gamma's direction

Here, we only smeared gamma's direction, while keeping the resolutions of K_L energy, gamma's energy were to zero, and the detector length to infinite.

We studied two case for gamma's direction, b=1 and 5. Figure 4.26 shows the background level after smearing gamma's direction. For b=1 and 5, the background levels increase by a factor 1.1$\sim$3.1 and 2.2$\sim$9.3, respectively, from the ideal model.

4.4.4 Finite Detector Length

Here, we assumed that the detector has a finite length, instead of an infinite length. The resolutions of energies and direction are assumed to be perfect.

We prepared three types of detectors, L=50, 100, 1000. Figure 4.27 shows the background levels for three difference detector lengths. As shown in this figure, the influence of the detector length is smaller than in the simple case. This is because 'Missing mass VS. $E_{\gamma\gamma}$ Cut' suppresses the background caused by shortening detector length.

The acceptances for different detector lengths are shown in Table 4.7.

K_L momentum =500MeV/c

L	Acceptance for signal	Acceptance for background
ideal model	0.062	7.5×10^{-11}
1000	0.062	7.6×10^{-11}
100	0.063	1.2×10^{-10}
50	0.063	1.4×10^{-10}

K_L momentum =1GeV/c

L	Acceptance for signal	Acceptance for background
ideal model	0.060	6.8×10^{-12}
1000	0.060	7.5×10^{-12}
100	0.060	1.1×10^{-11}
50	0.060	1.4×10^{-11}

K_L momentum =5GeV/c

L	Acceptance for signal	Acceptance for background
ideal model	0.060	2.7×10^{-13}
1000	0.060	4.6×10^{-13}
100	0.060	8.4×10^{-13}
50	0.060	2.2×10^{-12}

K_L momentum =10GeV/c

L	Acceptance for signal	Acceptance for background
ideal model	0.060	3.7×10^{-14}
1000	0.060	9.6×10^{-14}
100	0.060	4.6×10^{-13}
50	0.083	1.1×10^{-9}

K_L momentum =50GeV/c

L	Acceptance for signal	Acceptance for background
ideal model	0.060	8.4×10^{-15}
1000	0.060	1.2×10^{-14}

Table 4.7: Acceptance for the signal and background using a finite length detector in the case where vertex and E_{K_L} are known. The 1mmPb/5mmScint sampling calorimeter was used as the photon counter.

4.4.5 Realistic model

At the end, we simulated a realistic experiment by choosing a set of detector resolutions and a length.

For the reason explained in Section 4.1.4, we chose $L = P_{K_L}/10MeV/c$ as the detector length. We chose a K_L energy resolution of $\Delta E_{K_L}/E_{K_L} = 5\%$, a direction resolution of $\Delta\theta = 1/E(MeV)$, and the energy resolution of $\Delta E/E = 1\%/\sqrt{E(GeV)}$.

Figure 4.28 shows the background levels for the realistic model. The background levels for a realistic model is lager than those for the ideal model by a factor 4.4∼25.4. With this condition, we can achieve our goal even with low K_L momentum of 500MeV/c. The S/N ratio at this momentum is 6.2. For higher K_L momentum, we do not need background level as low as $< O(10^{-13})$. Therefore we can measure η with a better accuracy by loosening the cut region to collect more signal events, while allowing the background level to increase.

The acceptances for these realistic cases are shown in Table 4.8.

4.4.6 Summary

We have studied the effect of finite detector resolutions and length in the case where we know the decay vertex and K_L energy in addition to the gamma's energy and position.

Smearing the K_L energy with $\Delta E_{K_L}/E_{K_L}$=10% increases the background level by a factor 3.2 ∼ 20.6 from the ideal model. Smearing gamma's energy with $\Delta E/E = 1\%/\sqrt{E(GeV)}$ increases the background

K_L momentum =500MeV/c

L	Acceptance of signal	Acceptance of background
ideal model	0.062	7.5×10^{-11}
realistic model	0.069	3.7×10^{-10}

K_L momentum =1GeV/c

L	Acceptance of signal	Acceptance of background
ideal model	0.060	6.8×10^{-12}
realistic model	0.063	1.2×10^{-10}

K_L momentum =5GeV/c

L	Acceptance of signal	Acceptance of background
ideal model	0.060	2.7×10^{-13}
realistic model	0.060	4.2×10^{-12}

K_L momentum =10GeV/c

L	Acceptance of signal	Acceptance of background
ideal model	0.060	3.7×10^{-14}
realistic model	0.060	9.5×10^{-13}

K_L momentum =50GeV/c

L	Acceptance of signal	Acceptance of background
ideal model	0.060	8.4×10^{-15}
realistic model	0.060	9.7×10^{-14}

Table 4.8: Acceptance for the signal and background for the ideal and realistic models in the case where vertex and K_L energy are known. The realistic model uses a detector with $L = P_{K_L}/10MeV/c$, $\Delta E_{K_L}/E_{K_L} = 0.05$, $\Delta\theta = 1/E(MeV)$, and $\Delta E/E = 1\%/\sqrt{1E(GeV)}$. We studied K_L momentum of 500MeV/c, 1GeV/c, 5GeV/c, 10GeV/c, and 50GeV/c. The detector was assumed to be made of 1mmPb/ 5mmScint calorimeter.

level by a factor $1.4 \sim 2.9$ from the ideal model. Smearing gamma's direction with $\Delta\theta = 1/E(MeV)$ increases the background level by a factor $1.1 \sim 3.1$ from the ideal model.

As shown in Figure 4.28, if we prepared a detector with the following specifications, we can achieve our goal of measuring η with a 10% error and $S/N \geq 1$

- K_L momentum: P_{K_L} ≥500MeV/c
- K_L energy resolution: $\Delta E_{K_L}/E_{K_L}$=0.05
- gammas energy resolution: $\Delta E/E = 1\%/\sqrt{E(GeV)}$
- gammas direction resolution: $\Delta\theta = 1/E(MeV)$ (corresponding to using the thin slabs of 0.005 radiation lengths each)
- Detector length; $L = P_{K_L}$/10MeV/c for a detector radius of '1'

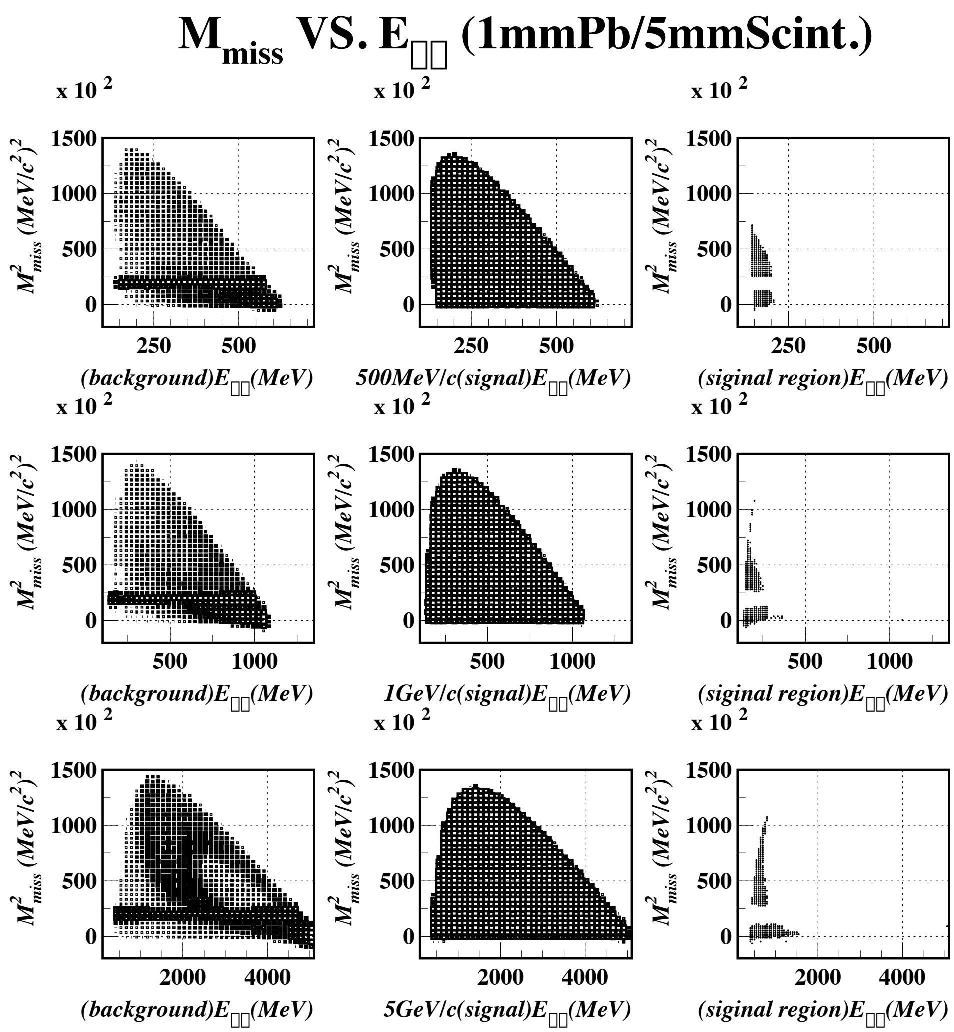

Figure 4.22: Missing mass VS. $E_{\gamma\gamma}$ for the K_L momentum of 500MeV/c, 1GeV/c, and 5GeV/c in the case where vertex and E_{K_L} are known. The 1mmPb/5mmScint sampling calorimeter was used as the photon counter. We smeared the K_L energy by 1% in sigma. The left row shows the distribution for the background, and the center row shows the distribution for the signal. The right row shows the signal region selected by the method described in the text.

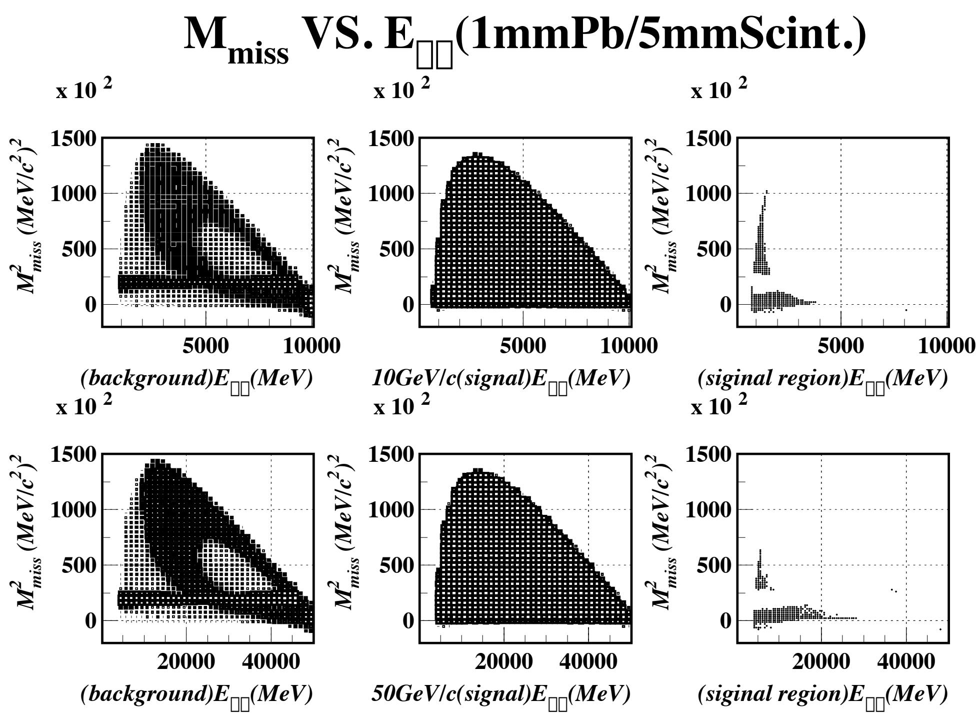

Figure 4.23: Missing mass VS. $E_{\gamma\gamma}$ for the K_L momentum of 10GeV/c, and 50GeV/c in the case where vertex and E_{K_L} are known. The 1mmPb/5mmScint sampling calorimeter was used as the photon counter. We smeared the K_L energy by 1% in sigma. The left row shows the distribution for the background, and the center row shows the distribution for the signal. The right row shows the signal region selected by the method described in the text.

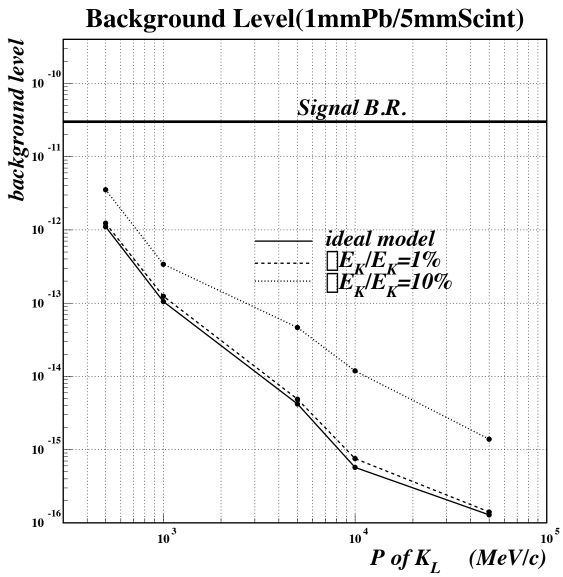

Figure 4.24: Background level after smearing the K_L energy with $\Delta E_{K_L}/E_{K_L} = 1\%$ and 10% in the case where vertex and E_{K_L} are known. The 1mmPb/5mmScint sampling calorimeter was used as the photon counter.

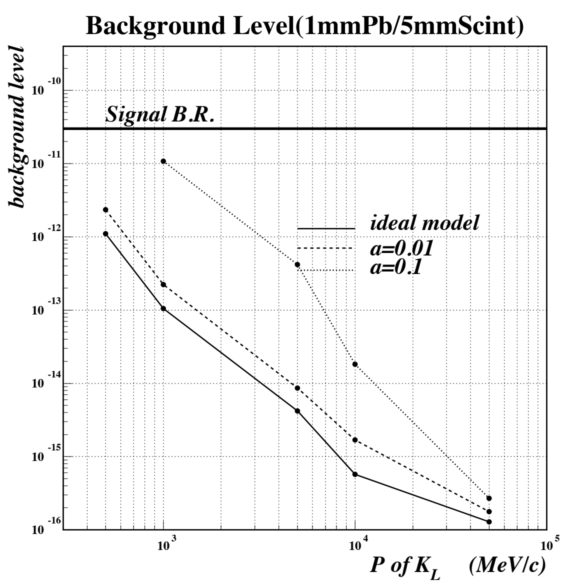

Figure 4.25: Background level after smearing gammas energy with a=1% and 10% in the case where vertex and E_{K_L} are known. The 1mmPb/5mmScint sampling calorimeter was used as the photon counter. The background level at 500MeV for a=0.1 does not exist, because $\Delta\eta/\eta$ can not reach 10% with any cut region.

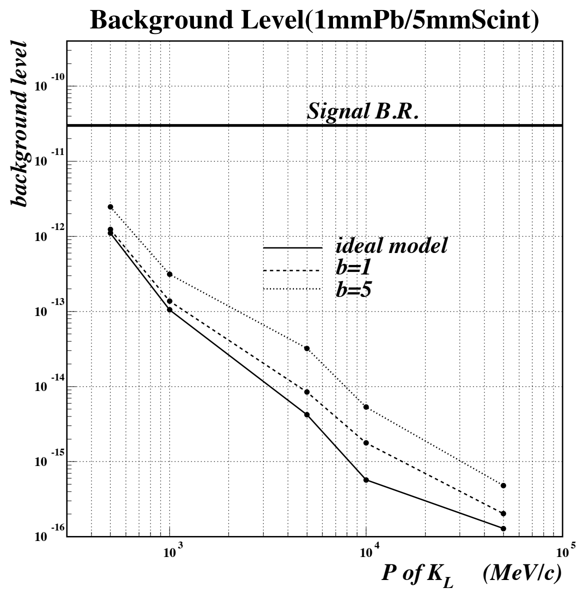

Figure 4.26: Background level after smearing gammas direction with b=1 and 5 in the case where vertex and E_{K_L} are known. The 1mmPb/5mmScint sampling calorimeter was used as the photon counter.

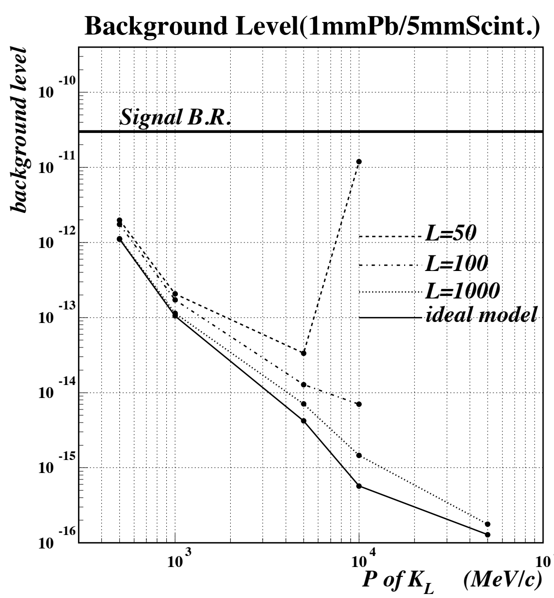

Figure 4.27: Background level for a detector with a finite length in the case where vertex and E_{K_L} are known. The 1mmPb/5mmScint sampling calorimeter was used as the photon counter. The background level at 50GeV in L=50 and L=100 are absent, because most of gammas escape the detector.

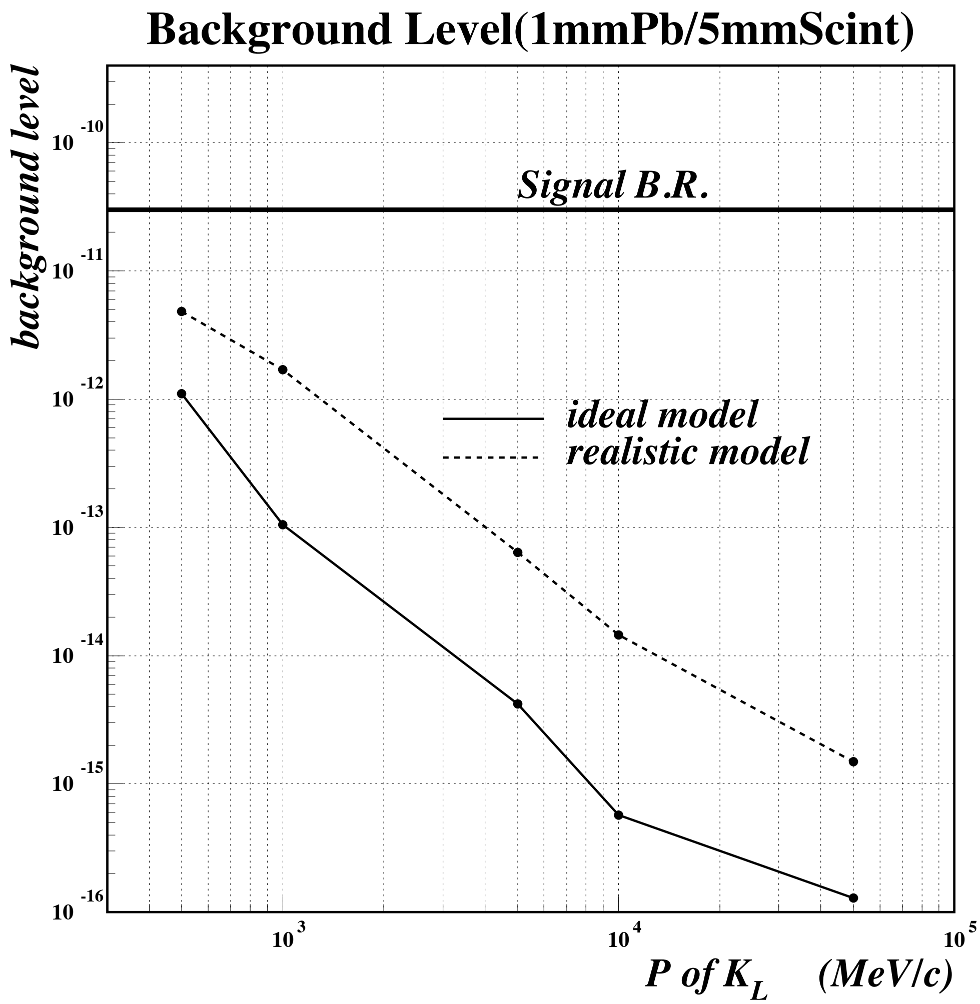

Figure 4.28: Background level for a realistic detector with a finite length and finite resolutions in the case where vertex and K_L energy are known. The conditions are $\Delta E_{K_L}/E_{K_L}$=5%, a=0.01, b=1, and L=P_{K_L}/10MeV. The 1mmPb/5mmScint sampling calorimeter was used as the photon counter.

Chapter 5

Discussion

5.1 Examination of Experiments

In this section, based on our results we will examine the main experiments which are being planned currently.

5.1.1 BNL

Brookhaven National Laboratory (BNL) KOPIO experiment[8] is proposing to measure K_L energy and decay vertex by measuring the time of flight (TOF) of K_L and the direction of gamma. In order to measure the K_L momentum by TOF, they plan to use a K_L beam with a low momentum around 700 MeV/c.

As shown in Fig. 4.28, at 700MeV/c, the background level is about 3×10^{-12}. However, BNL is proposing to use Pb/Scinti sampling calorimeter as calorimeter, but it is very difficult to achieve a gammas energy resolution of $\Delta E/E = 1\%/\sqrt{E(GeV)}$. If we assume the energy resolution of $\Delta E/E = 10\%/\sqrt{E(GeV)}$ for Pb/Scinti detector, Fig. 4.25 shows that the background level increases by a factor $\cong$100 from the ideal model. Therefore the background level with Pb/Scinti detector is expected to be about 3×10^{-10}, which means, S/N is 0.1. Therefore, it is very difficult to measure η with a 10% error. In order to measure $K_L \to \pi^0 \nu \bar{\nu}$ in this K_L energy, they probably have to use a better calorimeter such as CsI.

5.1.2 KAMI

KAMI (Kaons At the Main Injector) experiment [9] is planning to use high momentum K_L beam with typical momentum of 13 GeV/c. They are planing to measure only gamma's energy and position.

As shown in Fig. 4.7, at 13GeV/c, the background level is about 2.2×10^{-11}, that is, S/N is about 1.4. However, KAMI is proposing to use CsI as a calorimeter, and CsI has better detection inefficiency than Pb/Scint sampling calorimeter. Therefore we expect the that the S/N ratio in KAMI is less than 1. If KAMI also measures the direction of gammas, the background level reduces to about 4.5×10^{-12} as shown in Figure 4.14 where S/N ratio is about 6. Since KAMI use CsI as a calorimeter, the background level and S/N should be even less. This would allow them to make a clean measurement of the branching ratio of $K_L \to \pi^0 \nu \bar{\nu}$.

5.1.3 E391

E391[7] is planing to use 2 GeV K_L beam, and surround the decay region with a hermetic veto. They are planning to measure only gamma's energy and position. At JHF (Japan Hadron Facility), the number of total K_L decays is 2.1×10^{14}.

As shown in Fig. 4.14, at 2GeV/c, $\Delta\eta/\eta = 10\%$ can not be reached with any signal region. However, in our study, the number of total K_L decays is 1.4×10^{13}, 1/15 of JHF's yield. In addition, E391 is proposing to use CsI. They also plan to use 1MeV threshold instead of 10MeV in our study, for photon veto. Therefore they should have a lower background level than our result.

5.2 Suggestions

In our study, 'the realistic model' are still far from reality mainly in following points.

At first, in our model, all the area of photon counter can measure the energy and position of gamma. However, it is not realistic because of its high cost, so we should instrument a part of the detector as a calorimeter, and use the rest of the part as a photon veto.

Next, we assumed that the beam size is infinitely small. The beam size is sensitive to P_t distribution in simple case, so we should estimate the effect of the finite beam size.

In this study, we considered only background from $K_L \to \pi^0\pi^0$. However there are many other backgrounds, and it is probable that the signal region in our study is not optimum for rejecting other backgrounds. Moreover, the backgrounds originated from target(ex, Λ, multi πs, etc.) may raise the background level at high K_L momentum.

In order to design the experiment to measure the branching ratio of $K_L \to \pi^0\nu\bar{\nu}$, we suggest to study above subjects.

Chapter 6

Conclusion

By using Monte Carlo simulation, we studied the conditions necessary for measuring the branching ratio of $K_L \to \pi^0 \nu \bar{\nu}$ while suppressing major background from $K_L \to \pi^0 \pi^0$. In this study, we assumed that K_L's decay at the same point, which was surrounded by a cylindrical photon counter. The length of this detector was assumed to be infinite in the upstream direction and P_{K_L}/10MeV/c times the detector radius in the downstream direction, where P_{K_L} is the K_L momentum. This detector length was chosen to keep the effect of finite detector length small. The photon counter was assumed to have the energy resolution of $\Delta E/E = 1\%/\sqrt{E(GeV)}$ and position resolution of ΔX=0.01 for a detector radius of '1'. The detection inefficiency was assumed to be the same as 1mmPb/5mmScintillator calorimeter.

Using this detector, in order to measure η to 10% of itself and to keep the background level below 3×10^{-11} with 1.4×10^{13} K_L decays, the incident K_L momentum needs to satisfy at least the following conditions.

- If we only measure gammas energy and position,
  $P_{K_L} \geq$ 10GeV/c.
- If we know the decay vertex in addition to gammas energy and position
  (here we assumed that we obtain the decay vertex position by measuring gammas direction with a resolution $\Delta\theta = 1/E(MeV)$),
  $P_{K_L} \geq$5GeV/c.
- If we know K_L energy($\Delta E_{K_L}/E_{K_L} = 0.05$) in addition to gammas energy and position
  $P_{K_L} \geq$5GeV/c.
- If we know K_L energy and decay vertex with the resolutions described above, in addition to gammas energy and position,
  $P_{K_L} \geq$500MeV/c.

Addendum I

CsI Photon Counter

In this addendum, we will use the CsI as the photon counter instead of lead/scintillator, and study how much the background level would be improved compared to using lead/scintillator.

I.1 Inefficiency of CsI photon counter

In this section, we will describe the detection inefficiency of the photon counter made of CsI.

The inefficiency of CsI photon counter due to photo-nuclear interaction was also studied by ES171 experiment [14]. In this experiment, they used stacked nine CsI blocks to make the total volume of 15cm$\times$ 15cm$\times$ 50cm which corresponds to 27 radiation length and 2 moliere radius. The energy threshold was set to 10MeV. Figure I.1 shows the inefficiency of CsI photon counter due to photo-nuclear interaction measured by ES171.

Since CsI photon counter is a fully active calorimeter, the inefficiency due to sampling effect does not exist, and since this photon counter is 27 radiation lengths long, the inefficiency due to punch through is negligible. Therefore Figure I.1 shows the total photon detection inefficiency of CsI photon counter.

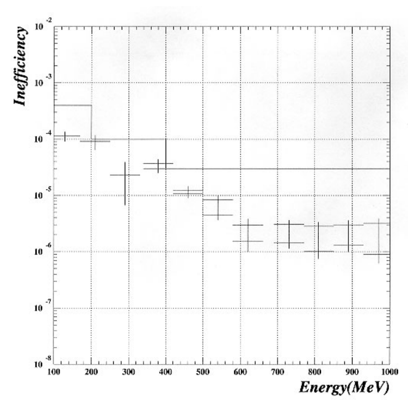

Figure I.1: Photon detection inefficiency for CsI photon counter as a function of gamma's energy, measured by ES171 [14]. The cross correspond to the data, and the solid line is the inefficiency which KAMI experiment required in EOI.

The inefficiencies due to photo-nuclear interaction are almost similar between CsI and lead/scintillator.

However since CsI photon counter does not have the sampling effect, total inefficiency of CsI is lower than lead/scintillator for gammas below 30MeV.

I.2 Detector parameters

In this and next section, by using CsI photon counter described in the previous section, we will study the background levels for the four cases; the simple case, the case where vertex is known, the case where E_{K_L} is known, and the case where both vertex and E_{K_L} are known. The methods for rejecting background events are the same as in Chapter3 and Chapter4. The detector performances are kept the same as in Chapter4 except for the inefficiency, as shown in the following table.

	Simple case	Case where vertex is known	Case where E_{K_L} is known	Case where E_{K_L} and vertex are known
K_L energy resolution($\Delta E_{K_L}/E_{K_L}$)			5%	5%
gamma's energy resolution($\Delta E/E$)	$1\%/\sqrt{E(GeV)}$	$1\%/\sqrt{E(GeV)}$	$1\%/\sqrt{E(GeV)}$	$1\%/\sqrt{E(GeV)}$
gamma's position resolution(ΔX)	0.01		0.01	
gamma's direction resolution($\Delta\theta$)		$1/E(MeV)$		$1/E(MeV)$
detector length(L)	$P_{K_L}/10MeV/c$	$P_{K_L}/10MeV/c$	$P_{K_L}/10MeV/c$	$P_{K_L}/10MeV/c$

Where the position resolution and detector length are scaled for a detector radius of '1'.

I.3 Background Level

Figures I.2, I.3, I.4, and I.5 show the background levels using CsI photon counter for the simple case, the case where vertex is known, the case where K_L energy is known, and the case where vertex and K_L energy are known, respectively.

As shown in these figures, the background levels using CsI are generally lower than that using lead/scint, and this difference is lager for lower K_L momentum. This is because the difference of photon detection inefficiency between CsI and lead/scint is larger for lower energy gamma(Fig 2.12 and I.1), since CsI photon counter does not have a sampling effect.

I.4 Discussion

In a real experiment, we will most likely use CsI for only part of the detector, so the background level would be somewhere between the background levels for CsI and lead/scintillator.

As shown in Fig.I.2, at 13GeV/c which is the mean E_{K_L} for KAMI, the background level is $\simeq 2.2 \times 10^{-11}$ for lead/Scint and $\simeq 1.5 \times 10^{-11}$ for CsI. Therefore if KAMI measures only gammas energy and position, the background level is between 1.5×10^{-11} and 2.2×10^{-11}. This corresponds to S/N of about $1.4 \sim 2.0$. If KAMI measures the decay vertex in addition to gammas energy and position, even with lead/scintillator calorimeter the S/N is high enough to detect $K_L \to \pi^0 \nu\bar{\nu}$, as shown in Fig.I.3.

If BNL experiment uses CsI for a part of photon counter, the background level will be reduced to $2 \times 10^{-13} \sim 3 \times 10^{-12}$, that is, S/N of 10$\sim$150.(See Fig.I.5 at 700MeV/c) This is enough to detect $K_L \to \pi^0 \nu\bar{\nu}$.

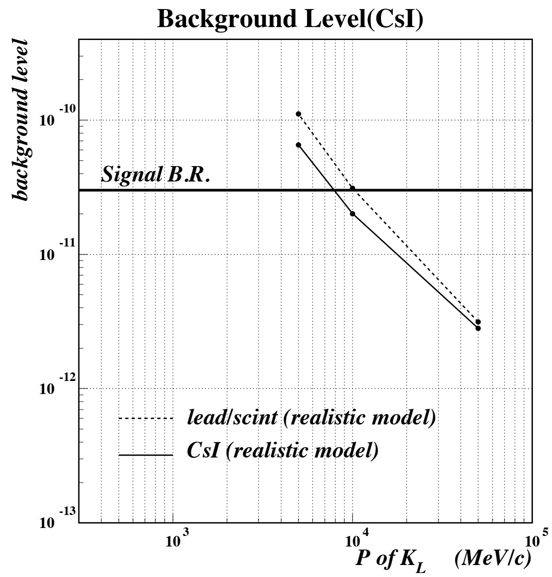

Figure I.2: The background level for a realistic model in the simple case is shown. The solid line and the dashed line show the background level using CsI photon counter and 1mmPb/5mmScint sampling detector, respectively.

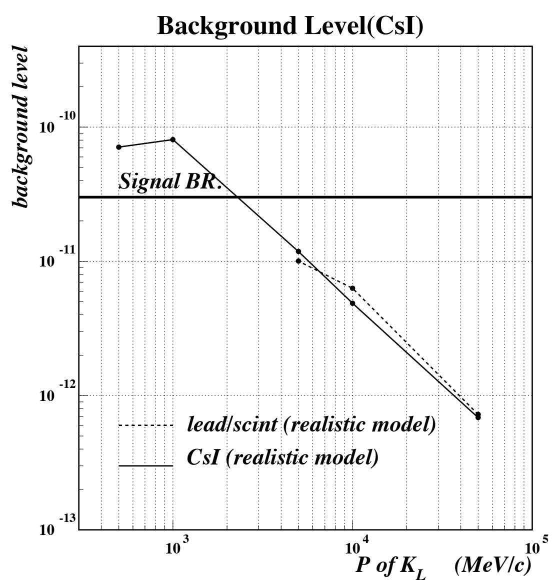

Figure I.3: The background level for a realistic model in the case where vertex is known is shown. The solid line and the dashed line show the background level using CsI photon counter and 1mmPb/5mmScint sampling detector, respectively.

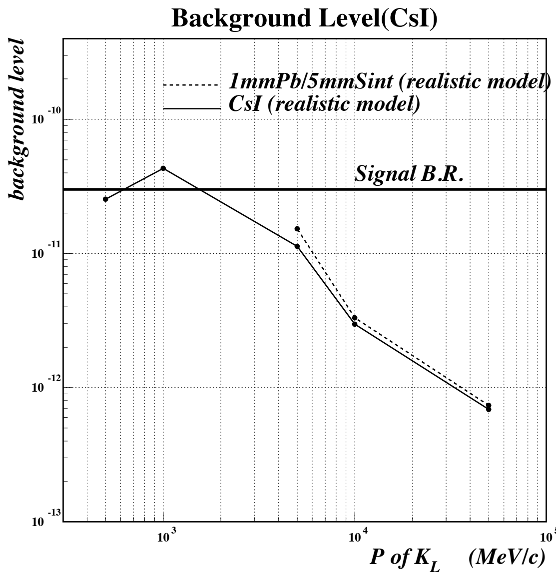

Figure I.4: The background level for a realistic model in the case where K_L energy is known is shown. The solid line and the dashed line show the background level using CsI photon counter and 1mmPb/5mmScint sampling detector, respectively.

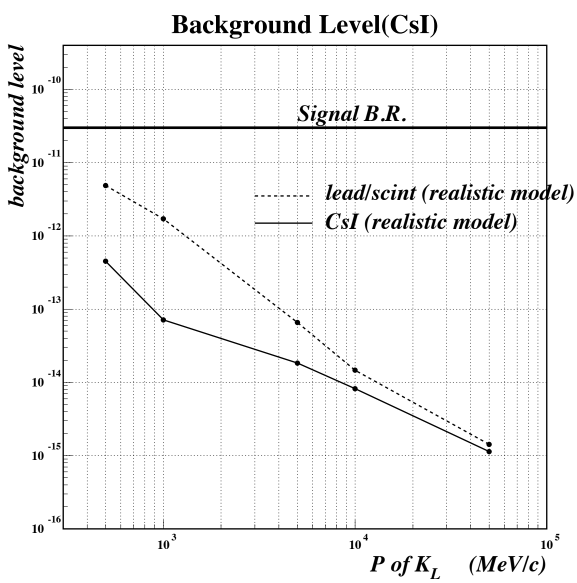

Figure I.5: The background level for a realistic model in the case where vertex and K_L energy are known is shown. The solid line and the dashed line show the background level using CsI photon counter and 1mmPb/5mmScint sampling detector, respectively.

Addendum II

Reconstructed Decay Vertex Position

In the simple case and the case where E_{K_L} is known, we reconstructed the vertex position assuming that two gammas originated from one pion. However, the reconstructed vertex position is not correct for odd pair background events. Therefore in this chapter we will study the property of the reconstructed decay position.

Figure II.1 shows the distribution of the reconstructed vertex position of $K_L \to \pi^0\pi^0$ before cuts. The detector condition is the same as in the realistic model described in Section 4.1.4, that is $\Delta E/E = 1\%/\sqrt{E(GeV)}$, $\Delta X = 0.01$, and $L = P_{K_L}/10MeV/c$.

In this study, we assumed that all K_L decayed at Z=0. Therefore, in Fig. II.1, the peak at Z=0 shows the even pair background and other events are due to odd pair background, because two detected gammas of odd pair(even pair) background originated from different(same) pions and we calculated vertex position assuming that two gammas came from the same pion.

As shown in Fig. II.1, most of the odd pair background events are reconstructed upstream. We do not know this reason in detail. However, this is related to the property where events reconstructed upstream have higher two gammas energy($E\gamma\gamma$). For higher $E\gamma\gamma$, since the energy of missing gammas is low, the possibility of becoming a background is higher, so in result, the distribution increased for upstream Z.

The distribution drops sharply at some Z(for example, this edge is $Z = -50$ for K_L momentum of 10GeV/c). The edge is caused by a kinematic limit where the E_{K_L} is shared by two observed gammas.

In the real experiment, since the K_L decay position spreads over decay region and we do not know the true vertex position, we cannot use the reconstructed position for cutting background events. However by shortening the distance between the upstream edge of decay region and the downstream edge of detector, we can reject the odd pair background events which are reconstructed far upstream than true vertex. For example, if we choose this distance of 20, we can reject the odd pair background below $Z = -20$ as shown in Fig.II.1.

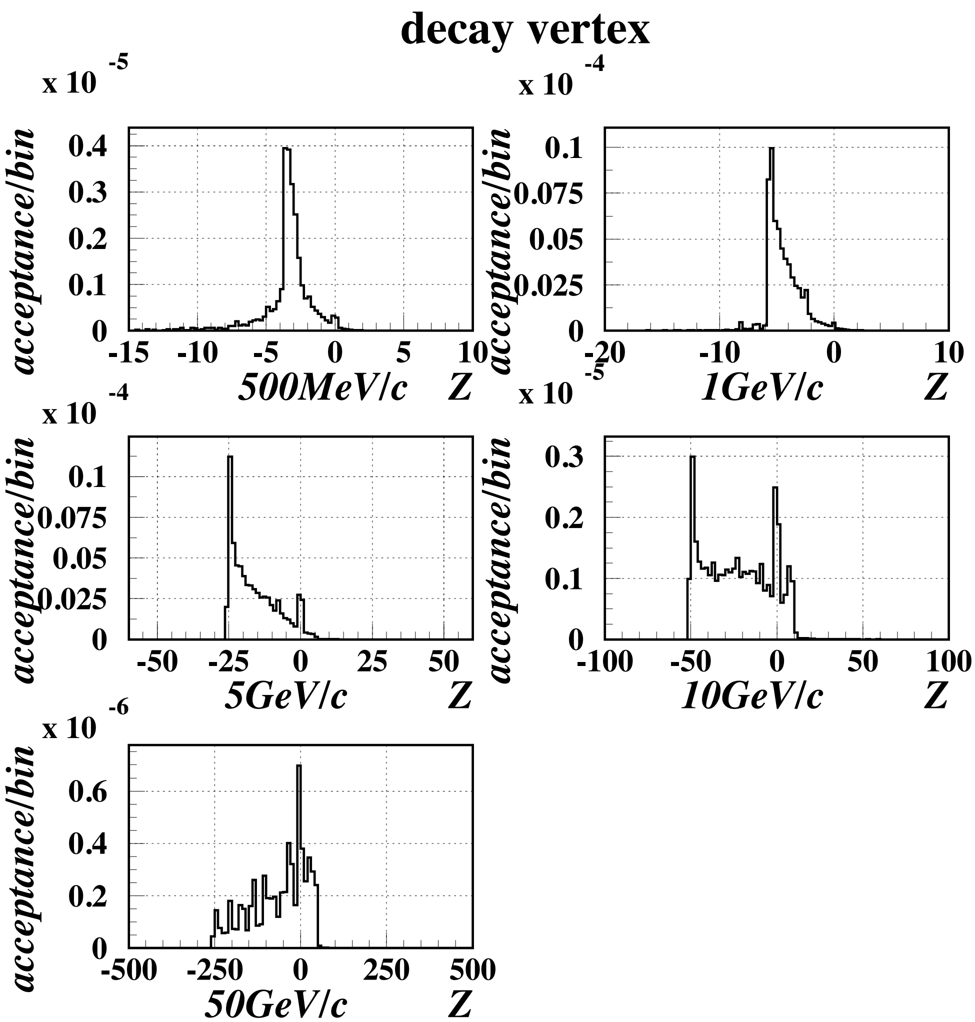

Figure II.1: Distribution of reconstructed vertex position before cuts for a detector with finite resolutions and length. The real vertex position is zero.

Addendum III

Effect of the realistic K_L momentum

In the previous chapters, we assumed that incident momentum of K_L is monochromatic, but in reality, K_L momentum has a finite width. Therefore we studied the effect caused by the spread of K_L momentum for the simple case and the case where vertex is known, and further we examined whether we can use the '$E_{\gamma\gamma}$ VS.M_{miss} cut' for the these cases.

III.1 K_L momentum distribution

In this study, as the distribution of incident K_L momentum(P_{K_L}), we referred to the result in KAMI beam test. This beam test was performed by KTeV with a 150GeV proton beam during Jan. and Feb. of 2000. Figure III.1 shows the distribution of incident K_L momentum which was obtained by using the $K_L \to \pi^+\pi^-\pi^0$.

We fitted this distribution with a Gaussian whose standard deviation depended on K_L momentum with a linearity:

$$f(P_{K_L}) = \exp\left(\frac{-(P_{K_L} - a)^2}{2(b + c \times P_{K_L})^2}\right). \tag{III.1}$$

The fitted result is

$$a = 24650MeV,\ b = 4020MeV,\ c = 0.1640\ . \tag{III.2}$$

To make P_{K_L} distributions for different momentum ranges, we simply scaled the Equation(III.1) with the momentum at the peak of the distribution, P_{peak}, as shown in

$$f(P_{K_L}) = \exp\left(\frac{-(P_{K_L} - P_{peak})^2}{2(b\frac{P_{peak}}{a} + c \times P_{K_L})^2}\right). \tag{III.3}$$

We generated the events with Equation(III.3) for P_{peak} of 500MeV/c, 1GeV/c, 5GeV/c, 10GeV/c, and 50GeV/c.

III.2 Effect of the realistic K_L momentum

In this section, we studied the effect caused by the realistic K_L momentum spectrum for the simple case and the case where vertex is known.

The detector condition is the same as the realistic model used in section 4.1.4 and 4.2.4. For the simple case, $\Delta E/E = 1\%/\sqrt{E(GeV)}$, $\Delta X = 0.01$, and $L = P_{peak}/10MeV/c$. For the case where vertex is known, $\Delta E/E = 1\%/\sqrt{E(GeV)}$, $\Delta\theta = 1/E(MeV)$, and $L = P_{peak}/10MeV/c$.

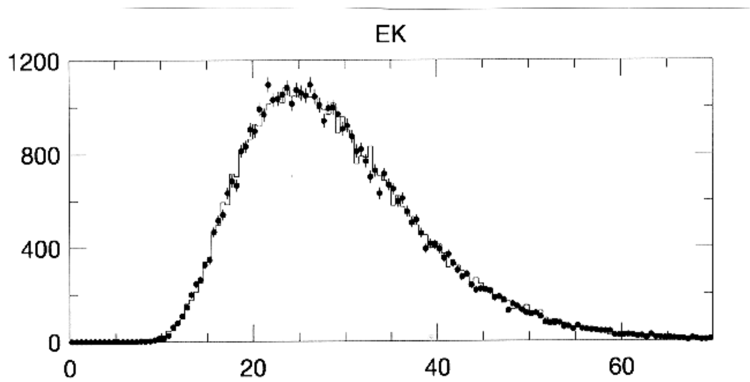

Figure III.1: The K_L momentum(GeV/c) distribution, measured in KAMI beam test. The dots and histogram correspond to the data and MC, respectively.

Figure III.2 and III.3 show the background level for simple case and the case where vertex is known, respectively. As shown in these figures, the effect caused by the spread of K_L momentum is small for the simple case, because the transverse momentum distribution is not affected by the K_L momentum, and for the case where vertex is known, the background level is not also affected by the realistic K_L momentum except for 10GeV/c. The increase at 10MeV/c is due to a step in photon detection inefficiency curve.

III.3 $E_{\gamma\gamma}$ VS. M_{miss} Cut

In this section, we examined whether we can use the '$E_{\gamma\gamma}$ VS. M_{miss} cut' for the simple case and the case where vertex known. In these cases, we do not know the K_L energy event by event. Therefore, in order to calculate the M_{miss}, we assumed the peak of K_L momentum distribution(P_{peak}) as K_L momentum.

Figure III.4 shows the $E_{\gamma\gamma}$ VS.M_{miss} using realistic E_{K_L} distribution for the simple case. Compared to the $E_{\gamma\gamma}$ VS. M_{miss} using monochromatic K_L energy(Figure 3.12, 3.13), this distribution spreads into negative M^2_{miss} area in both high $E_{\gamma\gamma}$ and low $E_{\gamma\gamma}$ regions. The negative M^2_{miss} in high(low) $E_{\gamma\gamma}$ are caused by events whose K_L momentum is larger(smaller) than P_{peak}.

Figure III.5 shows the background level for the simple case. Using the $E_{\gamma\gamma}$ VS. M_{miss} cut instead of P_t cut lowers the background level by 1.1$\sim$1.9 times than P_t cut.

Figure III.6 shows the background level for the case where vertex is known. The $E_{\gamma\gamma}$ VS. M_{miss} cut in addition to $M_{\gamma\gamma}$ cut lowers the background level up to 2.5 times than $M_{\gamma\gamma}$ cut only. The cut also allows us to measure the η with error of 10% at 1GeV/c.

Since $E_{\gamma\gamma}$ VS. M_{miss} distribution for background events is very sensitive to photon counter inefficiency, we need to know the property of photon counter well to use this cut. However, if we know this property well, this $E_{\gamma\gamma}$ VS. M_{miss} cut is effective for the simple case and the case where vertex is known.

The acceptances after these cuts are shown in Table III.1.

Simple case

Momentum of K_L (GeV)	Acceptance of signal	Acceptance of signal ($M^2_{miss} > m^2_{\pi^0}$)	Acceptance of signal ($M^2_{miss} \leq m^2_{\pi^0}$)	Acceptance of background
5	0.20	0.15	0.05	1.5×10^{-8}
10	0.094	0.041	0.052	1.8×10^{-9}
50	0.067	0.027	0.040	2.4×10^{-10}

Case where vertex is known

Momentum of K_L (GeV)	Acceptance of signal	Acceptance of signal ($M^2_{miss} > m^2_{\pi^0}$)	Acceptance of signal ($M^2_{miss} \leq m^2_{\pi^0}$)	Acceptance of background
1	0.27	0.24	0.03	3.2×10^{-8}
5	0.076	0.043	0.032	6.6×10^{-10}
10	0.066	0.031	0.035	2.1×10^{-10}
50	0.062	0.025	0.037	6.4×10^{-11}

Table III.1: Acceptance for the simple case and the case where vertex is known with a realistic K_L momentum. For the simple case, $E_{\gamma\gamma}$ VS. M_{miss} cut is used to rejected backgrounds, and for the case where vertex is known, $M_{\gamma\gamma}$ cut and $E_{\gamma\gamma}$ VS. M_{miss} cut are used. The 1mmPb/5mmScint calorimeter was used as photon counter.

.

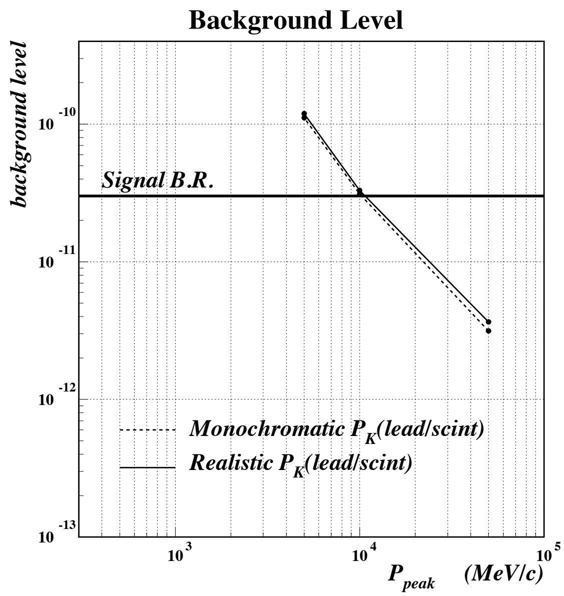

Figure III.2: The background level as a function of the peak K_L momentum(P_{peak}) for the simple case. The solid line and dashed line show the case where realistic K_L momentum and a monochromatic K_L momentum are used, respectively.

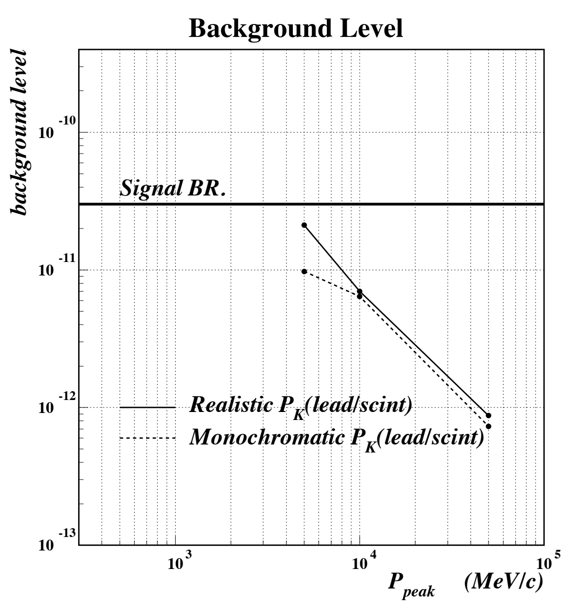

Figure III.3: The background level as a function of the peak K_L momentum(P_{peak}) for the case where vertex is known. The solid line and dashed line show the case where the realistic K_L momentum and a monochromatic K_L momentum are used, respectively.

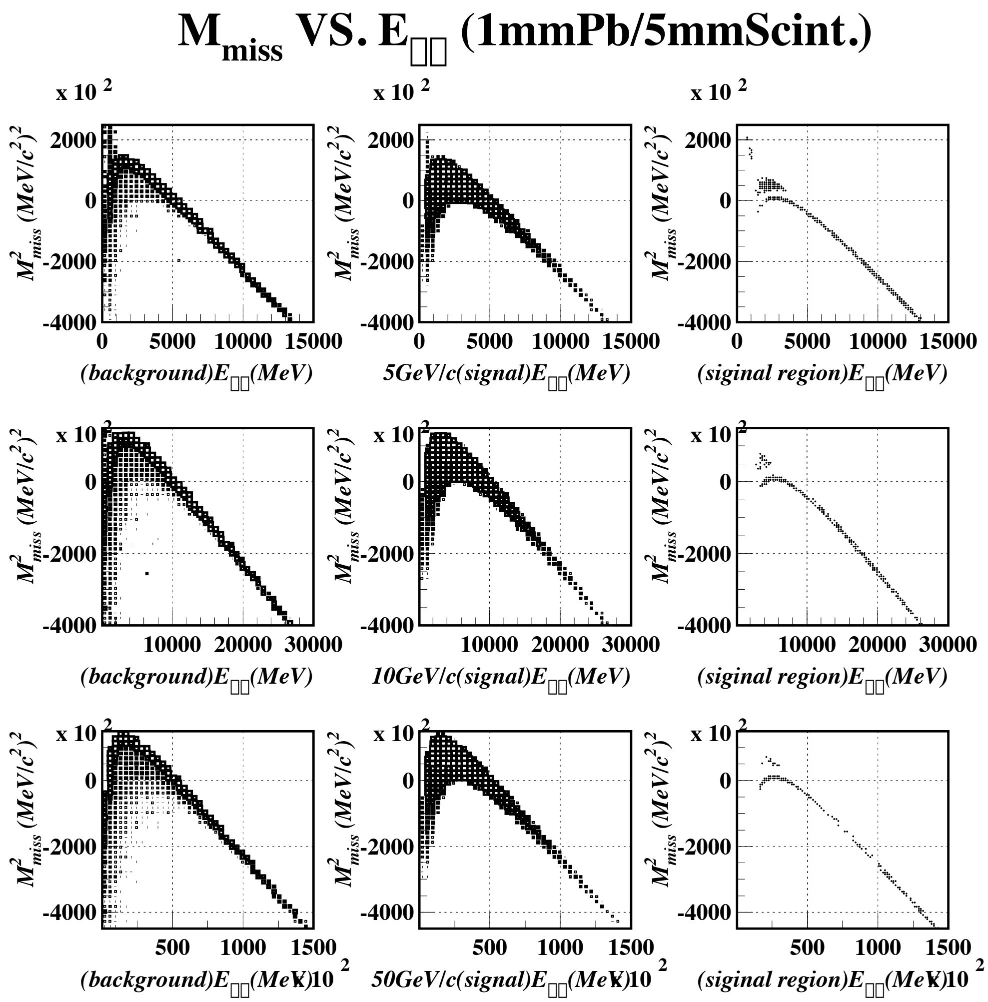

Figure III.4: M_{miss} VS. $E_{\gamma\gamma}$ for P_{peak} of 5GeV/c, 10GeV/c, and 50GeV/c in the simple case. The E_{K_L} which is necessary to calculate M_{miss} is assumed to be the K_L momentum at the peak of the distribution. The 1mmPb/5mmScint sampling calorimeter was used as the photon counter. The left row shows the distribution for the background, and the center row shows the distribution for the signal. The right row shows the signal region selected by the method described in Section3.4.2.

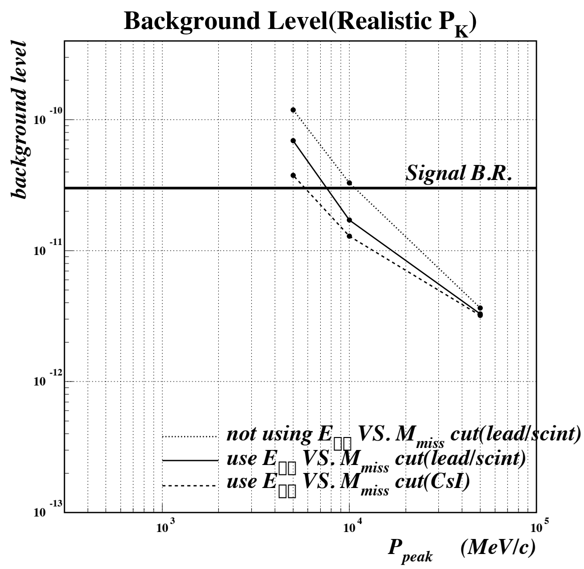

Figure III.5: The background level as a function of P_{peak} for the simple case. The dotted line shows the case where transverse momentum cut is used and the lead/scint is used as detector. The solid line and dashed line show the cases where E_{K_L} VS. M_{miss} cut is used instead of transverse momentum cut, and for solid line the lead/scint is used as detector and for dashed line the CsI is used as detector.

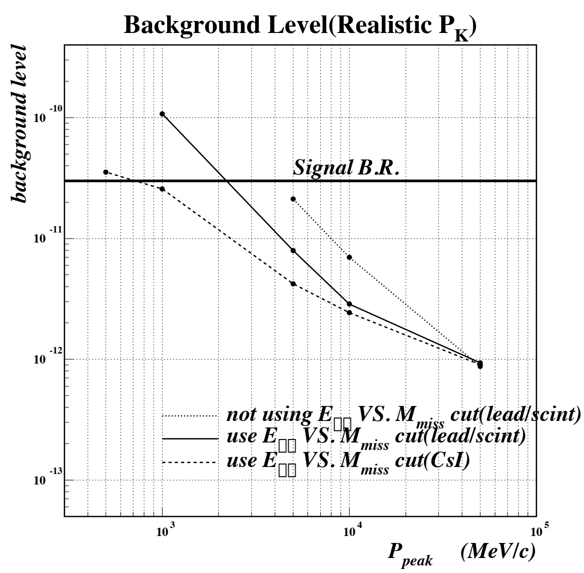

Figure III.6: The background level as a function of P_{peak} for the case where vertex is known. The dotted line shows the case where only $M_{\gamma\gamma}$ cut is used and the lead/scint is used as detector. The solid line and dashed line show the cases where E_{K_L} VS. M_{miss} cut is used in addition to $M_{\gamma\gamma}$ cut, and for solid line the lead/scint is used as detector and for dashed line the CsI is used as detector.

Addendum IV

Threshold of Photon Counter

The background level is very sensitive to photon detection inefficiency, and this inefficiency depends largely on the threshold of the photon counter. Therefore, in this addendum, we studied the effect of the threshold of photon counter by changing the threshold from 10MeV to lower values.

IV.1 Inefficiency of Photon Counter

Here, we used the 1mmPb/5mmScintillator calorimeter as the photon counter, and we studied the threshold of 1MeV and 5MeV. The inefficiency was estimated by the same method as in Chapter2, that is, we used the ES171 experiments result for photo-nuclear interaction and used EGS simulation for sampling effect and punch through. Figure IV.1 shows the photon detection inefficiencies using the threshold of 1MeV and 5MeV. As shown in this figure, the inefficiencies are reduced in all gamma's energy region.

IV.2 Background Level

By using the photon detection inefficiency described above section, we estimated the background level for the simple case. Figure IV.2 shows the background levels using the threshold of 1MeV, 5MeV, and 10MeV. As shown in this figure, by using the threshold of 5MeV and 1MeV, the background levels are reduced by a factor 1.7∼4.3 and 2.5∼13.3 compared to the threshold of 10MeV, respectively, and this factor is lager for lower K_L momentum.

IV.3 Conclusion

As shown in Figure IV.2, by lowering the threshold, the background level was reduced significantly, and the technique of reducing the threshold seems to be easier than other techniques described in previous chapters, that is, the measurement of the vertex position, gammas direction, and K_L momentum. Therefore, we suggest that at first we should try to lower the photon counter threshold.

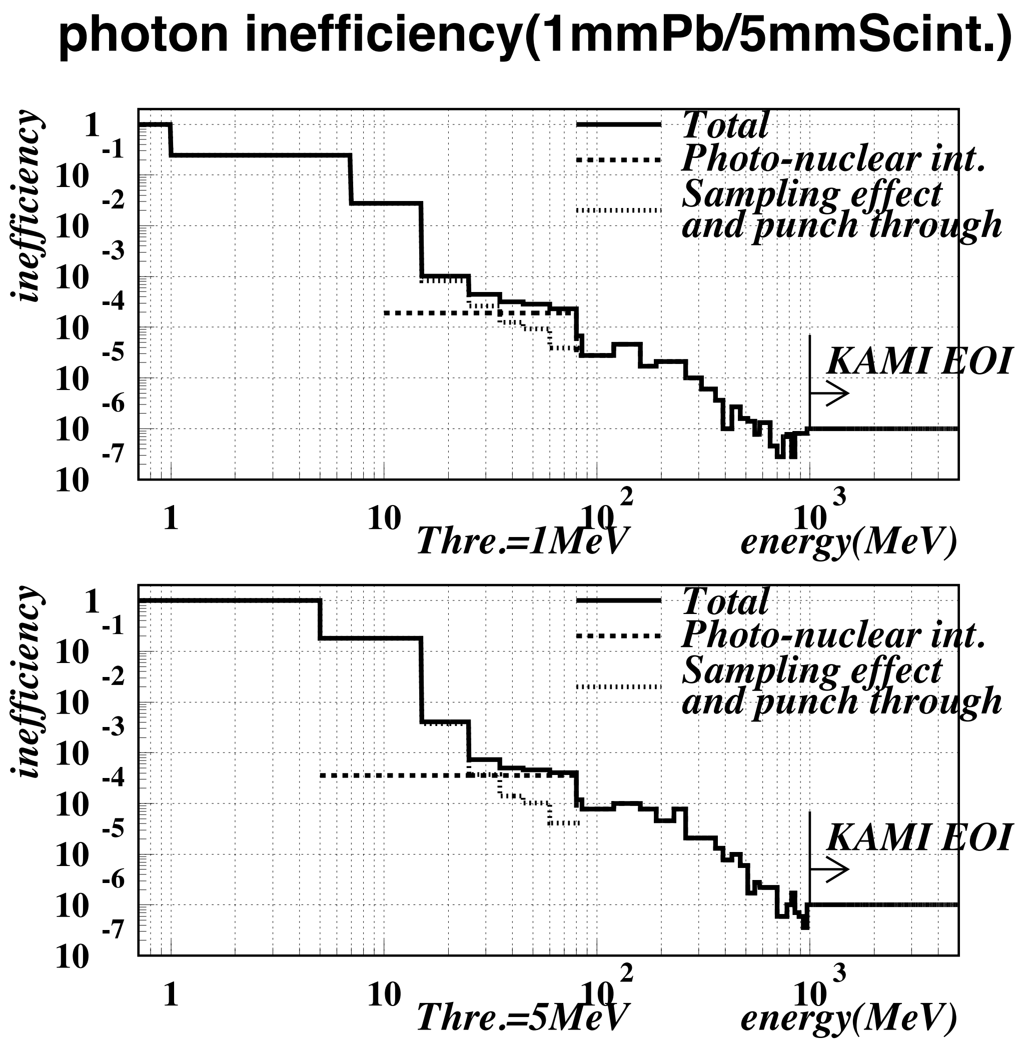

Figure IV.1: Total detection inefficiency as a function of the photon energy for 1mmPb/5mmScint sampling calorimeters. The upper(lower) figure shows the inefficiency whose threshold is 1MeV(5MeV). The dashed line and dotted line show the inefficiency due to the photo-nuclear interaction and the sum of sampling effect and punch through, respectively. Above 1GeV, the inefficiency required by KAMI is used.

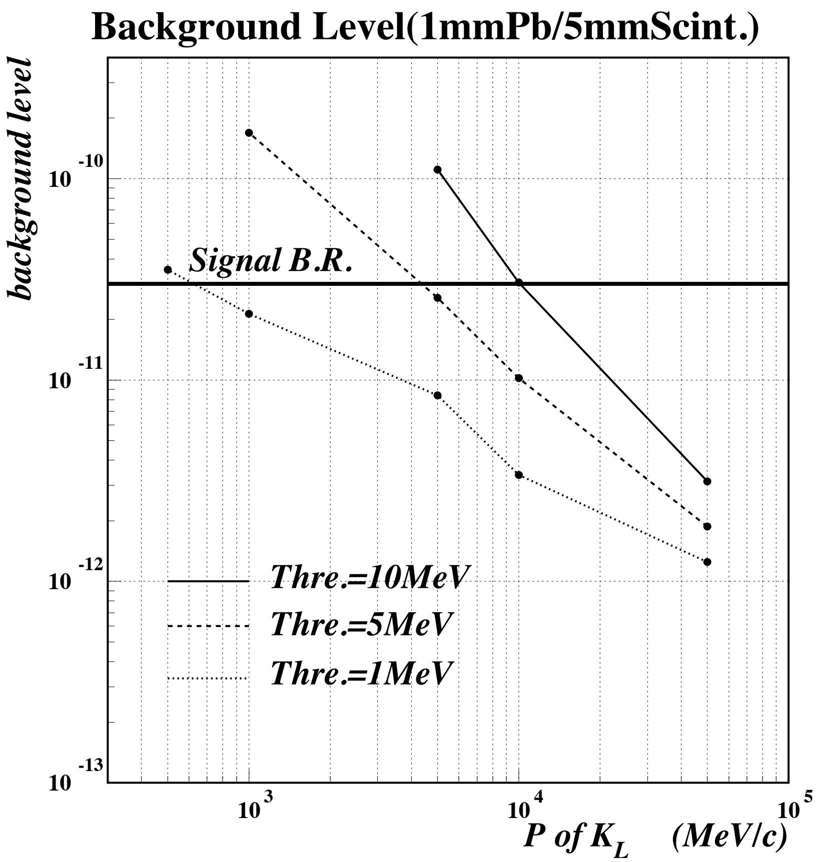

Figure IV.2: The background level as a function of K_L momentum for simple case. The solid line shows the inefficiency using threshold of 10MeV, which was used in previous chapters. The dashed and dotted lines show the background levels using the threshold of 5MeV and 1MeV, respectively. The 1mm Pb/5mm Scint detector is used as photon counter.

Appendix A

Contribution of Punch Through

When gammas deposit the energy in lead/scintillator sampling calorimeter, a peak exists at 0MeV in the distribution of deposit energy in scintillator (Fig. 2.8, 2.9, and 2.10). The probability of this peak is about 3×10^{-4} and 1.8×10^{-5} for incident gammas energy of 20 MeV and 100MeV in 1mmPb/ 5mmScint detector, respectively, and this probability is reduced as gammas incident energy gets higher. In this appendix, we will explain about this peak.

This peak comes from two sources. First source is a backward scattering of the incident photon in the first lead layer. This effect contributes about 10% of the peak for photon energy of 20MeV, but $O(10^{-7})$ for 100MeV. This is a reasonable result because photon which have higher energy can not go back at the first lead. Another source is punch through, and this is actually more dominant.

The total probability for photon interaction in matter is described by a cross section. The cross section(σ) is shown in Fig. A.1 [13] for lead. If we now multiply σ by the density of atoms, N, we then obtain the probability per unit length for an interaction,

$$\mu = N\sigma = \sigma(N_a \rho / A) \tag{A.1}$$

with N_a: Avogadro's Number; ρ:density of the material; A: molecular weight. The fraction of photons surviving a distance x is then

$$I/I_o = exp(-\mu x), \tag{A.2}$$

where I_o is the incident intensity.

For 1mmPb/ 5mmScinti detector, since its length is 18.2 radiation lengths, we assumed x=10.2cm. For example, for 20MeV photon, μ is $\cong 0.69 cm^{-1} atom^{-1}$, and I/I_0 is 9×10^{-4} at the downstream end of our detector. For 100MeV photon energy, μ is $\cong 1.0 cm^{-1} atom^{-1}$, and the I/I_0 is 4×10^{-5}. From Figure 2.8, for 20MeV photon, the peak hight at 0MeV is 8×10^{-4}(1bin=0.2MeV), and for 100MeV photon, the peak hight is 1.8×10^{-5}. These number agree within a factor $\cong$2.5.

We should note that the well known equation for a fraction of photons surviving a radiation length L,

$$I/I_o = exp(-\frac{7}{9}L) \cong exp(-0.78L) \tag{A.3}$$

is an approximation at high energy and it is not correct in the low energy such as 20MeV and 100MeV. For example, for 20MeV photon, if we use this equation, $I/I_o = 6.8 \times 10^{-7}$ at the downstream end of our detector, but Figure 2.8 shows the $I/I_o = 8 \times 10^{-4}$, and the difference is about factor of 100. Therefore we should not use this expression in these energy.

Actually, for high energy($\cong$100GeV) photon, μ is $\cong 1.4 cm^{-1} atom^{-1}$, which gives

$$I/I_o = exp(-1.41x) \cong exp(-0.78L), \tag{A.4}$$

consistent with Equation(A.3). The difference of μ between 20MeV and 100GeV is only a factor 2, but in here we consider exponential, so this value is not small. In result, low energy photons pass through more material than high energy photons.

In Fig. 2.11 which shows the photon detection inefficiency due to electro-magnetic interaction, the inefficiency at energy greater than 50MeV is actually dominated by punch through effect. However, in this energy region, the effect of photo-nuclear interaction is more dominant by a factor > 10 than the punch through effect.

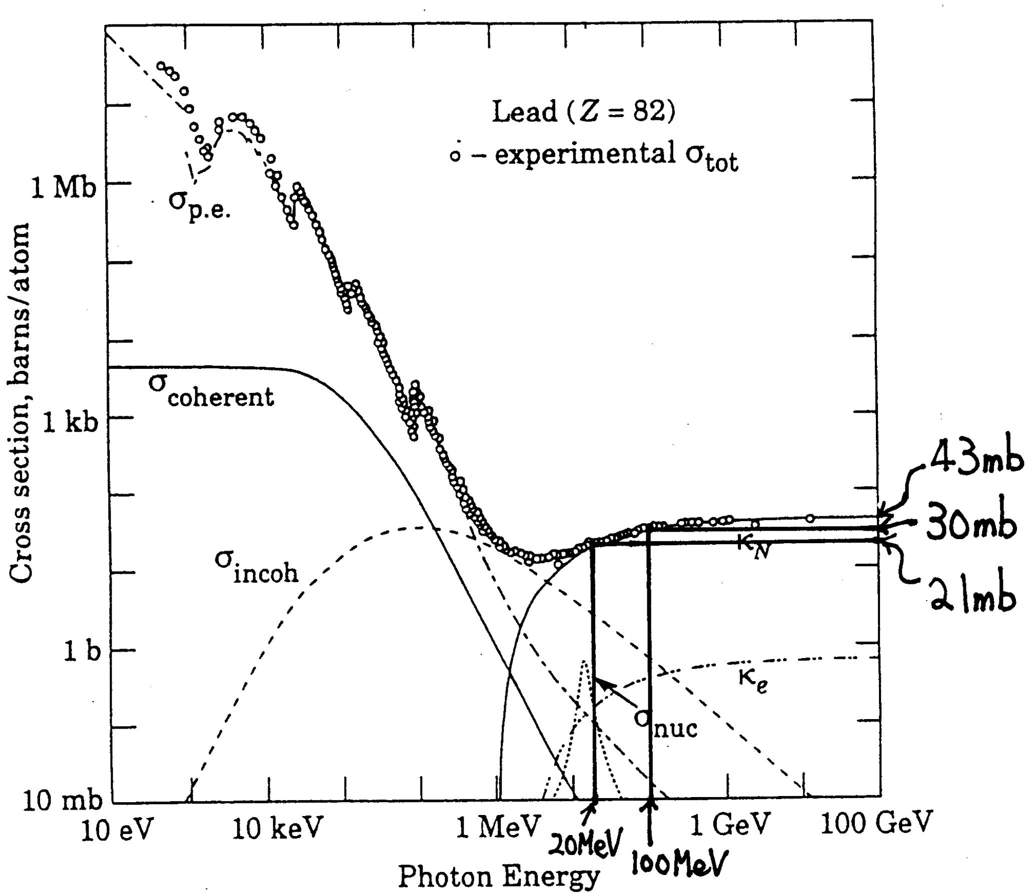

Figure A.1: Total photon absorption cross section for lead

Appendix B

Step in P_t distribution

In this appendix, we will explain the step at about 180MeV/c in the P_t distribution(K_L momentum of 10GeV/c in Fig. 3.3, and 3.7).

This step comes from the step in the photon detection inefficiency we used (Fig. 2.12), and cased by the even pair background.

If we assume the even pair background where two detected gammas come from the same pion, the transverse momentum, P_t, and the energy of missing two gammas, $E_{miss\gamma\gamma}$ (or missing pion energy), are expressed as:

$$P_t = \sin\theta \sqrt{\left(\frac{M_{K_L}}{2}\right)^2 - M_{\pi^0}^2} \tag{B.1}$$

$$E_{miss\gamma\gamma} = \frac{E_{K_L}}{2} - \frac{P_{ZK_L}}{M_{K_L}} \cos\theta \sqrt{\left(\frac{M_{K_L}}{2}\right)^2 - M_{\pi^0}^2} \tag{B.2}$$

where M_{K_L} and M_{π^0} are the masses of K_L and π^0, E_{K_L} is the energy of K_L, P_{ZK_L} and θ are Z component of K_L momentum and angle between the directions of incident K_L and pion. The above equations represent a part of an eclipse with θ parameter in the P_t-$E_{miss\gamma\gamma}$ plane, as shown in Fig. B.1(b).

Therefore, P_t and $E_{miss\gamma\gamma}$ are constrained on this line.

As described in Appendix D, the even pair background prefers to have one high energy missing gamma and one low energy missing gamma. Thus we can approximate the higher gamma's energy with the missing pion energy($E_{miss\gamma\gamma}$).

Therefore, the big step at 3GeV in the photon detection inefficiency we used(Figure 2.12) corresponds to the 3GeV in the vertical axis in Figure B.1(b) and this energy corresponds to the transverse momentum of 185MeV/c. This is in good agreement with the step in P_t distribution(Fig B.1(a)).

On the other hand, the step in the inefficiency curve for low energy photon does not produce a step in the P_t distribution, because there is no good correlation between the lower energy of missing gammas and missing pion energy($E_{miss\gamma\gamma}$).

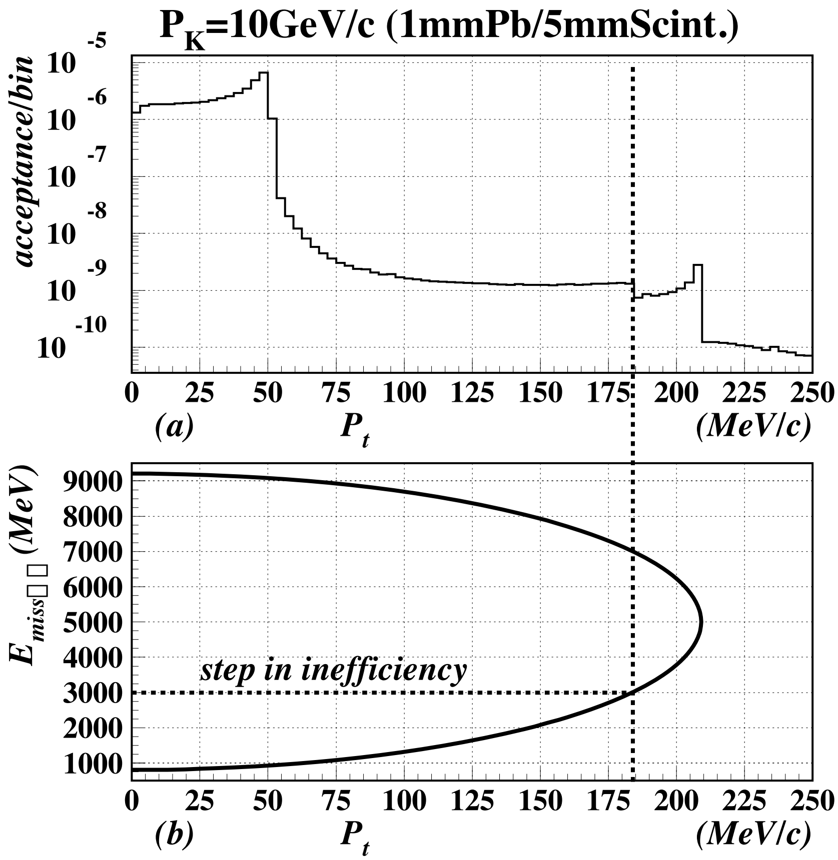

Figure B.1: (a)transverse momentum for K_L momentum of 10GeV/c in 1mmPb/5mmScint detector. (b)Relation between P_t and energy of two missing gammas,$E_{miss\gamma\gamma}$ for even pair background.

Appendix C

Error on η

In this appendix, we will explain how we derived the error on $\eta(\Delta\eta/\eta)$, Equation(3.3), in detail.

As described in Introduction, the branching ratio of the signal, BR_{sig}, is proportional to η^2 (Equation(1.12)). Therefore the error on η is expressed as:

$$\frac{\Delta\eta}{\eta} = \frac{1}{2} \times \frac{\Delta BR_{sig}}{BR_{sig}}. \tag{C.1}$$

The BR_{sig} is defined as:

$$BR_{sig} \equiv \frac{\overline{N_{sig}}/A_{sig}}{\overline{N_{norm}}/(A_{norm}BR_{norm})}, \tag{C.2}$$

where $\overline{N_{sig}}$ and $\overline{N_{norm}}$ are the observed numbers for signal and normalization mode events, and A_{sig} and A_{norm} are the acceptances for signal and normalization mode event, and BR_{norm} is the branching ratio of normalization mode event.

In this case, since the errors on $\overline{N_{norm}}$ and A_{sig}/A_{norm} are very small as compared to error on $\overline{N_{sig}}$ $(\Delta\overline{N_{sig}}/\overline{N_{sig}} \gg \Delta N_{norm}/N_{norm}, \Delta(A_{sig}/A_{norm})/(A_{sig}/A_{norm}))$, the error on signal branching ratio can be written as,

$$\frac{\Delta BR_{sig}}{BR_{sig}} = \frac{\Delta\overline{N_{sig}}}{\overline{N_{sig}}}. \tag{C.3}$$

Using the total observed number of decays($\overline{N_{decay}}$) and the estimated number of background events($\overline{N_{bkg}}$), $\overline{N_{sig}}$ is expressed as,

$$\overline{N_{sig}} = \overline{N_{decay}} - \overline{N_{bkg}}. \tag{C.4}$$

Assuming that the number of background events is known well from other studies,

$$\Delta\overline{N_{sig}} = \Delta\overline{N_{decay}}. \tag{C.5}$$

From (C.3) and (C.5),

$$\frac{\Delta BR_{sig}}{BR_{sig}} = \frac{\Delta\overline{N_{decay}}}{\overline{N_{sig}}} \tag{C.6}$$

$$= \frac{\sqrt{\overline{N_{decay}}}}{\overline{N_{sig}}} \tag{C.7}$$

where we only considered a statistics error, $\Delta\overline{N} = \sqrt{\overline{N}}$.

Using the total number of decays(N_{decay}), BR_{sig}, and background branching ratio(BR_{bkg}), $\overline{N_{sig}}$ and $\overline{N_{bkg}}$ are written as,

$$\overline{N_{sig}} = N_{decay} \times BR_{sig} \times Asig, \tag{C.8}$$

$$\overline{N_{bkg}} = N_{decay} \times BR_{bkg} \times Abkg. \tag{C.9}$$

Then $\overline{N_{decay}}$ is

$$\overline{N_{decay}} = \overline{N_{sig}} + \overline{N_{bkg}} \tag{C.10}$$

$$= N_{decay} \times (BR_{sig} \times A_{sig} + BR_{bkg} \times A_{bkg}). \tag{C.11}$$

Substituting these $\overline{N_{sig}}$ and $\overline{N_{decay}}$ for Equation(C.7),

$$\frac{\Delta BR_{sig}}{BR_{sig}} = \frac{\sqrt{BR_{sig} \times A_{sig} + BR_{bkg} \times A_{bkg}}}{\sqrt{N_{decay}} \times BR_{sig} \times A_{sig}}. \tag{C.12}$$

Using Equations(C.1) and (C.12), we get

$$\frac{\Delta\eta}{\eta} = \frac{\sqrt{BR_{sig} \times A_{sig} + BR_{bkg} \times A_{bkg}}}{2 \times \sqrt{N_{decay}} \times BR_{sig} \times A_{sig}}. \tag{C.13}$$

In this thesis, we used $BR_{bkg} = BR(K_L \to \pi^0\pi^0) = 9.36 \times 10^{-4}$, $BR_{sig} = BR(K_L \to \pi^0\nu\bar{\nu}) = 3 \times 10^{-11}$, and $N_{decay} = 1.4 \times 10^{13}$ as described in Chapter 4. The acceptances (A_{sig} and A_{bkg}) depend on the cut region.

Appendix D

Dominant of Odd Pair Background

In this appendix, we will explain why the background events are dominated by the odd pair background, as shown in Fig. 3.3 and Fig. 3.6 etc..

The two gammas missed in even pair background come from one pion. Therefore the sum of these missing gamma's energy is equal to the energies of pion.

$$E_{\gamma 1} + E_{\gamma 2} = E_{\pi^0} \tag{D.1}$$

where $E_{\gamma 1}$ and $E_{\gamma 2}$ are the energy of two missing gammas, and E_{π^0} is the energy of the parent pion in the lab frame. The energy of pion, E_{π^0}, is expressed as:

$$E_{\pi^0} = \frac{E_{K_L}}{M_{K_L}} \left(\frac{M_{K_L}}{2} + \sqrt{\left(\frac{M_{K_L}}{2}\right)^2 - M_{\pi^0}^2} \frac{P_{ZK_L}}{E_{K_L}} \cos\theta \right) \tag{D.2}$$

where M_{K_L} and M_{π^0} are the mass of K_L and π^0, E_{K_L}, P_{ZK_L}, and θ are the energy of K_L, Z component of K_L momentum, and the angle between the directions of incident K_L and pion, respectively. As shown this equation at $\cos\theta = -1$, E_{π^0} becomes the minimum energy, $E_{\pi^0 min}$.

$$E_{\pi^0 min} = \frac{E_{K_L}}{M_{K_L}} \left(\frac{M_{K_L}}{2} - \sqrt{\left(\frac{M_{K_L}}{2}\right)^2 - M_{\pi^0}^2} \frac{P_{ZK_L}}{E_{K_L}} \right) \tag{D.3}$$

From (D.1) and (D.3), we get a constraint on two missing gammas.

$$E_{\gamma 1} + E_{\gamma 2} \geq \frac{E_{K_L}}{M_{K_L}} \left(\frac{M_{K_L}}{2} - \sqrt{\left(\frac{M_{K_L}}{2}\right)^2 - M_{\pi^0}^2} \frac{P_{ZK_L}}{E_{K_L}} \right) \tag{D.4}$$

Using the actual values in Equation(D.4), we get

$$E_{\gamma 1} + E_{\gamma 2} \geq 142.7 MeV \qquad for\ P_{ZK_L} = 500 MeV/c \tag{D.5}$$

$$E_{\gamma 1} + E_{\gamma 2} \geq 4.0 GeV \qquad for\ P_{ZK_L} = 50 GeV/c \tag{D.6}$$

On other hand, odd pair backgrounds does not have such constraint, since two gammas come from different pions.

Figure D.1 shows the distributions of missing two gamma's energies. The constraint described above(Equation(D.5) and (D.6)) are shown as solid line in Fig. D.1, and the area below this line is forbidden for even pair background.

Since the inefficiency of photon counter is higher for lower gammas energy, events in the lower left corner has a higher probability of becoming background. However even pair background is not allowed in the region below the line, while odd pair background is allowed this region(right row in Fig. D.1). For this reason, the size of odd pair background is greater than the size of even pair background. At higher K_L energy, this area becomes wider as shown in the lower row in Fig. D.1, so the even pair background becomes far less at higher K_L energy.

Also, as shown in Figure D.1(c), since the photon inefficiency is higher for lower gammas energy, one of the missing gamma's from the even pair background tends to have a low energy.

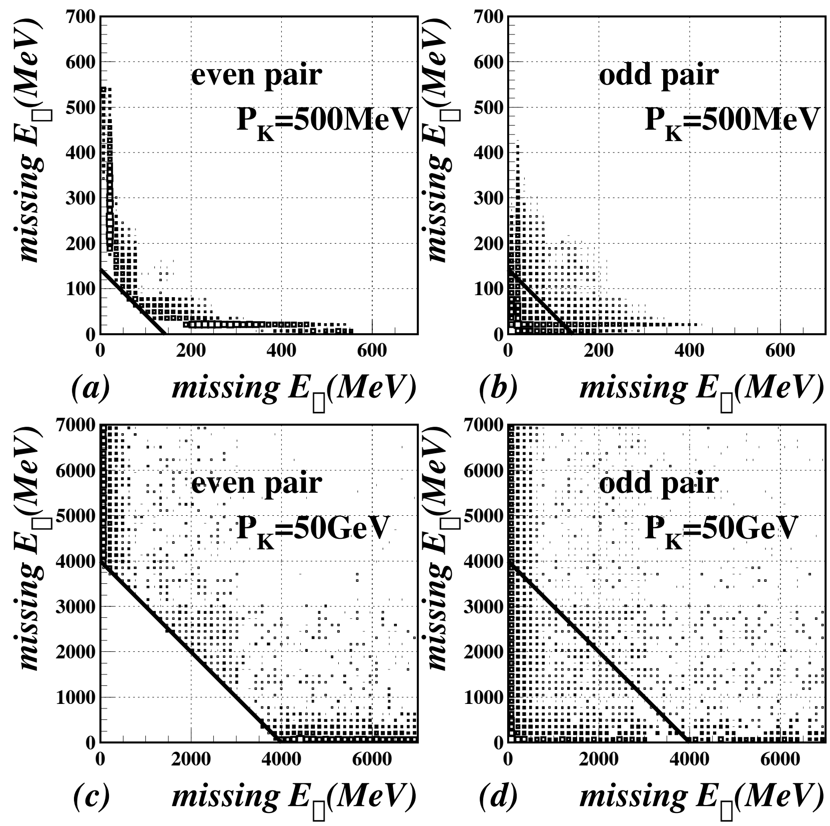

Figure D.1: Distribution of energies of two missing gammas. (a)even pair background from 500MeV/c K_L (b)odd pair background from 1GeV/c K_L (c)even pair background from 5GeV/c K_L (d)odd pair background from 50GeV/c K_L. The area below the solid line is forbidden for even pair background. The detector is assumed to be made of 1mmPb/5mmScint calorimeter.

Bibliography

[1] J. Cronin, V. Fitch *et al.*, Phys. Rev. Lett. **13**, 138 (1964).

[2] M. Kobayashi and T. Maskawa, Prog. Theor. Phys. **49**, 652 (1973).

[3] L. Wolfenstein, Phys. Rev. Lett. **51**, 1945 (1983).

[4] A. Buras, Phys. Lett. **B333**, 476 (1994).

[5] G. Buchalla and A. Buras, Phys. Rev. **D54**, 6782 (1996).

[6] A. Alavi-Harati *et al.*, To be published in Phys. Rev. D, "Search for the Decay $K_L \to \pi^0 \nu \bar{\nu}$ using $\pi^0 \to e^+ e^- \gamma$".

[7] T. Inagaki *et al.*, KEK Proposal, "Measurement of the $K_L \to \pi^0 \nu \overline{\nu}$ decay", (June, 1996).

[8] MECO collaboration and KOPIO collaboration, "A Proposal to the National Science Foundation to Construct the MECO and KOPIO Experiments." (Oct.,1999)

[9] K. Arisaka *et al.*, "An Expression of Interest to Detect and Measure the Direct CP Violating Decay $K_L \to \pi^0 \nu \bar{\nu}$ and Other Rare Decays at Fermilab Using the Main Injector", (Sept., 1997).

[10] K. Kurebayashi, Master Thesis, Osaka Univ., "Measurement of inefficiency of photo-nuclear interaction with lead/scintillator sampling calorimeter", (Feb., 1999).

[11] Peter Mikelsons, PhD thesis, Colorado Univ., "Search for the Decay $K_L \to \pi^0 e^+ e^-$ and Study of the Decay $K_L \to e^+ e^- \gamma\gamma$", (Dec.,1999).

[12] Peter S. Shawhan, PhD thesis, The University of Chicago,"Observation of direct CP Violation in $K_{S,L} \to \pi\pi$ Decays", (Sep., 1999).

[13] Particle Data Group, Phys. Rev. **D54,** 146(1996).

[14] K. Mori, Master Thesis, Osaka Univ., "Measurement of inefficiency of photo-nuclear interaction with CsI photon counter", (Feb., 1999).